5. Lattice Boltzmann Models

5.1 From lattice-gas cellular automata to lattice Boltzmann models

Lattice-gas cellular automata for Navier-Stokes equations are plagued by several *diseases*. Only for some of them therapies and cures could be found (compare Table 5.1.1).

Table 5.1.1. Diseases of lattice-gas cellular automata: its causes and therapies and cures.

disease	cause	therapy/cure	remarks
non-isotropic advection term	lattice tensor of 4th rank is non-isotropic	higher symmetry of lattice add inner degree of freedom multi-speed models	HPP → FHP HPP → PI
violation of the Galilei invariance	Fermi-Dirac distributions	rescaling (symptomatic treatment)	FHP, FCHC, PI
spurious invariants	regular lattices	as much collisions as possible	Zanetti invariants
noise	Boolean variables	averaging (coarse graining)	enormous memory demand
pressure depends explicitly on velocity		multi-speed models	Chen et al. 1989

Historically the following stages in the development of lattice Boltzmann models[1] (LBM) can be distinguished:

[1] A lattice Boltzmann model encompasses a lattice, an equilibrium distribution and a kinetic equation which is called lattice Boltzmann equation (LBE). In

D.A. Wolf-Gladrow: LNM 1725, pp. 159–246, 2000.

1. Lattice Boltzmann equations have been used already at the cradle of lattice-gas cellular automata by Frisch et al. (1987) to calculate the viscosity of LGCA.
2. Lattice Boltzmann models as an independent numerical method for hydrodynamic simulations were introduced by McNamara and Zanetti in 1988. The main motivation for the transition from LGCA to LBM was the desire to get rid of the noise. The Boolean fields were replaced by continuous distributions over the FHP and FCHC lattices. Fermi-Dirac distributions were used as equilibrium functions.
3. Linearized collision operator (Higuera and Jiménez, 1989).
4. Boltzmann instead of Fermi-Dirac distributions.
5. The collision operator, which is based on the collisions of a certain LGCA, has been replaced by the BGK (also called single time relaxation) approximation by Koelman (1991), Qian et al. (1992) and others. These lattice BGK models (*LBGK*) mark a new level of abstraction: collisions are not anymore defined explicitly.

Multi-speed LBGK models are most popular today. However, more complex collision operators are still in use in models of multi-phase flows (Rothman and Zaleski, 1994).

5.1.1 Lattice Boltzmann equation and Boltzmann equation

The microdynamics of LGCA are described by kinetic equations of the type

$$n_i\left(\boldsymbol{x}+\boldsymbol{c}_i\Delta t, t+\Delta t\right)=n_i\left(\boldsymbol{x},t\right)+\Delta_i \tag{5.1.1}$$

(compare, for example, eq. 3.2.15 where Δt was set to 1). Δ_i is the collision function of the respective model. Discrete equations of the form (5.1.1) are referred to as *lattice Boltzmann equations*. The correspondence to the Boltzmann equation

$$\frac{\partial f}{\partial t}+\boldsymbol{v}\boldsymbol{\nabla}f=Q \tag{5.1.2}$$

(Q is the collision integral; external forces have been neglected) can be shown by expansion of the left hand side of eq. (5.1.1):

$$n_i\left(\boldsymbol{x}+\boldsymbol{c}_i\Delta t, t+\Delta t\right)=n_i\left(\boldsymbol{x},t\right)+\Delta t\frac{\partial n_i}{\partial t}+\boldsymbol{c}_i\Delta t\boldsymbol{\nabla}n_i+\mathcal{O}\left(\left(\Delta t\right)^2\right).$$

Neglecting higher order terms, one obtains

$$\frac{\partial n_i}{\partial t}+\boldsymbol{c}_i\boldsymbol{\nabla}n_i=\frac{\Delta_i}{\Delta t}$$

---

the literature you will find other names like 'lattice Boltzmann equation' or 'Boltzmann cellular automata' instead of lattice Boltzmann model.

which by substituting $n_i \to f$, $\boldsymbol{c}_i \to \boldsymbol{v}$, $\Delta_i/\Delta t \to Q$ gives the Boltzmann equation (5.1.2).

Sterling and Chen (1996) show that this is more than pure formal correspondence. They derive the lattice Boltzmann equation as a special discretization of the Boltzmann equation. The Boltzmann equation with BGK approximation reads

$$\frac{\partial f}{\partial t} + \boldsymbol{v}\boldsymbol{\nabla} f = -\frac{1}{\tau}\left(f - f^{(eq)}\right).$$

The distribution function f depends on space, velocity and time: $f(\boldsymbol{x}, \boldsymbol{v}, t)$. The $\boldsymbol{v}$-space is discretized by introducing a finite set of velocities, $\boldsymbol{v}_i$, and associated distribution functions, $f_i(\boldsymbol{x}, t)$, which are governed by the *discrete Boltzmann equation*:

$$\frac{\partial f_i}{\partial t} + \boldsymbol{v}_i\boldsymbol{\nabla} f_i = -\frac{1}{\tau}\left(f_i - f_i^{(eq)}\right)$$

(please note that this equation is different from the *discretized Boltzmann equation*, see below). The discrete Boltzmann equation will be nondimensionalized by the characteristic length scale, L, the reference speed, U, the reference density, n_r, and the time between particle collisions, t_c,

$$\frac{\partial F_i}{\partial \hat{t}} + \boldsymbol{c}_i\hat{\boldsymbol{\nabla}} F_i = -\frac{1}{\hat{\tau}\epsilon}\left(F_i - F_i^{(eq)}\right) \tag{5.1.3}$$

where $\boldsymbol{c}_i = \boldsymbol{v}_i/U$, $\hat{\boldsymbol{\nabla}} = L\boldsymbol{\nabla}$, $\hat{t} = t \cdot U/L$, $\hat{\tau} = \tau/t_c$, $F_i = f_i/n_r$. The parameter

$$\epsilon = t_c\frac{U}{L}$$

may be interpreted as either the ratio of collision time to flow time or as the ratio of mean free path to the characteristic length (i.e., Knudsen number). A discretization of eq. (5.1.3) is given by:

$$\begin{aligned}
&\frac{F_i\left(\hat{\boldsymbol{x}}, \hat{t} + \Delta\hat{t}\right) - F_i\left(\hat{\boldsymbol{x}}, \hat{t}\right)}{\Delta\hat{t}} + c_{ix}\frac{F_i\left(\hat{\boldsymbol{x}} + \Delta\hat{x}, \hat{t} + \Delta\hat{t}\right) - F_i\left(\hat{\boldsymbol{x}}, \hat{t} + \Delta\hat{t}\right)}{\Delta\hat{x}} \\
&+c_{iy}\frac{F_i\left(\hat{\boldsymbol{x}} + \Delta y, \hat{t} + \Delta\hat{t}\right) - F_i\left(\hat{\boldsymbol{x}}, \hat{t} + \Delta\hat{t}\right)}{\Delta y} \\
&+c_{iz}\frac{F_i\left(\hat{\boldsymbol{x}} + \Delta z, \hat{t} + \Delta\hat{t}\right) - F_i\left(\hat{\boldsymbol{x}}, \hat{t} + \Delta\hat{t}\right)}{\Delta z} \\
= \quad &-\frac{1}{\hat{\tau}\epsilon}\left(F_i - F_i^{(eq)}\right)
\end{aligned}$$

where $\Delta\hat{t} = \Delta t \cdot U/L$. Lagrangian behavior is then obtained by the selection of the lattice spacing divided by the time step to equal the lattice velocity ($\Delta\hat{\boldsymbol{x}}/\Delta\hat{t} = \boldsymbol{c}_i$):

$$\frac{F_i\left(\hat{\boldsymbol{x}},\hat{t}+\hat{\Delta t}\right)-F_i\left(\hat{\boldsymbol{x}},\hat{t}\right)}{\hat{\Delta t}}+\frac{F_i\left(\hat{\boldsymbol{x}}+\boldsymbol{c}_i\hat{\Delta t},\hat{t}+\hat{\Delta t}\right)-F_i\left(\hat{\boldsymbol{x}},\hat{t}+\hat{\Delta t}\right)}{\hat{\Delta t}}$$

$$= \frac{F_i\left(\hat{\boldsymbol{x}}+\boldsymbol{c}_i\hat{\Delta t},\hat{t}+\hat{\Delta t}\right)-F_i\left(\hat{\boldsymbol{x}},\hat{t}\right)}{\hat{\Delta t}}=-\frac{1}{\hat{\tau}\epsilon}\left(F_i-F_i^{(eq)}\right). \qquad (5.1.4)$$

Thus two terms on the left hand side cancel each other and thereby the method becomes explicit. Choosing $\Delta t = t_c$, multiplying eq. (5.1.4) by $\hat{\Delta t}$ and dropping all carets leads to the *(BGK) lattice Boltzmann equation*

$$\boxed{F_i\left(\boldsymbol{x}+\boldsymbol{c}_i\Delta t,t+\Delta t\right)-F_i\left(\boldsymbol{x},t\right)=-\frac{1}{\tau}\left(F_i-F_i^{(eq)}\right)} \qquad (5.1.5)$$

Sterling and Chen (1996, p.200) give the following interpretation of Eq. (5.1.5)[2]:

> "This equation has a particular simple physical interpretation in which the collision term is evaluated locally and there is only one streaming step or 'shift' operation per lattice velocity. This stream-and-collide particle interpretation is a result of the fully Lagrangian character of the equation for which the lattice spacing is the distance travelled by the particle during a time step. Higher order discretizations of the discrete Boltzmann equation typically require several 'shift' operations for the evaluation of each derivative and a particle interpretation is less obvious. ... It did not originally occur to the authors" [i.e. McNamara and Zanetti in 1988] "that the LB method could be considered a particular discretization for the discrete Boltzmann equation (G. McNamara, private communication)."

[2] Readers not familiar with lattice-gas cellular automata should skip this quotation.

Table 5.1.2. From the Boltzmann equation to the lattice Boltzmann equation.

Boltzmann equation:

$$\frac{\partial f}{\partial t} + \boldsymbol{v}\boldsymbol{\nabla} f = Q$$

Boltzmann equation (BGK approximation):

$$\frac{\partial f}{\partial t} + \boldsymbol{v}\boldsymbol{\nabla} f = -\frac{1}{\tau}\left(f - f^{(eq)}\right)$$

discrete Boltzmann equation:

$$\frac{\partial f_i}{\partial t} + \boldsymbol{v}_i\boldsymbol{\nabla} f_i = -\frac{1}{\tau}\left(f_i - f_i^{(eq)}\right)$$

non-dimensional discrete Boltzmann equation:

$$\frac{\partial F_i}{\partial \hat{t}} + \boldsymbol{c}_i\hat{\boldsymbol{\nabla}} F_i = -\frac{1}{\hat{\tau}\epsilon}\left(F_i - F_i^{(eq)}\right)$$

discretized Boltzmann equation:

$$\frac{F_i\left(\hat{\boldsymbol{x}}, \hat{t} + \Delta\hat{t}\right) - F_i\left(\hat{\boldsymbol{x}}, \hat{t}\right)}{\Delta\hat{t}} + c_{ix}\frac{F_i\left(\hat{\boldsymbol{x}} + \Delta\hat{x}, \hat{t} + \Delta\hat{t}\right) - F_i\left(\hat{\boldsymbol{x}}, \hat{t} + \Delta\hat{t}\right)}{\Delta\hat{x}} \ldots$$
$$= -\frac{1}{\hat{\tau}\epsilon}\left(F_i - F_i^{(eq)}\right)$$

lattice Boltzmann equation:

$$F_i\left(\boldsymbol{x} + \boldsymbol{c}_i\Delta t, t + \Delta t\right) - F_i\left(\boldsymbol{x}, t\right) = -\frac{1}{\tau}\left(F_i - F_i^{(eq)}\right)$$

5.1.2 Lattice Boltzmann models of the first generation

The following remarks are mainly of historical interest and should be skipped by readers not familiar with LGCA.
LGCA are plagued by noise which can be suppressed by coarse graining over large domains and/or time intervals. Thus low noise levels are costly in terms of memory and computer time (see Dahlburg et al., 1987, for further discussion). In order to get rid of this noise McNamara and Zanetti (1988) proposed to use directly the mean occupation numbers instead of the Boolean fields. The lattice Boltzmann equation (LBE) had been applied already before by Wolfram (1986) and Frisch et al. (1987) as an analytical tool to calculate the viscosity coefficients of LGCA. McNamara and Zanetti for the first time used the LBE as a numerical scheme.

The mean occupation numbers F_i $(0 \leq F_i \leq 1)$ develop in time according to the following kinetic equation

$$F_i(\boldsymbol{r}+\boldsymbol{c}_i, t+1) = F_i(\boldsymbol{r}, t) + \Omega_i\left(\{F_j(\boldsymbol{r}, t)\}\right), \tag{5.1.6}$$

where the form of the collision operator Ω_i is identical to the arithmetic form of the microscopic collision operator of the corresponding LGCA. For FHP, for example, the Boolean (discrete) variables n_i in (3.2.17) are replaced by mean (continuous) occupation numbers F_i:

$$\begin{aligned}\Omega_i(N) \quad = \quad & F_{i+1}F_{i+3}F_{i+5}(1-F_i)(1-F_{i+2})(1-F_{i+4}) \\ & -F_iF_{i+2}F_{i+4}(1-F_{i+1})(1-F_{i+3})(1-F_{i+5}) \\ & +\xi F_{i+1}F_{i+4}(1-F_i)(1-F_{i+2})(1-F_{i+3})(1-F_{i+5}) \\ & +(1-\xi)F_{i+2}F_{i+5}(1-F_i)(1-F_{i+1})(1-F_{i+3})(1-F_{i+4}) \\ & -F_iF_{i+3}(1-F_{i+1})(1-F_{i+2})(1-F_{i+4})(1-F_{i+5}).\end{aligned} \tag{5.1.7}$$

This type of LBM has been improved by Higuera and Jiménez (1989). They could show that the nonlinear collision operator which evaluation is time consuming can be approximated by a linear operator.

Further reading: Benzi et al. (1992) give an extensive review on LBMs based on the FHP and FCHC models.

5.2 BGK lattice Boltzmann model in 2D

Lattice Boltzmann models (LBMs) of the first generation are plagued by the same problems as the corresponding lattice-gas cellular automata except for the noise. Modern LBMs with Boltzmann distribution functions, several lattice speeds and BGK approximation of the collision operator are free of all problems mentioned in Table 5.1.1. In this chapter a detailed discussion of such a model in 2D will be given. The derivations of the equilibrium distributions and the Navier-Stokes equation will be presented in full length. We will refer to this model as the D2Q9-LBM.

A LBM has three main ingredients:

1. the lattice: D2Q9 (multi-speed model),
2. the equilibrium distributions: Maxwell (see below),
3. the kinetic equation: BGK approximation.

On the contrary, a LGCA is basically defined by the lattice and the collision rules.
Koelman (1991) defines his LBM for the Navier-Stokes equation over the lattice with the following lattice velocities $\boldsymbol{c}_i$

$$\begin{aligned} \boldsymbol{c}_0^K &= (0,0) \\ \boldsymbol{c}_{1,2,3,4}^K &= (\pm a, \pm b) \\ \boldsymbol{c}_{5,6}^K &= (\pm 2a, 0) \\ \boldsymbol{c}_{7,8}^K &= (0, \pm 2b) \end{aligned}$$

where the lattice constants a and b are restricted by $a^2/3 \leq b^2 \leq 3a^2$. The special choice $a = b = \dfrac{1}{\sqrt{2}}c$ and rotation of the lattice velocities by 45° leads to the D2Q9 lattice (compare Section 3.3 and Fig. 5.2.1) with

$$\begin{aligned} \boldsymbol{c}_0 &= (0,0) \\ \boldsymbol{c}_{1,3}, \boldsymbol{c}_{2,4} &= (\pm c, 0), (0, \pm c) \\ \boldsymbol{c}_{5,6,7,8} &= (\pm c, \pm c). \end{aligned} \tag{5.2.1}$$

Fig. 5.2.1. *The D2Q9 lattice.*

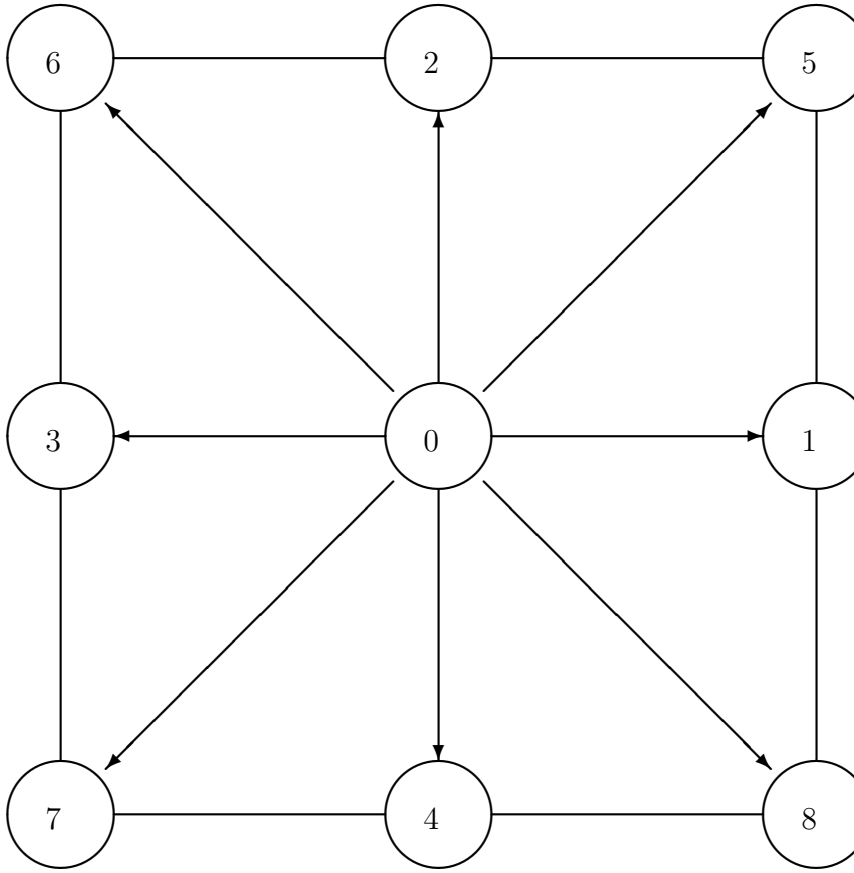

In what follows the D2Q9 lattice will be used exclusively.
The mass density, ρ, and the momentum density, $\boldsymbol{j}$, are defined by sums over the distribution functions $F_i(\boldsymbol{x}, t)$

$$\rho(\boldsymbol{x}, t) = \sum_i F_i(\boldsymbol{x}, t) \tag{5.2.2}$$

$$\boldsymbol{j}(\boldsymbol{x}, t) = \rho(\boldsymbol{x}, t)\boldsymbol{v}(\boldsymbol{x}, t) = \sum_i \boldsymbol{c}_i F_i(\boldsymbol{x}, t) \tag{5.2.3}$$

For vanishing velocities a global equilibrium distribution W_i ("fluid at rest") is defined. In the vicinity (small Mach numbers) of this resting equilibrium, distribution functions can be written as sums of the W_i and small perturbations $f_i(\boldsymbol{x}, t)$

$$F_i(\boldsymbol{x}, t) = W_i + f_i(\boldsymbol{x}, t) \tag{5.2.4}$$

with $|f_i(\boldsymbol{x}, t)| << W_i$.
The W_i should be positive to assure positive mass density. They are chosen of Maxwell type in the following sense. The lattice velocity moments up to fourth order over the W_i shall be identical to the respective velocity moments over the Maxwell distribution

$$w_B(v) = \rho_0 \left(\frac{m}{2\pi k_B T}\right)^{D/2} \exp\left[-mv^2/2k_B T\right] \tag{5.2.5}$$

(D dimension, ρ_0 mass density, m particle mass, v particle speed, k_B Boltzmann constant, T temperature). Thus the odd moments vanish

$$\sum_i W_i c_{i\alpha} = 0$$

$$\sum_i W_i c_{i\alpha} c_{i\beta} c_{i\gamma} = 0$$

and the even moments read

$$\sum_i W_i = \int d\boldsymbol{v}\, w_B(v) = \rho_0 \tag{5.2.6}$$

$$\sum_i W_i c_{i\alpha} c_{i\beta} = \int d\boldsymbol{v}\, w_B(v) v_\alpha v_\beta = \rho_0 \frac{k_B T}{m} \delta_{\alpha\beta} \tag{5.2.7}$$

$$\begin{aligned} \sum_i W_i c_{i\alpha} c_{i\beta} c_{i\gamma} c_{i\delta} &= \int d\boldsymbol{v}\, w_B(v) v_\alpha v_\beta v_\gamma v_\delta \\ &= \rho_0 \left(\frac{k_B T}{m}\right)^2 (\delta_{\alpha\beta}\delta_{\gamma\delta} + \delta_{\alpha\gamma}\delta_{\beta\delta} + \delta_{\alpha\delta}\delta_{\beta\gamma}) \end{aligned} \tag{5.2.8}$$

Note that the constraint (5.2.8) is more rigorous than pure isotropy (compare Section 3.3).

Exercise 5.2.1. (**)
Calculate the velocity moments up to fourth order over the Maxwell distribution in $D \geq 2$ dimensions.

Nonnegative solutions of Eqs. (5.2.6 - 5.2.8) for the W_i can be found whenever the number of lattice velocities $\boldsymbol{c}_i$ is large enough. For the D2Q9 lattice (5.2.1) one obtains (see Section 5.2.1 for derivation):

$$\begin{aligned} W_0/\rho_0 &= \frac{4}{9} \\ W_1/\rho_0 &= \frac{1}{9} \\ W_2/\rho_0 &= \frac{1}{36} \\ \frac{k_B T}{m} &= \frac{c^2}{3}. \end{aligned}$$

The evolution of the LBM consists of the recurring alternation between transition to the local equilibrium and propagation of the distributions to neighboring sites according to the lattice velocities. The BGK (compare Section 4.1.3) kinetic equation reads

$$\boxed{\begin{aligned} &F_i(\boldsymbol{x}+\boldsymbol{c}_i\Delta t, t+\Delta t) - F_i(\boldsymbol{x},t) = -\frac{\Delta t}{\tau}\left[F_i(\boldsymbol{x},t) - F_i^{(0)}(\boldsymbol{x},t)\right] \\ &+\frac{\Delta t c_{i\alpha}}{12c^2}\left[K_\alpha(\boldsymbol{x},t) + K_\alpha(\boldsymbol{x}+\boldsymbol{c}_i\Delta t, t+\Delta t)\right] \end{aligned}} \tag{5.2.9}$$

or

$$\boxed{\begin{aligned} &F_i(\boldsymbol{x}+\boldsymbol{c}_i\Delta t, t+\Delta t) = (1-\omega)F_i(\boldsymbol{x},t) + \omega F_i^{(0)}(\boldsymbol{x},t) \\ &+\frac{\Delta t c_{i\alpha}}{12c^2}\left[K_\alpha(\boldsymbol{x},t) + K_\alpha(\boldsymbol{x}+\boldsymbol{c}_i\Delta t, t+\Delta t)\right] \end{aligned}} \tag{5.2.10}$$

where τ is the collision time, $\omega = \Delta t/\tau$ is the collision frequency, and $\boldsymbol{K}$ is an applied body force. The local equilibrium distributions $F_i^{(0)}$ depend only on the local values of mass and momentum density

$$F_i^{(0)}(\boldsymbol{x},t) = F_i^{(0)}\left(\rho(\boldsymbol{x},t), \boldsymbol{j}(\boldsymbol{x},t)\right).$$

They can be derived by applying the maximum entropy principle under the constraints of mass and momentum conservation (see Section 5.2.2). Up to second order in $\boldsymbol{j}$ one obtains

$$\boxed{F_i^{(0)}(\rho,\boldsymbol{j}) = \frac{W_i}{\rho_0}\left\{\rho + \frac{m}{k_BT}\boldsymbol{c}_i\cdot\boldsymbol{j} + \frac{m}{2\rho k_BT}\left[\frac{m}{k_BT}\left(\boldsymbol{c}_i\cdot\boldsymbol{j}\right)^2 - \boldsymbol{j}^2\right]\right\}} \quad (5.2.11)$$

or more explicitly

$$\begin{aligned}
F_i &= \frac{4}{9}\rho\left[1-\frac{3}{2}\frac{\boldsymbol{u}^2}{c^2}\right] && i=0\\
F_i &= \frac{1}{9}\rho\left[1+3\frac{\boldsymbol{c}_i\cdot\boldsymbol{u}}{c^2}+\frac{9}{2}\frac{(\boldsymbol{c}_i\cdot\boldsymbol{u})^2}{c^4}-\frac{3}{2}\frac{\boldsymbol{u}^2}{c^2}\right] && i=1,2,3,4\\
F_i &= \frac{1}{36}\rho\left[1+3\frac{\boldsymbol{c}_i\cdot\boldsymbol{u}}{c^2}+\frac{9}{2}\frac{(\boldsymbol{c}_i\cdot\boldsymbol{u})^2}{c^4}-\frac{3}{2}\frac{\boldsymbol{u}^2}{c^2}\right] && i=5,6,7,8.
\end{aligned}$$

Application of the multi-scale technique (Chapman-Enskog expansion) yields the Navier-Stokes equation with pressure $p=\rho k_BT/m$, kinematic shear viscosity

$$\nu = \frac{k_BT}{m}\left(\frac{1}{\omega}-\frac{1}{2}\right)\Delta t = \frac{c^2}{3}\left(\frac{1}{\omega}-\frac{1}{2}\right)\Delta t = \frac{2-\omega}{6\omega}c^2\Delta t = \frac{c^2}{3}\left(\tau-\frac{\Delta t}{2}\right) \quad (5.2.12)$$

and an advection term with Galilean invariance[3]. The Galilean invariance breaking *g-factor* (compare Section 3.2) never arises (see Section 5.2.3).
The above given presentation of the LBM contains all informations necessary to set up the computer code. The algorithm proceeds as follows:

1. For given initial values of mass $\rho(\boldsymbol{x},t)$ and momentum density $\boldsymbol{j}(\boldsymbol{x},t)$ calculate the equilibrium distributions $F_i^{(0)}(\rho(\boldsymbol{x},t),\boldsymbol{j}(\boldsymbol{x},t))$ according to Eq. (5.2.11) and set $F_i = F_i^{(0)}$. Remark: Global equilibrium distributions (5.2.11) but with different values of ρ and $\boldsymbol{j}$ are used for local initialization, i.e. in the beginning there is a patchwork of local equilibria which is far from a global equilibrium.
2. Apply the kinetic equation (5.2.10), i.e. add the (non-equilibrium) distribution function $F_i(\boldsymbol{x},t)$ and the equilibrium distribution function $F_i^{(0)}(\boldsymbol{x},t)$ with the appropriate weights $(1-\omega)$ and ω, and then propagate it to the next neighbor (except for the distribution of 'rest particles' with $\boldsymbol{c}_0=\boldsymbol{0}$).
3. Calculate from the propagated distributions new values of $\rho(\boldsymbol{x},t)$ and $\boldsymbol{j}(\boldsymbol{x},t)$ according to the definitions (5.2.2) und (5.2.3).
4. The next time step starts with the calculation of new equilibrium distributions. Thereafter proceed with the second step of the algorithm.

[3] But: There is always a disturbing fly or two in the ointment. Qian and Orszag (1993) and Qian and Zhou (1998) have shown that a higher order term (slightly compressible regime) leads to frame-velocity-dependent viscosity.

In BGK-LBMs collisions are not explicitly defined. They are kind of fictive and make themselves felt only by the transition to local equilibrium (the term $\omega F_i^{(0)}(\boldsymbol{x}, t)$ in the kinetic equation). On the other hand for LGCA the collisions are explicitly defined and the distribution functions are theoretical constructs which can not be observed on the lattice because of their continuous nature.

5.2.1 Derivation of the W_i

The D2Q9 model includes three different speeds (compare Table 5.2.1). The W_i for directions with identical speeds are equal for reason of symmetry.

Table 5.2.1. Lattice speeds, cells and W_i of the D2Q9 lattice.

$\boldsymbol{c}_i^2$	cells	number of cells	W_i
0	0	1	W_0
1	1, 2, 3, 4	4	W_1
2	5, 6, 7, 8	4	W_2

The non-vanishing elements of the even moments up to fourth order read:

– 0. moment:

$$\sum_i W_i = W_0 + 4W_1 + 4W_2 = \rho_0 \tag{5.2.13}$$

Remark: The only equation which includes W_0. It will be used to calculate W_0.

– 2. moment:

$$\sum_i c_{i1}^2 W_i = 2c^2 W_1 + 4c^2 W_2 = \rho_0 \frac{k_B T}{m} \tag{5.2.14}$$

Remark: $(k_B T)/m$ will be calculated from Eqs. (5.2.14) and (5.2.15).

$$\sum_i c_{i2}^2 W_i = 2c^2 W_1 + 4c^2 W_2 = \rho_0 \frac{k_B T}{m}$$

Remark: This constraint is identical with (5.2.14).

– 4. Moment:

$$\sum_i c_{i1}^4 W_i = 2c^4 W_1 + 4c^4 W_2 = 3\rho_0 \left(\frac{k_B T}{m}\right)^2 \tag{5.2.15}$$

Remark: W_1 will be calculated from Eq. (5.2.15).

$$\sum_i c_{i2}^4 W_i = 2c^4 W_1 + 4c^4 W_2 = 3\rho_0 \left(\frac{k_B T}{m}\right)^2$$

Remark: This constraint is identical with (5.2.15).

$$\sum_i c_{i1}^2 c_{i2}^2 W_i = 4c^4 W_2 = \rho_0 \left(\frac{k_B T}{m}\right)^2 \tag{5.2.16}$$

Remark: W_2 will be calculated from Eq. (5.2.16).

The solution reads:

$$\begin{aligned} W_0/\rho_0 &= \frac{4}{9} \\ W_1/\rho_0 &= \frac{1}{9} \\ W_2/\rho_0 &= \frac{1}{36} \\ \frac{k_B T}{m} &= \frac{c^2}{3}. \end{aligned}$$

One readily confirms that the first and third moments of the lattice velocities over W_i vanish.

5.2.2 Entropy and equilibrium distributions

Koelman defines the *relative entropy*[4] density by

$$\boxed{S(\rho, \boldsymbol{j}) := -\frac{k}{m} \sum_i F_i^{(0)}(\rho, \boldsymbol{j}) \ln \frac{F_i^{(0)}(\rho, \boldsymbol{j})}{W_i}.} \tag{5.2.17}$$

The weighting by $1/W_i$ in the logarithmic factor will lead to equilibrium distributions of the form $F_i^{(0)} = W_i e^{h(\rho, \boldsymbol{j}, \boldsymbol{c}_i)}$ and implies $S = 0$ for $F_i^{(0)} = W_i$. The equilibrium distributions $F_i^{(0)}$ will be calculated by maximizing the entropy for given constraints which for the case under consideration are the mass and momentum density

[4] Kullback (1959) and Cover and Thomas (1991) are standard references on relative entropy.

$$\begin{aligned}\rho(\rho,\boldsymbol{j}) &= \sum_i F_i^{(0)}(\rho,\boldsymbol{j})\\ \boldsymbol{j}(\rho,\boldsymbol{j}) &= \sum_i \boldsymbol{c}_i F_i^{(0)}(\rho,\boldsymbol{j}).\end{aligned}$$

The functional

$$\begin{aligned}\hat{S} &:= S + \tilde{A}\rho + \tilde{\boldsymbol{B}}\cdot\boldsymbol{j}\\ &= -\frac{k}{m}\sum_i F_i^{(0)}(\rho,\boldsymbol{j})\ln\frac{F_i^{(0)}(\rho,\boldsymbol{j})}{W_i} + \tilde{A}\sum_i F_i^{(0)}(\rho,\boldsymbol{j}) + \tilde{\boldsymbol{B}}\sum_i \boldsymbol{c}_i F_i^{(0)}(\rho,\boldsymbol{j})\end{aligned}$$

encompasses the constraints coupled by Lagrange multipliers $\tilde{A}$ und $\tilde{\boldsymbol{B}}$. The necessary conditions for an extremum of $\hat{S}$ read

$$\forall i: \quad \frac{\partial\hat{S}}{\partial F_i^{(0)}} = -\frac{k}{m}\left[\ln\frac{F_i^{(0)}}{W_i} + 1\right] + \tilde{A} + \tilde{\boldsymbol{B}}\cdot\boldsymbol{c}_i = 0. \tag{5.2.18}$$

The solutions of (5.2.18) are of the form

$$F_i^{(0)} = W_i e^{A(\rho,\,\boldsymbol{j}) + \boldsymbol{B}(\rho,\,\boldsymbol{j})\cdot\boldsymbol{c}_i}$$

with

$$A = \frac{m}{k}\tilde{A} - 1, \quad \text{and} \quad \boldsymbol{B} = \frac{m}{k}\tilde{\boldsymbol{B}}.$$

A and $\boldsymbol{B}$ can be determined by Taylor series expansions of $F_i^{(0)}$ around $\boldsymbol{j}=0$ (same procedure as for the FHP lattice-gas cellular automata). Because of the symmetry of the D2Q9 lattice the ansatz

$$\begin{aligned}A(\rho,\boldsymbol{j}) &= A_0(\rho) + A_2(\rho)\boldsymbol{j}^2 + \mathcal{O}(\boldsymbol{j}^4)\\ \boldsymbol{B}(\rho,\boldsymbol{j}) &= B_1(\rho)\boldsymbol{j} + \mathcal{O}(\boldsymbol{j}^3).\end{aligned}$$

is sufficient. The expansion of $F_i^{(0)}$ around $\boldsymbol{j}=0$ reads

$$\begin{aligned}\frac{\partial F_i^{(0)}}{\partial j_\alpha} &= (2A_2 j_\alpha + B_1 c_{i\alpha})F_i^{(0)}\\ &\to B_1 c_{i\alpha} W_i e^{A_0} \quad \text{at } \boldsymbol{j}=0\\ \frac{\partial^2 F_i^{(0)}}{\partial j_\alpha^2} &= \left[(2A_2 j_\alpha + B_1 c_{i\alpha})^2 + 2A_2\right]F_i^{(0)}\\ &\to (B_1^2 c_{i\alpha}^2 + 2A_2)W_i e^{A_0} \quad \text{at } \boldsymbol{j}=0\\ \frac{\partial^2 F_i^{(0)}}{\partial j_\alpha \partial j_\beta} &= (2A_2 j_\alpha + B_1 c_{i\alpha})(2A_2 j_\beta + B_1 c_{i\beta})F_i^{(0)}\\ &\to B_1^2 c_{i\alpha}c_{i\beta}W_i e^{A_0} \quad \text{at } \boldsymbol{j}=0\end{aligned}$$

and finally up to terms of second order in $\boldsymbol{j}$

$$F_i^{(0)} = W_i e^{A_0} \left\{ 1 + B_1 \boldsymbol{c}_i \cdot \boldsymbol{j} + \frac{B_1^2}{2} (\boldsymbol{c}_i \cdot \boldsymbol{j})^2 + A_2 \boldsymbol{j}^2 \right\}. \tag{5.2.19}$$

Now the definitions of ρ and $\boldsymbol{j}$ will be exploited to calculate the unknown coefficients $A_0(\rho)$, $A_2(\rho)$ and $B_1(\rho)$:

$$\sum_i F_i^{(0)} = \rho = e^{A_0} \left\{ \rho_0 + \frac{B_1^2}{2} \rho_0 \frac{k_B T}{m} \boldsymbol{j}^2 + \rho_0 A_2 \boldsymbol{j}^2 \right\} \tag{5.2.20}$$

$$\sum_i \boldsymbol{c}_i F_i^{(0)} = \boldsymbol{j} = e^{A_0} B_1 \rho_0 \frac{k_B T}{m} \boldsymbol{j}. \tag{5.2.21}$$

The vector equation (5.2.21) reduces to a scalar constraint

$$B_1 = \frac{1}{e^{A_0}} \frac{m}{\rho_0 k_B T},$$

i.e. an auxiliary condition is required to solve for all three unknowns (A_0, A_2, B_1). Solving Eq. (5.2.20) for A_2 yields

$$A_2 = -\frac{B_1^2}{2} \frac{k_B T}{m} + \frac{1}{\boldsymbol{j}^2} \underbrace{\left(\frac{\rho}{\rho_0 e^{A_0}} - 1 \right)}_{(*)}.$$

To obtain A_2 independent of $\boldsymbol{j}$ (as implied by the ansatz) the expression $(*)$ must vanish. This is the third constraint looked for. It immediately follows that

$$e^{A_0} = \frac{\rho}{\rho_0}, \quad B_1 = \frac{m}{\rho k_B T}, \quad \text{and} \quad A_2 = -\frac{1}{2\rho^2} \frac{m}{k_B T}.$$

Insertion into (5.2.19) finally yields the equilibrium distributions

$$F_i^{(0)}(\rho, \boldsymbol{j}) = \frac{W_i}{\rho_0} \left\{ \rho + \frac{m}{k_B T} \boldsymbol{c}_i \cdot \boldsymbol{j} + \frac{m}{2\rho k_B T} \left[\frac{m}{k_B T} (\boldsymbol{c}_i \cdot \boldsymbol{j})^2 - \boldsymbol{j}^2 \right] \right\}. \tag{5.2.22}$$

Koelman (1991) used $1/\rho_0$ instead of $1/\rho$ in the coefficient of the third term which is a good approximation for small Mach numbers.

Further reading: Karlin et al. (1998) construct local equilibrium functions, $F_i^{(0)}$, that maximize the entropy $S_K = \sum_i F_i^{(0)} \sqrt{F_i^{(0)}}$.

5.2.3 Derivation of the Navier-Stokes equations by multi-scale analysis

The derivation of the macroscopic equations (Navier-Stokes) proceeds in close analogy to the multi-scale analysis discussed in Section 4.2 and for the FHP model in Section 3.2. For the BGK-LBM the calculation of terms of second order in the expansion parameter ϵ is much simpler than for LGCA. Here the complete derivation of the Navier-Stokes equation will be given.
The distributions $F_i(\boldsymbol{x},t)$ are expanded around the equilibrium distributions $F_i^{(0)}(\boldsymbol{x},t)$

$$F_i(\boldsymbol{x},t) = F_i^{(0)}(\boldsymbol{x},t) + \epsilon F_i^{(1)}(\boldsymbol{x},t) + \epsilon^2 F_i^{(2)} + \mathcal{O}(\epsilon^3) \tag{5.2.23}$$

with

$$\begin{aligned} \sum_i F_i^{(1)}(\boldsymbol{x},t) &= 0, \quad \sum_i \boldsymbol{c}_i F_i^{(1)}(\boldsymbol{x},t) = 0, \\ \sum_i F_i^{(2)}(\boldsymbol{x},t) &= 0, \quad \sum_i \boldsymbol{c}_i F_i^{(2)}(\boldsymbol{x},t) = 0, \end{aligned} \tag{5.2.24}$$

i.e. the perturbations $F_i^{(1)}(\boldsymbol{x},t)$ and $F_i^{(2)}(\boldsymbol{x},t)$ do not contribute to the mass and momentum density. The small expansion parameter ϵ can be viewed as the Knudsen number K_n which is the ratio between the mean free path and the characteristic length scale of the flow.

The left hand side of the kinetic equation (5.2.10) and the forcing term are expanded into a Taylor series up to terms of second order ($\Delta\boldsymbol{x}_i = \Delta t \cdot \boldsymbol{c}_i$):

$$\begin{aligned} F_i(\boldsymbol{x} + \boldsymbol{c}_i\Delta t, t + \Delta t) &= F_i(\boldsymbol{x},t) + \Delta t\partial_t F_i + \Delta t c_{i\alpha}\partial_{x_\alpha} F_i \\ &+ \frac{(\Delta t)^2}{2}\left[\partial_t\partial_t F_i + 2c_{i\alpha}\partial_t\partial_{x_\alpha} F_i + c_{i\alpha}c_{i\beta}\partial_{x_\alpha}\partial_{x_\beta} F_i\right] + \mathcal{O}\left(\partial^3 F_i\right) \end{aligned} \tag{5.2.25}$$

and

$$\begin{aligned} \frac{\Delta t}{c^2}\ \frac{c_{i\alpha}}{12}\ & [K_\alpha(\boldsymbol{x},t) + K_\alpha(\boldsymbol{x} + \boldsymbol{c}_i\Delta t, t + \Delta t)] \\ = \ & \frac{\Delta t}{c^2}\frac{c_{i\gamma}}{6}K_\gamma(\boldsymbol{x},t) + \frac{(\Delta t)^2}{c^2}\frac{c_{i\gamma}}{12}\left[\partial_t K_\gamma + c_{i\beta}\partial_{x_\beta}K_\gamma\right] + \mathcal{O}\left[(\Delta t)^3\right]. \end{aligned} \tag{5.2.26}$$

As for the FHP model two time scales and one spatial scale with the following scaling will be introduced

$$\begin{aligned} \partial_t &\rightarrow \epsilon\partial_t^{(1)} + \epsilon^2\partial_t^{(2)} \\ \partial_{x_\alpha} &\rightarrow \epsilon\partial_{x_\alpha}^{(1)}. \end{aligned} \tag{5.2.27}$$

Conservation of mass and momentum. The expansions given above are substituted into the kinetic equation (Eq. 5.2.10)

$$\begin{aligned} 0 \;=\; & F_i(\boldsymbol{x}+\boldsymbol{c}_i\Delta t, t+\Delta t) - F_i(\boldsymbol{x},t) + \omega\left[F_i(\boldsymbol{x},t) - F_i^{(0)}(\boldsymbol{x},t)\right] \\ & -\frac{\Delta t}{c^2}\frac{c_{i\alpha}}{12}\left[K_\alpha(\boldsymbol{x},t) + K_\alpha(\boldsymbol{x}+\boldsymbol{c}_i\Delta t, t+\Delta t)\right] \end{aligned}$$

which leads to

$$\begin{aligned} 0 \underbrace{=}_{(5.2.25)} \; & F_i(\boldsymbol{x},t) + \Delta t\partial_t F_i + \Delta t c_{i\gamma}\partial_{x_\gamma}F_i \\ & + \frac{(\Delta t)^2}{2}\left[\partial_t\partial_t F_i + 2c_{i\gamma}\partial_t\partial_{x_\gamma}F_i + c_{i\beta}c_{i\gamma}\partial_{x_\beta}\partial_{x_\gamma}F_i\right] \\ & + \mathcal{O}\left[\partial^3 F_i\right] - F_i(\boldsymbol{x},t) + \omega\left[F_i(\boldsymbol{x},t) - F_i^{(0)}(\boldsymbol{x},t)\right] \\ & - \frac{\Delta t}{c^2}\frac{c_{i\gamma}}{6}K_\gamma(\boldsymbol{x},t) - \frac{(\Delta t)^2}{c^2}\frac{c_{i\gamma}}{12}\left[\partial_t K_\gamma + c_{i\beta}\partial_{x_\beta}K_\gamma\right] \\ & + \mathcal{O}\left[(\Delta t)^3\right] \\ \underbrace{=}_{(5.2.23),(5.2.27)} \; & \epsilon\Delta t\left[\partial_t^{(1)}F_i^{(0)} + c_{i\gamma}\partial_{x_\gamma}^{(1)}F_i^{(0)}\right] \\ & + \epsilon^2\Delta t\left[\partial_t^{(1)}F_i^{(1)} + \partial_t^{(2)}F_i^{(0)} + c_{i\gamma}\partial_{x_\gamma}^{(1)}F_i^{(1)}\right] \\ & + \epsilon^2\frac{(\Delta t)^2}{2}\left[\partial_t^{(1)}\partial_t^{(1)}F_i^{(0)} + 2c_{i\gamma}\partial_t^{(1)}\partial_{x_\gamma}^{(1)}F_i^{(0)}\right. \\ & \left. + c_{i\beta}c_{i\gamma}\partial_{x_\beta}^{(1)}\partial_{x_\gamma}^{(1)}F_i^{(0)}\right] + \epsilon\omega F_i^{(1)} \\ & + \epsilon^2\omega F_i^{(2)} - \epsilon\frac{\Delta t}{c^2}\frac{c_{i\gamma}}{6}K_\gamma \\ & - \epsilon^2\frac{(\Delta t)^2}{c^2}\frac{c_{i\gamma}}{12}\left[\partial_t^{(1)}K_\gamma + c_{i\beta}\partial_{x_\beta}^{(1)}K_\gamma\right] + \mathcal{O}\left[\epsilon^3\right] \end{aligned}$$

Please note that the leading order of the body forcing was set proportional to ϵ. Sorting according to orders in ϵ yields

$$0 = \epsilon E_i^{(0)} + \epsilon^2 E_i^{(1)} + \mathcal{O}\left[\epsilon^3\right] \tag{5.2.28}$$

with

$$E_i^{(0)} = \partial_t^{(1)} F_i^{(0)} + c_{i\gamma}\partial_{x_\gamma}^{(1)} F_i^{(0)} + \frac{\omega}{\Delta t} F_i^{(1)} - \frac{c_{i\gamma}}{6c^2} K_\gamma \tag{5.2.29}$$

$$\begin{aligned} E_i^{(1)} = {} & \partial_t^{(1)} F_i^{(1)} + \partial_t^{(2)} F_i^{(0)} + c_{i\gamma}\partial_{x_\gamma}^{(1)} F_i^{(1)} + \frac{\Delta t}{2}\partial_t^{(1)}\partial_t^{(1)} F_i^{(0)} \\ & + \Delta t c_{i\gamma}\partial_t^{(1)}\partial_{x_\gamma}^{(1)} F_i^{(0)} + \frac{\Delta t}{2} c_{i\beta}c_{i\gamma}\partial_{x_\beta}^{(1)}\partial_{x_\gamma}^{(1)} F_i^{(0)} \\ & + \frac{\omega}{\Delta t} F_i^{(2)} - \Delta t \frac{c_{i\gamma}}{12c^2}\partial_t^{(1)} K_\gamma - \Delta t \frac{c_{i\gamma}}{12c^2} c_{i\beta}\partial_{x_\beta}^{(1)} K_\gamma. \end{aligned} \tag{5.2.30}$$

We will now calculate the zeroth and first lattice velocity moments of $E_i^{(0)}$ and $E_i^{(1)}$ (conservation of mass and momentum density).

Terms of first order in ϵ. The zeroth and first lattice velocity moments of $E_i^{(0)}$ can be readily calculated:

$$\begin{aligned} \sum_i E_i^{(0)} &= \sum_i \left\{ \partial_t^{(1)} F_i^{(0)} + c_{i\gamma}\partial_{x_\gamma}^{(1)} F_i^{(0)} + \frac{\omega}{\Delta t} F_i^{(1)} - \frac{c_{i\gamma}}{6c^2} K_\gamma \right\} \\ &= \partial_t^{(1)}\rho + \partial_{x_\gamma}^{(1)} j_\gamma \end{aligned}$$

$$\begin{aligned} \sum_i c_{i\alpha} E_i^{(0)} &= \sum_i c_{i\alpha} \left\{ \partial_t^{(1)} F_i^{(0)} + c_{i\beta}\partial_{x_\beta}^{(1)} F_i^{(0)} + \frac{\omega}{\Delta t} F_i^{(1)} - \frac{c_{i\beta}}{6c^2} K_\beta \right\} \\ &= \partial_t^{(1)} j_\alpha + \partial_{x_\beta}^{(1)} P_{\alpha\beta}^{(0)} - K_\alpha \end{aligned} \tag{5.2.31}$$

where we have used

$$\sum_i c_{i\alpha} c_{i\beta} = 6c^2 \delta_{\alpha\beta}. \tag{5.2.32}$$

The momentum flux tensor in first order of ϵ reads

$$P_{\alpha\beta}^{(0)} := \sum_i c_{i\alpha} c_{i\beta} F_i^{(0)} = \frac{1}{\rho} \begin{pmatrix} j_1^2 & j_1 j_2 \\ j_1 j_2 & j_2^2 \end{pmatrix} + p\delta_{\alpha\beta} \tag{5.2.33}$$

where $p = \dfrac{k_B T}{m}\rho$ is the pressure (a detailed calculation of $P^{(0)}_{\alpha\beta}$ will be given below).

Thus to first order in ϵ we obtain the *continuity equation*

$$\boxed{\partial_t \rho + \boldsymbol{\nabla} \cdot \boldsymbol{j} = 0} \tag{5.2.34}$$

and (in the incompressible limit: $\rho =$ constant) the *Euler equation* (Navier-Stokes equation without friction):

$$\boxed{\frac{\partial \boldsymbol{u}}{\partial t} + \boldsymbol{u}\boldsymbol{\nabla}\boldsymbol{u} = -\frac{1}{\rho}\boldsymbol{\nabla} p + \boldsymbol{K}.} \tag{5.2.35}$$

Calculation of the momentum flux tensor. In the calculation of $P^{(0)}_{\alpha\beta}$ the detailed form of the equilibrium distribution has to be taken into account for the first time. Four different summands $P^{(0.1)}_{\alpha\beta}$ to $P^{(0.4)}_{\alpha\beta}$ have to be evaluated. The first term reads:

$$P^{(0.1)}_{\alpha\beta} := \frac{\rho}{\rho_0}\sum_i c_{i\alpha}c_{i\beta}W_i = \underbrace{\rho\frac{k_B T}{m}}_{=p}\delta_{\alpha\beta} = p\delta_{\alpha\beta}.$$

For the pressure $p = \dfrac{k_B T}{m}\rho = \dfrac{c^2}{3}\rho$ the speed of sound c_s is given by

$$c_s = \sqrt{\frac{dp}{d\rho}} = \frac{c}{\sqrt{3}}.$$

The second summand

$$P^{(0.2)}_{\alpha\beta} := \frac{m}{\rho_0 k_B T}\sum_i c_{i\alpha}c_{i\beta}(\boldsymbol{c}_i \cdot \boldsymbol{j})W_i = 0$$

vanishes because it is an odd moment in $\boldsymbol{c}_i$ over W_i. The third summand reads:

$$P^{(0.3)}_{\alpha\beta} := \frac{1}{2\rho_0\rho}\left(\frac{m}{k_B T}\right)^2 \sum_i c_{i\alpha}c_{i\beta}\left(\boldsymbol{c}_i \cdot \boldsymbol{j}\right)^2 W_i.$$

Prefactor:

$$\frac{1}{2\rho_0\rho}\left(\frac{m}{k_B T}\right)^2 \cdot \rho_0 \left(\frac{k_B T}{m}\right)^2 = \frac{1}{2\rho}$$

Tensor of fourth rank:

$$T_{\alpha\beta\gamma\delta} = \delta_{\alpha\beta}\delta_{\gamma\delta} + \delta_{\alpha\gamma}\delta_{\beta\delta} + \delta_{\alpha\delta}\delta_{\beta\gamma} \tag{5.2.36}$$

- $\alpha = \beta = 1$:
  - $\gamma = \delta = 1 \rightarrow T_{1111} = 3 \rightarrow \dfrac{1}{2\rho} 3 j_1^2$
  - $\gamma = \delta = 2 \rightarrow T_{1122} = 1 \rightarrow \dfrac{1}{2\rho} j_2^2$
  - $\gamma \neq \delta \rightarrow T_{1112} = T_{1121} = 0$
- $\alpha = \beta = 2$: $\rightarrow \dfrac{1}{2\rho} \left(j_1^2 + 3 j_2^2 \right)$
- $\alpha = 1$ $\beta = 2$:
  - $\gamma = \delta \rightarrow T_{1211} = T_{1222} = 0$
  - $\gamma \neq \delta \rightarrow T_{1212} = T_{1221} = 1 \rightarrow \dfrac{1}{2\rho} \cdot 2 j_1 j_2$

$$P_{\alpha\beta}^{(0.3)} = \frac{1}{2\rho} \boldsymbol{j}^2 \delta_{\alpha\beta} + \frac{1}{\rho} \begin{pmatrix} j_1^2 & j_1 j_2 \\ j_1 j_2 & j_2^2 \end{pmatrix}$$

The fourth summand reads:

$$\begin{aligned} P_{\alpha\beta}^{(0.4)} &:= -\frac{1}{2\rho_0 \rho} \frac{m}{k_B T} \boldsymbol{j}^2 \sum_i c_{i\alpha} c_{i\beta} W_i \\ &= -\frac{1}{2\rho} \boldsymbol{j}^2 \delta_{\alpha\beta} \end{aligned}$$

Summing up all terms yields

$$P_{\alpha\beta}^{(0)} = \frac{1}{\rho} \begin{pmatrix} j_1^2 & j_1 j_2 \\ j_1 j_2 & j_2^2 \end{pmatrix} + p \delta_{\alpha\beta} \tag{5.2.37}$$

The pressure of the D2Q9-LBM does not depend explicitly on the flow speed (see to the contrary the FHP model) because the summand $P_{\alpha\beta}^{(0.4)}$ is exactly compensated by a part of $P_{\alpha\beta}^{(0.3)}$.

Terms of second order in ϵ: mass. As for lattice-gas cellular automata one has to take into account terms of second order in ϵ to derive the dissipative terms of the macroscopic equations. Mass conservation leads to

$$
\begin{aligned}
0 &= \sum_i E_i^{(1)} \\
&= \sum_i \partial_t^{(1)} F_i^{(1)} + \partial_t^{(2)} F_i^{(0)} + c_{i\gamma}\partial_{x_\gamma}^{(1)} F_i^{(1)} + \frac{\Delta t}{2}\partial_t^{(1)}\partial_t^{(1)} F_i^{(0)} \\
&\quad + \Delta t c_{i\gamma}\partial_t^{(1)}\partial_{x_\gamma}^{(1)} F_i^{(0)} + \frac{\Delta t}{2} c_{i\beta}c_{i\gamma}\partial_{x_\beta}^{(1)}\partial_{x_\gamma}^{(1)} F_i^{(0)} \qquad (5.2.38) \\
&\quad + \frac{\omega}{\Delta t} F_i^{(2)} - \Delta t \frac{c_{i\gamma}}{12c^2}\partial_t^{(1)} K_\gamma - \Delta t \frac{c_{i\gamma}}{12c^2} c_{i\beta}\partial_{x_\beta}^{(1)} K_\gamma .
\end{aligned}
$$

The following summands vanish:

$$
\partial_t^{(1)} \sum_i F_i^{(1)} \underbrace{=}_{(5.2.24)} 0,
$$

$$
\partial_{x_\gamma}^{(1)} \sum_i c_{i\gamma} F_i^{(1)} \underbrace{=}_{(5.2.24)} 0,
$$

$$
\frac{\omega}{\Delta t} \sum_i F_i^{(2)} \underbrace{=}_{(5.2.24)} 0,
$$

and

$$
\frac{\Delta t}{12c^2}\partial_t^{(1)} K_\gamma \sum_i c_{i\gamma} = 0.
$$

The second term of Eq. (5.2.38) is the time derivative of the density:

$$
\partial_t^{(2)} \sum_i F_i^{(0)} = \partial_t^{(2)} \rho. \qquad (5.2.39)
$$

The spatial gradient of the body force yields

$$
-\frac{\Delta t}{12c^2}\partial_{x_\alpha}^{(1)} K_\beta \sum_i c_{i\alpha}c_{i\beta} = -\frac{\Delta t}{2}\partial_{x_\alpha}^{(1)} K_\alpha . \qquad (5.2.40)
$$

In the transformation of the following summands the time derivatives are substituted by spatial derivative using (5.2.34) and (5.2.31):

$$
\begin{aligned}
\frac{\Delta t}{2}\partial_t^{(1)}\partial_t^{(1)} \sum_i F_i^{(0)} &= \frac{\Delta t}{2}\partial_t^{(1)}\partial_t^{(1)}\rho = -\frac{\Delta t}{2}\partial_t^{(1)}\partial_{x_\beta}^{(1)}\rho u_\beta \\
&= \frac{\Delta t}{2}\partial_{x_\alpha}^{(1)}\partial_{x_\beta}^{(1)} P_{\alpha\beta}^{(0)} - \frac{\Delta t}{2}\partial_{x_\alpha}^{(1)} K_\alpha \\
\Delta t\partial_t^{(1)}\partial_{x_\alpha}^{(1)} \sum_i c_{i\alpha} F_i^{(0)} &= \Delta t\partial_{x_\alpha}^{(1)}\partial_t^{(1)}(\rho u_\alpha) \\
&= -\Delta t\partial_{x_\alpha}^{(1)}\partial_{x_\beta}^{(1)} P_{\alpha\beta}^{(0)} + \Delta t\partial_{x_\alpha}^{(1)} K_\alpha \\
\frac{\Delta t}{2}\partial_{x_\alpha}^{(1)}\partial_{x_\beta}^{(1)} \sum_i c_{i\alpha}c_{i\beta} F_i^{(0)} &= \frac{\Delta t}{2}\partial_{x_\alpha}^{(1)}\partial_{x_\beta}^{(1)} P_{\alpha\beta}^{(0)}
\end{aligned}
$$

The sum of these three terms yields $\Delta t \partial_{x_\alpha}^{(1)} K_\alpha/2$ which cancels with the term derived from the body force gradient (Eq. 5.2.40), i.e. inclusion of the spatial gradient of the body force is essential to ensure that there is no mass diffusion:

$$\boxed{\partial_t^{(2)} \rho = 0.} \tag{5.2.41}$$

Terms of second order in ϵ: momentum. Conservation of momentum leads to

$$\begin{aligned} 0 &= \sum_i c_{i\alpha} E_i^{(1)} \\ &= \sum_i c_{i\alpha}\partial_t^{(1)} F_i^{(1)} + c_{i\alpha}\partial_t^{(2)} F_i^{(0)} + c_{i\alpha}c_{i\beta}\partial_{x_\beta}^{(1)} F_i^{(1)} + \frac{\Delta t}{2} c_{i\alpha}\partial_t^{(1)}\partial_t^{(1)} F_i^{(0)} \\ &\quad + \Delta t c_{i\alpha}c_{i\gamma}\partial_t^{(1)}\partial_{x_\gamma}^{(1)} F_i^{(0)} + \frac{\Delta t}{2} c_{i\alpha}c_{i\beta}c_{i\gamma}\partial_{x_\beta}^{(1)}\partial_{x_\gamma}^{(1)} F_i^{(0)} \\ &\quad + \frac{\omega}{\Delta t} c_{i\alpha} F_i^{(2)} - \Delta t c_{i\alpha}\frac{c_{i\gamma}}{12c^2}\partial_t^{(1)} K_\gamma - c_{i\alpha}c_{i\beta}c_{i\gamma}\frac{\Delta t}{12c^2}\partial_{x_\beta}^{(1)} K_\gamma. \end{aligned}$$

An approximation of $F_i^{(1)}$ can be derived from the first order in ϵ: $E_i^{(0)} = 0$ $\Rightarrow$

$$\boxed{F_i^{(1)}(\boldsymbol{x}, t) = -\frac{\Delta t}{\omega}\partial_t^{(1)} F_i^{(0)} - \frac{\Delta t}{\omega} c_{i\gamma}\partial_{x_\gamma}^{(1)} F_i^{(0)} + \frac{\Delta t\, c_{i\gamma}}{6c^2\omega} K_\gamma,} \tag{5.2.42}$$

i.e. deviations from local equilibrium are driven by gradients in time and space (compare Eq. 4.2.25) and by applied body forces.
In the transformation of the following summands terms of the order $\mathcal{O}(\boldsymbol{j}^2)$ will be neglected (indicated by $\approx$ instead of $=$). Thus the Navier-Stokes equation will be recovered in the limit of *low Mach numbers* only.

$$\partial_t^{(1)} \sum_i c_{i\alpha} F_i^{(1)} \underbrace{=}_{(5.2.24)} 0$$

$$\partial_t^{(2)} \sum_i c_{i\alpha} F_i^{(0)} = \partial_t^{(2)} j_\alpha \tag{5.2.43}$$

$$\partial_{x_\beta}^{(1)} \sum_i c_{i\alpha}c_{i\beta} F_i^{(1)} \underbrace{=}_{(5.2.42)} \underbrace{-\frac{\Delta t}{\omega}\partial_t^{(1)}\partial_{x_\beta}^{(1)} \sum_i c_{i\alpha}c_{i\beta} F_i^{(0)}}_{(*)} \underbrace{-\frac{\Delta t}{\omega}\partial_{x_\beta}^{(1)}\partial_{x_\gamma}^{(1)} \sum_i c_{i\alpha}c_{i\beta}c_{i\gamma} F_i^{(0)}}_{(**)}$$

$$+\frac{\Delta t}{6c^2\omega}\partial_{x_\beta}^{(1)}K_\gamma\underbrace{\sum_i c_{i\alpha}c_{i\beta}c_{i\gamma}}_{=0}$$

$$\begin{aligned}\frac{\Delta t}{2}\partial_t^{(1)}\partial_t^{(1)}\sum_i c_{i\alpha}F_i^{(0)} &= \frac{\Delta t}{2}\partial_t^{(1)}\partial_t^{(1)}j_\alpha\\ &= -\frac{\Delta t}{2}\partial_t^{(1)}\partial_{x_\beta}^{(1)}P_{\alpha\beta}^{(0)}+\frac{\Delta t}{2}\partial_t^{(1)}K_\alpha\\ &\approx -\frac{\Delta t}{2}\frac{k_BT}{m}\partial_t^{(1)}\partial_{x_\beta}^{(1)}\rho\delta_{\alpha\beta}+\frac{\Delta t}{2}\partial_t^{(1)}K_\alpha\\ &\Rightarrow \frac{\Delta t}{2}\frac{k_BT}{m}\boldsymbol{\nabla\nabla}\cdot\boldsymbol{j}+\frac{\Delta t}{2}\partial_t\boldsymbol{K}\end{aligned}\tag{5.2.44}$$

$$\underbrace{\frac{\Delta t}{2}\partial_{x_\beta}^{(1)}\partial_{x_\gamma}^{(1)}\sum_i c_{i\alpha}c_{i\beta}c_{i\gamma}F_i^{(0)}}_{(**)}$$

$$\underbrace{\Delta t\partial_{x_\beta}^{(1)}\partial_t^{(1)}\sum_i c_{i\alpha}c_{i\beta}F_i^{(0)}}_{(*)}$$

$$\frac{\omega}{\Delta t}\sum_i c_{i\alpha}F_i^{(2)}\underbrace{=}_{(5.2.24)}0$$

The term derived from the time derivative of the body force

$$-\frac{\Delta t}{12c^2}\partial_t^{(1)}K_\beta\sum_i c_{i\alpha}c_{i\beta}=-\frac{\Delta t}{2}\partial_t^{(1)}K_\alpha\Rightarrow-\frac{\Delta t}{2}\partial_t\boldsymbol{K}\tag{5.2.45}$$

cancels with the term in Eq. (5.2.44), i.e. inclusion of the time derivative of the body force is essential to obtain the exact form of the Navier-Stokes equation.

$$-\frac{\Delta t}{12c^2}\partial_{x_\beta}^{(1)}K_\gamma\sum_i c_{i\alpha}c_{i\beta}c_{i\gamma}=0$$

Summation of the $(*)$-terms results in

$$\Delta t\left(1-\frac{1}{\omega}\right)\partial_{x_\beta}^{(1)}\partial_t^{(1)}\underbrace{\sum_i c_{i\alpha}c_{i\beta}F_i^{(0)}}_{\approx\frac{k_BT}{m}\rho\delta_{\alpha\beta}}\Rightarrow-\Delta t\left(1-\frac{1}{\omega}\right)\frac{k_BT}{m}\boldsymbol{\nabla\nabla}\cdot\boldsymbol{j}.\tag{5.2.46}$$

The $(**)$-terms lead to

$$\begin{aligned} \Delta t & \left(\frac{1}{2}-\frac{1}{\omega}\right)\partial_{x_\beta}^{(1)}\partial_{x_\gamma}^{(1)}\sum_i c_{i\alpha}c_{i\beta}c_{i\gamma}F_i^{(0)} \\ = \quad & \Delta t\left(\frac{1}{2}-\frac{1}{\omega}\right)\frac{m}{k_BT}\frac{1}{\rho_0}\partial_{x_\beta}^{(1)}\partial_{x_\gamma}^{(1)}\sum_i W_i c_{i\alpha}c_{i\beta}c_{i\gamma}(\boldsymbol{c}_i\cdot\boldsymbol{j}) \\ \Rightarrow \quad & \Delta t\left(\frac{1}{2}-\frac{1}{\omega}\right)\frac{k_BT}{m}\left(\nabla^2\boldsymbol{j}+2\boldsymbol{\nabla}\boldsymbol{\nabla}\cdot\boldsymbol{j}\right). \end{aligned} \tag{5.2.47}$$

By adding up (5.2.43 – 5.2.47) one finally obtains

$$\boxed{\partial_t^{(2)}\boldsymbol{j}=\Delta t\left(\frac{1}{\omega}-\frac{1}{2}\right)\frac{k_BT}{m}\left(\nabla^2\boldsymbol{j}+\boldsymbol{\nabla}\boldsymbol{\nabla}\cdot\boldsymbol{j}\right),} \tag{5.2.48}$$

i.e. dynamic shear and compression viscosity are equal:

$$\mu_S=\mu_K=\Delta t\left(\frac{1}{\omega}-\frac{1}{2}\right)\frac{k_BT}{m}. \tag{5.2.49}$$

The viscosities can be tuned by an appropriate choice of the collision parameter ω. The equation for iterative solution of linear systems by the simultaneous over-relaxation (SOR) is of the same form as the BGK kinetic equation. The SOR method is convergent for $0<\omega<2$ (Kahan, 1958). This range of ω corresponds to positive viscosities in the BGK-LBM.
The sum of the first and second order terms yields (in the incompressible limit) the Navier-Stokes equation:

$$\boxed{\boldsymbol{\nabla}\cdot\boldsymbol{u}=0} \tag{5.2.50}$$

and

$$\boxed{\partial_t\boldsymbol{u}+(\boldsymbol{u}\boldsymbol{\nabla})\,\boldsymbol{u}=-\frac{1}{\rho}\boldsymbol{\nabla}p+\nu\nabla^2\boldsymbol{u}+\boldsymbol{K}} \tag{5.2.51}$$

with the kinematic shear viscosity

$$\nu=\Delta t\left(\frac{1}{\omega}-\frac{1}{2}\right)\frac{c^2}{3}=\frac{c^2}{3}\left(\tau-\frac{\Delta t}{2}\right). \tag{5.2.52}$$

5.2.4 Storage demand

For the special case $\omega=1$ the kinetic equation reduces to

$$F_i(\boldsymbol{x}+\boldsymbol{c}_i\Delta t,t+\Delta t)=F_i^{(0)}(\boldsymbol{x},t)$$

and the storage demand for ρ, $\boldsymbol{j}$, 9 distributions $F_i^{(eq)}$ and their propagated values F_i, i.e. 21 2D arrays, seems to be quite large. The required memory can, however, be drastically reduced by the following two procedures:

1. One after the next $F_i^{(eq)}$ can be evaluated, propagated and will contribute (independent of the other F_j) to the values of ρ and $\boldsymbol{j}$ at the next time level. Only 7 arrays, namely ρ and $\boldsymbol{j}$ at two time levels and one array F_i, are required, i.e. the reduction factor is $21/7 = 3$.
2. Because the collisions are strictly local and the propagation is almost local (to next neighbor nodes) the domain can be partitioned into subdomains which can be updated one after the other using smaller auxiliary arrays.

Procedure 1 leads to some increase in the length of the code but seems to be worth the effort especially in 3D where the reduction factor is even larger. The second procedure requires some additional coding to treat the boundaries of the subdomains but offers a further reduction in memory by a factor of almost 2.
The storage demand for BGK-LBM with $\omega \neq 1$ is substantially larger because one has to keep all (non-equilibrium) distributions F_i. The adventage is the tunable viscosity which allows simulation of flows with high Reynolds numbers.

5.2.5 Simulation of two-dimensional decaying turbulence

In 1994 Martinez et al. published a milestone paper. They simulated two-dimensional decaying turbulence over a square with periodic boundary conditions by the BGK lattice Boltzmann model over the D2Q9 lattice and compared this method to a spectral model[5] which is very efficient over this simple domain. The initial velocity distribution consists of two shear layers (realized by a truncated spectral representation of δ functions at $y = \pi/2$ and $y = 3\pi/2$) plus some noise over the whole domain. The characteristic velocity U is defined as the root mean square value

$$U = \sqrt{\langle \boldsymbol{u}^2 \rangle} = 0.04 \tag{5.2.53}$$

und the characteristic length L is given by

$$L = \frac{512}{2\pi} \tag{5.2.54}$$

where 512 is the number of grid points in each dimension. The viscosity parameter ω has been chosen such that the Reynolds number

$$R_e = \frac{UL}{\nu(\omega)} \tag{5.2.55}$$

[5] The spectral model actually does not solve the Navier-Stokes equation but the *vorticity equation* $\dfrac{\partial \varpi}{\partial t} + \boldsymbol{v} \cdot \boldsymbol{\nabla} \varpi = \nu \nabla^2 \varpi$ where $\varpi = (\boldsymbol{\nabla} \times \boldsymbol{v})_z$ is the z-component of the relative vorticity.

is 10000.
The following Figures (5.2.2 - 5.2.5) show isocontours of the vorticity $a = (\boldsymbol{\nabla} \times \boldsymbol{u})_z$ at four dimensionless times. Dashed lines indicate negative values. The upper plots show the results of the spectral model and the lower plots those of the lattice Boltzmann model. The features compare very well which gives confidence in both methods.
What is most surprising: the LBM is as fast as the spectral model! And the LBM keeps its efficiency in more complex geometries (porous media, for example) whereas spectral models may not be applicable anymore. These simulations clearly demonstrated the great potential of BGK-LBMs.

Fig. 5.2.2. *Isovorticity contour plots for time 1. Dashed lines correspond to negative values of vorticity. The values for the contours are the same for all cases (Figures 5.2.2 – 5.2.5). Strikingly similar features can be found for the lattice Boltzmann simulation, as compared with the spectral simulation. (SP refers to the spectral sumulation and LBE to the lattice Boltzmann simulation; Martinez et al., 1994)*

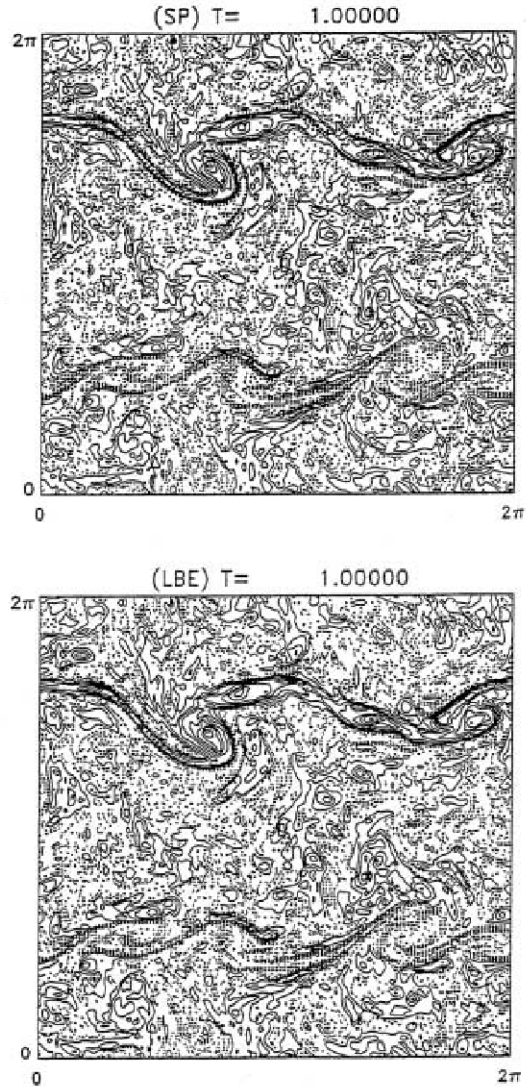

Fig. 5.2.3. *Same as in Fig. 5.2.2 for time 5 (Martinez et al., 1994).*

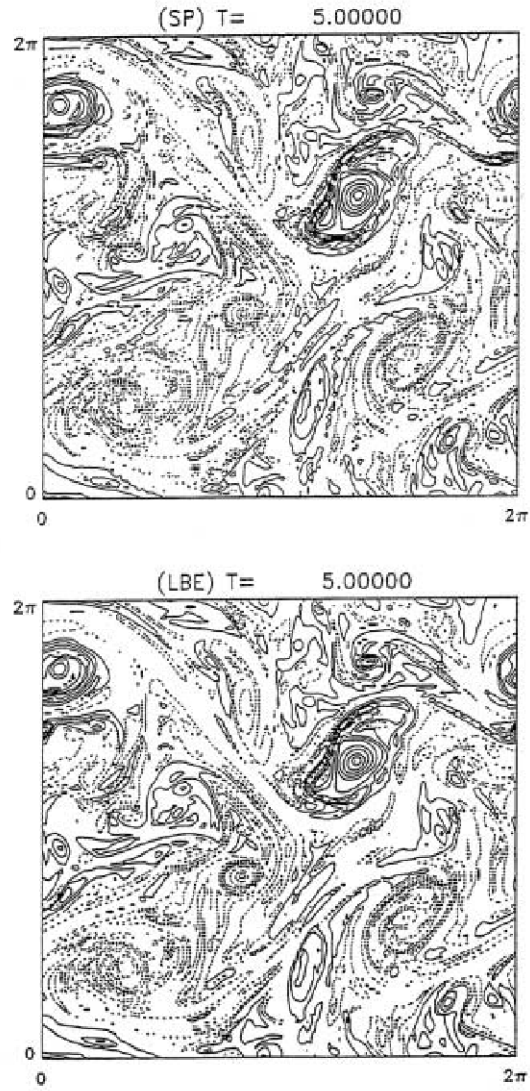

Fig. 5.2.4. *Same as in Fig. 5.2.2 for time 17 (Martinez et al., 1994).*

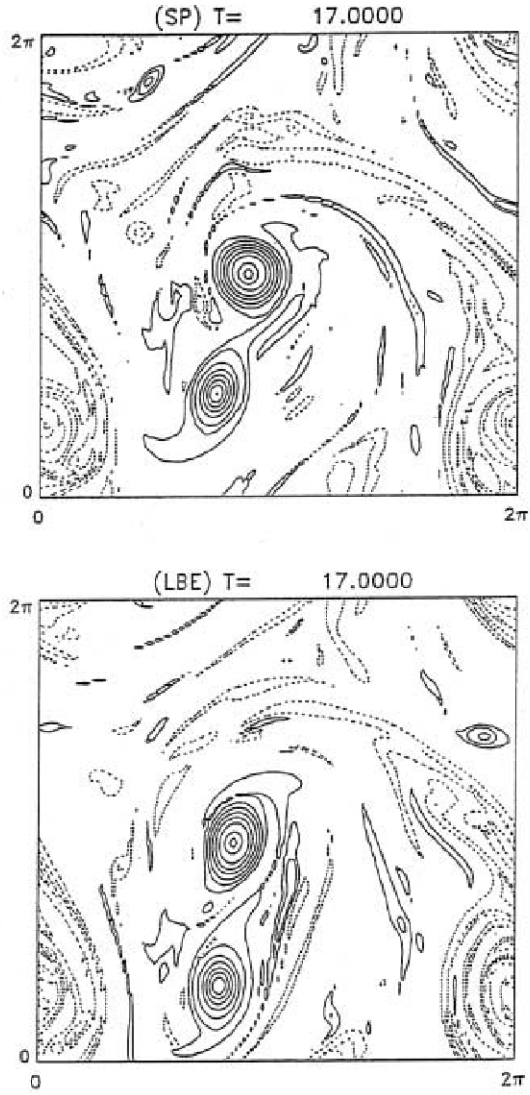

Fig. 5.2.5. *Same as in Fig. 5.2.2 for time 80 (Martinez et al., 1994).*

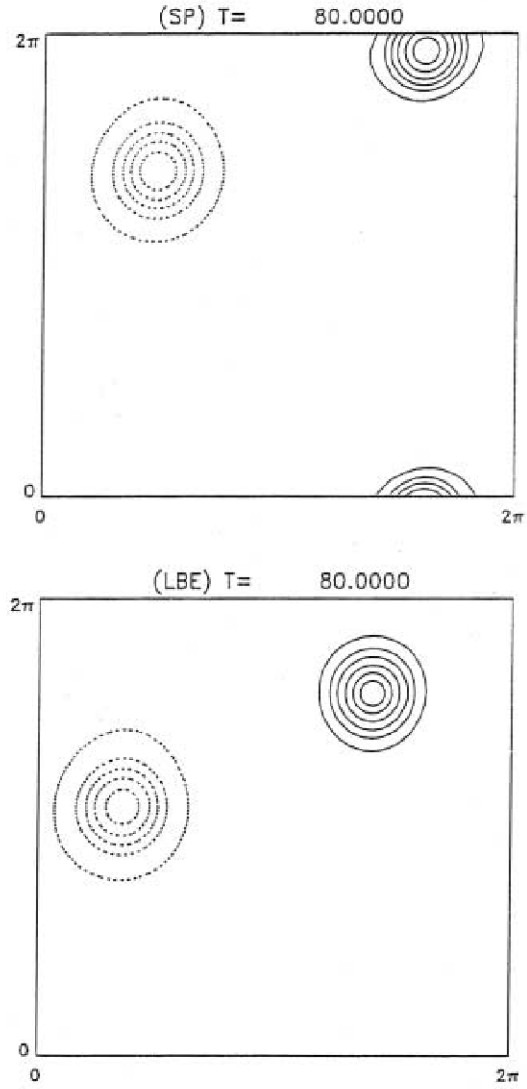

5.2.6 Boundary conditions for LBM

> "To a certain degree, achieving self-consistent boundary conditions with a given accuracy is as important as developing numerical schemes themselves."
> Chen et al. (1996)

The implementation of boundary conditions for LGCA has been discussed in Section 3.2.7. The same princles as outlined there can be applied also to LBM. In the following a self-contained discussion of no-slip and slip boundary conditions shall be given even risking the repetition of parts of Section 3.2.7. LGCA and LBM seem to be very attractive because the apparent ease to implement boundary conditions even in complicated geometry like porous media. You often can find quotes like 'difficult geometrical boundary conditions are readily handled' in the introduction of an article only to find out that the authors performed some simulation over a square with periodic boundary conditions. Much more realistic is the remark of He et al. (1997) that "the real hydrodynamic boundary conditions have not been fully understood". Accordingly various implementations of boundary conditions will be discussed here. Some of them have to be ruled out because they are only of first order of accuracy. You have to find out which of the remaining ones gives satisfying results for the actual flow problem considered.

In general, there are two ways to define a boundary: the boundary curve may include grid nodes (*'node boundary'*; the nodes on the boundary are called *'boundary nodes'*; Skordos, 1993; Inamuro et al., 1995; Noble et al., 1995a,b, 1996) or passes through the midpoints of links between nodes (*'link boundary'*; Cornubert et al., 1991; Ginzbourg and Adler, 1994; Ladd, 1994a,b). Node boundaries are appropriate for periodic and inflow boundary conditions.

No-slip boundary condition. Inamuro et al. (1995) He et al. (1997)

1. The *complete bounceback scheme*: Instead of collision assign each F_i the value of the F_i of its opposite direction, i.e. for a point on the lower boundary:

$$\begin{aligned} \text{in-state:} &\quad F_0, F_1, F_2, F_3, F_4, F_5, F_6, F_7, F_8 \\ \text{out-state:} &\quad F_0, F_1, F_4, F_3, F_2, F_7, F_8, F_5, F_6. \end{aligned}$$

2. The *half-way wall bounceback*: Consider a channel with periodic boundary conditions in x-directions and walls at the lower and upper boundary. The first and last nodes in y-direction, i.e. with indices $j = 1$ and $j = N$,

are 'dry' (*dry* or *wall nodes*), i.e. outside the 'wet' domain which encompasses nodes with $j = 2$ to $j = N - 1$ (*wet* or *interior* or *fluid nodes*). The lower (upper) boundary is located half-way between the first and second (last but one and last) nodes in y-direction. Particle distributions are propagated between wet and dry nodes and vice versa. On the dry nodes no collision or forcing is performed and the distributions are all bounced back. Note that the width of the channel is one unit smaller than that with the complete bounceback scheme.

Plane Poiseuille flow: analytic solution. Only few analytical solutions of the Navier-Stokes equation are known. One is the plane Poiseuille flow in a channel of width $2L$ where the flow is steady ($\partial/\partial t = 0$), in x-direction $\boldsymbol{u} = (u, v) = (u(y), 0)$, with constant pressure (p and ρ = constant) and without variations in x-direction ($\partial/\partial x = 0$). The flow is driven by a constant force $\boldsymbol{K} = K\boldsymbol{e}_x$. Accordingly the Navier-Stokes equation reduces to an ordinary differential equation for $u(y)$

$$\nu \frac{d^2u}{dy^2} + K = 0$$

and the continuity equation $\dfrac{du(y)}{dx} = 0$ is satisfied. At the channel walls no-slip boundary conditions apply, i.e. $u(y) = 0$ at $y = -L$ and $y = L$. The analytical solution is a parabola

$$u(y) = \frac{K}{2\nu}\left(L^2 - y^2\right). \tag{5.2.56}$$

Plane Poiseuille flow: numerical simulation. In the numerical simulation the velocity is initialized to zero and the mass density to a constant value of $\rho = 1$. In order to start the fluid flow a constant force has to be applied at every time step. Here the microscopic forcing method is applied.

First the simplest no-slip scheme, namely bounceback will be used. The result of an integration over a domain with 20 time 20 nodes is shown in Fig. 5.2.6 together with the analytical solution. The fluid is resting in the beginning and then is slowly accelarated. After $t = 1200$ time steps the mean x-momentum becomes steady (plot at lower right). The final velocity profile $u(y)$ (+ in plot at upper left) is compared with the analytical solution (Eq. 5.2.56) assuming a channel width $2L = YMAX - 1 = 19$ where $YMAX = 20$ is the number of nodes in y-direction. The numerical solution is zero on the boundary points (nodes $j = 1$ and $j = YMAX$ or $y = \pm 9.5$) and the profile looks similar to a parabola. The most striking difference compared to the analytical solution is the lower value of the maximum velocity. One can fit a parabola to the numerical data with equal values of the maximum velocity (plot at upper right). Deviations between this fit and the numerical values or most obvious

near the boundaries. The plot at the lower left shows the numerical solution together with the analytical solution but the latter one now based on a smaller channel width $2L = YMAX - 2 = 18$. This solution compares very well with the analytical solution except for the two boundary nodes. This figure suggests the following interpretation. The boundary is located half-way between the first and second node respectively half-way between the second to last and the last node. Therefore the 'wet' channel has only a width of $2L = YMAX - 2 = 18$. The nodes at $j = 1$ and $j = YMAX$ are auxiliary nodes which take care of the correct boundary conditions at $j = 3/2$ and $j = YMAX - 1/2$. The velocity values on these auxiliary nodes should not be interpreted as flow velocities (these nodes are located 'on land' and could by called 'dry nodes').

Fig. 5.2.6. *No-slip boundary conditions and Poiseuille flow (see text for discussion).*

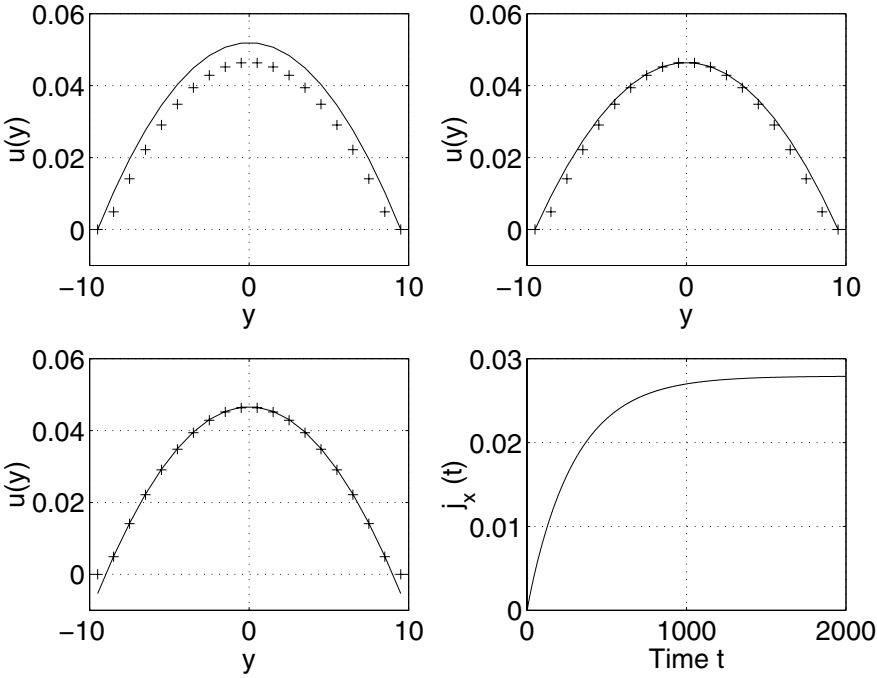

Numerical experiments with different channel widths $2L = 16, 32, 64, 128$ (different spatial resolutions of the parabola) have been performed while keeping constant the viscosity ν and the product of channel width and maximum speed (by varying the forcing). Thus the Reynolds number is kept constant. The Mach number varies but for $L \geq 16$ is small compared to 1. The error

has been calculated by

$$\text{Error} := \frac{1}{N}\sqrt{\sum_{i=1}^{N}\left(\hat{u}_i^{(n)} - \hat{u}_i^{(a)}\right)^2}$$

where the summation is over $N = 14$ inner points and $\hat{u}_i^{(n)}$ and $\hat{u}_i^{(a)}$ are the normalized numerical and analytical solutions with maximum speed equal to one. Fig. (5.2.7) shows the error as a function of L. The slop of the curve is close to -2 which indicates that this scheme is of second order in the spatial discretization.

Fig. 5.2.7. *Error of the numerical compared to the analytical solution of the Poiseuille flow as a function of spatial resolution. The bounceback scheme is applied and the resulting data are interpretated such that the boundaries are located between the first and second respectively between the second to last and the last node (compare also Fig. 5.2.6C). The slop of the curve is close to -2 which indicates that this scheme is of second order in the spatial discretization.*

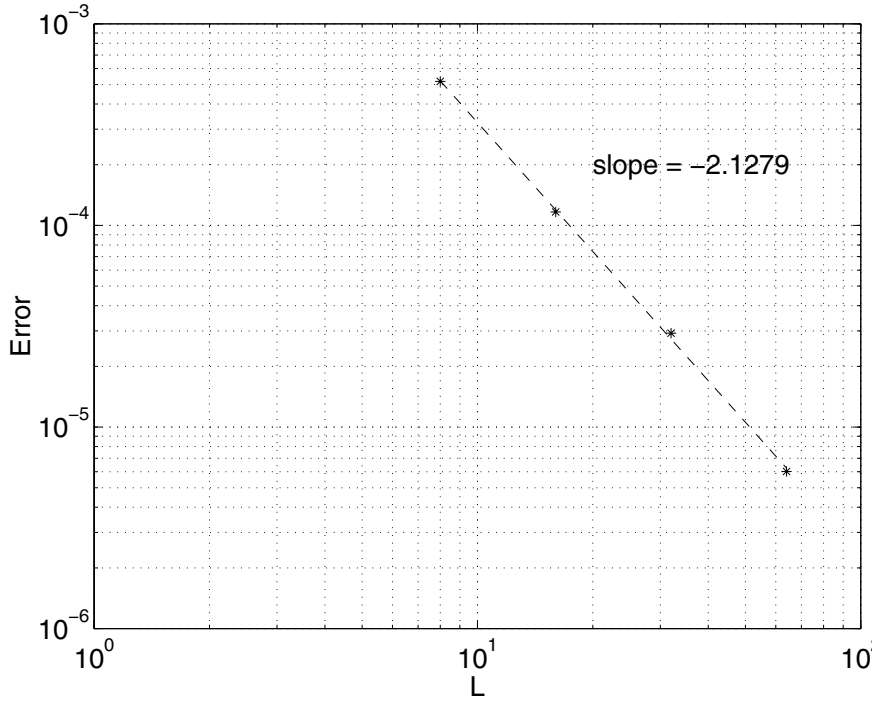

Slip boundary condition. To test slip boundary condition ($\frac{\partial u_t}{\partial x_n} = 0$ at $|y| \to \infty$, i.e. the normal derivative of the tangential velocity component u_t vanishes on the boundary) a shear layer with

$$u = \begin{cases} -U & \text{for} \quad y < 0 \\ +U & \text{for} \quad y > 0 \end{cases}, \quad v = 0$$

is initialized at $t = 0$. The analytical solution of the Navier-Stokes equation in $-\infty < y < \infty$ for this initial condition is known:

$$u(y,t) = U\, erf\left(\frac{y}{\sqrt{4\nu t}}\right), \quad v = 0$$

where $erf(arg)$ is the error function.
The slip conditions have been implemented by reflection of the distribution F_i on boundary nodes. The result of a numerical simulation ($U = 0.1$) in a channel of finite width ($2L = 18$) are shown together with the analytical solution in Fig. 5.2.8. The implementation of the simple slip scheme works very well. Small deviations between numerical and analytical solution are to be expected due to the finite width of the channel in the simulation.

Fig. 5.2.8. *Shear layer flow in a channel: test of slip boundary conditions (see text).*

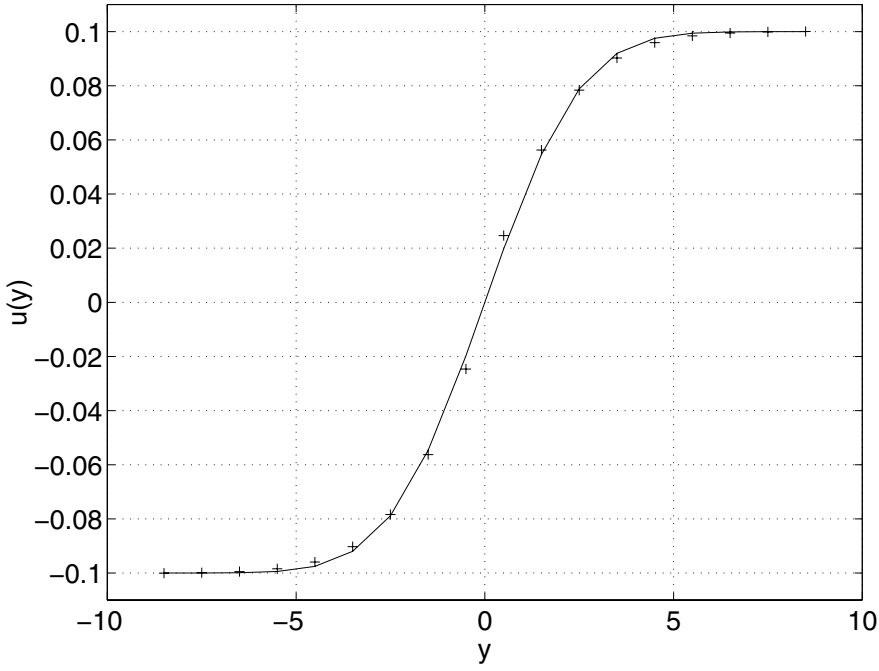

Further reading: boundary conditions for LBM
Skordos (1993), Ziegler (1993), Ginzbourg and Adler (1994), He and Zou

(1995), Noble et al. (1995a,b), Inamuro et al. (1995), Noble et al. (1996), Chen et al. (1996), Ginzbourg and d'Humiéres (1996), Maier et al. (1996), Filippova and Hänel (1997), Gallivan et al. (1997), Stockman et al. (1997), Kandhai et al. (1999).

5.3 Hydrodynamic lattice Boltzmann models in 3D

BGK-LBMs have been discussed so far only in two dimensions. The extension to three dimensions is straightforward. One just has to choose a 3D lattice and calculate appropriate equilibrium distributions. In this section we will calculate equilibrium distributions by the method of Koelman (1991) for 3D lattices with 19 *and* 15 *velocities.*
The derivation of the equilibrium distribution functions $F_i^{(eq)}$ (5.2.11) by minimizing the functional (5.2.18) is independent of the lattice velocities $\boldsymbol{c}_i$ and the dimension D. Only the constraints (5.2.6 to 5.2.8) for the velocity moments were used in Section (5.2). Thus one can use the form of the equilibrium distribution functions $F_i^{(eq)}$ (5.2.11) with the appropriate lattice velocities $\boldsymbol{c}_i$ and weights W_i.

5.3.1 3D-LBM with 19 velocities

For hydrodynamic simulation d'Humières et al. (1986) proposed a multi-speed lattice-gas cellular automata over a cubic lattice with 19 velocities (compare Section 3.3). This cubic lattice D3Q19 is defined by the following velocities

$$\begin{aligned} \boldsymbol{c}_0 &= (0,0) \\ \boldsymbol{c}_{1,2},\, \boldsymbol{c}_{3,4},\, \boldsymbol{c}_{5,6} &= (\pm 1,0,0),\, (0,\pm 1,0)\, (0,0,\pm 1) \\ \boldsymbol{c}_{7,\ldots,10},\, \boldsymbol{c}_{11,\ldots,14},\, \boldsymbol{c}_{15,\ldots,18} &= (\pm 1,\pm 1,0),\, (\pm 1,0,\pm 1),\, (0,\pm 1,\pm 1). \end{aligned}$$

The calculation of the W_i for the 3D model proceeds in close analogy with the 2D case. There are three different speeds: 1 time speed 0 (rest particle), 6 times speed 1 (1-particles) and 12 times speed $\sqrt{2}$ ($\sqrt{2}$-particles). The even moments yield four independent equations for the calculation of W_0, W_1, W_2 and k_bT/m:

– 0. moment:

$$\sum_i W_i = W_0 + 6W_1 + 12W_2 = \rho_0$$

– 2. moment:

$$\sum_i c_{\alpha x}^2 W_i = 2W_1 + 8W_2 = \rho_0 \frac{kT}{m}$$

– 4. moment:

$$\sum_i c_{\alpha x}^4 W_i = 2W_1 + 8W_2 = 3\rho_0 \left(\frac{kT}{m}\right)^2$$

$$\sum_i c_{\alpha x}^2 c_{\alpha y}^2 W_i = 4W_2 = \rho_0 \left(\frac{kT}{m}\right)^2$$

The solution reads

$$\begin{aligned} W_0 &= \frac{\rho_0}{3} \\ W_1 &= \frac{\rho_0}{2}\left(\frac{kT}{m}\right)^2 = \frac{\rho_0}{18} \\ W_2 &= \frac{\rho_0}{4}\left(\frac{kT}{m}\right)^2 = \frac{\rho_0}{36} \\ \frac{kT}{m} &= \frac{1}{3}. \end{aligned} \tag{5.3.1}$$

The odd velocity moments over W_i vanish.

5.3.2 3D-LBM with 15 velocities and Koelman distribution

The lattice velocities of the D3Q15 lattice read

$$\begin{aligned} \boldsymbol{c}_0 &= (0,0,0) && \text{rest particle} \\ \boldsymbol{c}_{1,2},\ \boldsymbol{c}_{3,4},\ \boldsymbol{c}_{5,6} &= (\pm 2,0,0),\ (0,\pm 2,0)\,(0,0,\pm 2) && \text{2-particles} \\ \boldsymbol{c}_{7,\ldots,14} &= (\pm 1,\pm 1,\pm 1) && \sqrt{3}\text{-particles.} \end{aligned}$$

There are three different speeds: 1 time speed 0, 6 times speed 2 and 8 times speed $\sqrt{3}$. The even moments yield four independent equations for the calculation of W_0, W_2, W_3 and k_bT/m:

– 0. moment:

$$\sum_i W_i = W_0 + 6W_2 + 8W_3 = \rho_0$$

– 2. moment:

$$\sum_i c_{\alpha x}^2 W_i = 8W_2 + 8W_3 = \rho_0 \frac{kT}{m}$$

– 4. moment:

$$\sum_i c_{\alpha x}^4 W_i = 32W_2 + 8W_3 = 3\rho_0 \left(\frac{kT}{m}\right)^2$$

$$\sum_i c_{\alpha x}^2 c_{\alpha y}^2 W_i = 8W_3 = \rho_0 \left(\frac{kT}{m}\right)^2$$

The solution reads

$$\begin{aligned} W_0 &= \frac{7}{18}\rho_0 \\ W_2 &= \frac{\rho_0}{16}\left(\frac{kT}{m}\right)^2 = \frac{\rho_0}{36} \\ W_3 &= \frac{\rho_0}{8}\left(\frac{kT}{m}\right)^2 = \frac{\rho_0}{18} \\ \frac{kT}{m} &= \frac{2}{3}. \end{aligned}$$

The odd velocity moments over W_i vanish.

5.3.3 3D-LBM with 15 velocities proposed by Chen et al. (D3Q15)

The equilibrium distributions are not unique and other choices are possible. As an example we give the equilibrium distributions proposed by Chen et al. (1992):

$$\begin{aligned} F_0^{eq} &= d^{(0)} + \delta^{(0)}\boldsymbol{v}^2 \\ F_i^{eq} &= d^{(1)} + \beta^{(1)}\boldsymbol{c}_i\cdot\boldsymbol{v} + \gamma^{(1)}(\boldsymbol{c}_i\cdot\boldsymbol{v})^2 + \delta^{(1)}\boldsymbol{v}^2 \quad \alpha = 1,...,6 \\ F_i^{eq} &= d^{(2)} + \beta^{(2)}\boldsymbol{c}_i\cdot\boldsymbol{v} + \gamma^{(2)}(\boldsymbol{c}_i\cdot\boldsymbol{v})^2 + \delta^{(2)}\boldsymbol{v}^2 \quad \alpha = 7,...,14 \end{aligned}$$

where

$$\begin{aligned} d^{(0)} &= d^{(1)} = \frac{\rho}{11}, \quad d^{(2)} = \frac{\rho}{22} \\ \alpha^{(1)} &= \frac{\rho}{24}, \quad \alpha^{(2)} = \frac{\rho}{12} \\ \gamma^{(1)} &= \frac{\rho}{32}, \quad \gamma^{(2)} = \frac{\rho}{16} \\ \delta^{(0)} &= -\frac{7}{24}\rho, \quad \delta^{(1)} = -\frac{\rho}{48}, \quad \delta^{(2)} = -\frac{\rho}{24}. \end{aligned}$$

These distributions will not be considered in the following.

5.4 Equilibrium distributions: the ansatz method

> "The question that we are most often asked about cellular automata is the following.
> 'I've been shown cellular automata that make surprisingly good models of, say, hydrodynamics, heat conduction, wave scattering, flow through porous media, nucleation, dendritic growth, phase separation, etc. But I'm left with the impression that these are all *ad hoc* models, arrived at by some sort of magic.'
> 'I'm a scientist, not a magician. Are there well-established *correspondence rules* that I can use to translate features of the system I want to model into specifications for an adequate cellular-automaton model of it?'
> Physical modeling with cellular automata is a young discipline. Similar questions were certainly asked when differential equations were new - and, despite three centuries of accumulated experience, modeling with differential equations still requires a bit of magic."
> Toffoli und Margolus (1990)

The problem addressed for CA by Toffoli and Margolus exists also for lattice Boltzmann models. However, in what follows it will be shown that a LBM for the Navier-Stokes equation can be developed by an almost straightforward method. In chapter 5.2 global equilibrium functions W_i for vanishing velocity ($\boldsymbol{u} = 0$) and constant density $\rho = \rho_0$ were determined in close analogy to the Maxwell distribution (more precise: the velocity moments of W_i up to fourth order are equal to the corresponding velocity moments over the Maxwell distribution; compare Eqs. 5.2.6 - 5.2.8). Subsequently the local equilibrium distributions F_i have been derived using the maximum entropy principle. These 'Koelman-distributions' lead to the Navier-Stokes equation with isotropic advection, Galilean invariance and pressure which does not explicitly depend on flow speed.

To be sure, these are not the only distributions over that lattice which in the macroscopic limit yield the Navier-Stokes equation. This is not a problem because the equilibrium distributions of our artificial microworld are not of interest by themselves.

In the current section I will discuss an alternative approach to suitable equilibrium distributions F_i whereby an ansatz for F_i will be used. After the multiscale analysis the free parameters in the ansatz will be chosen such that isotropy etc. are assured. This alternative approach will be of central importance for the development of lattice Boltzmann models for given differential equations.

To keep things simple the presentation will be restricted to a twodimensional model. The extension to 3D is straightforward. An LBM is defined by three ingredients:

1. A kinetic equation: here the meanwhile well-established BGK equation is chosen.
2. A lattice with sufficient symmetry: in order to compare results with those of the previous chapter the D2Q9 lattice is chosen; for a model based on D2Q7 see exercise (5.4.3).
3. Equilibrium distributions: see below.

Instead of using the maximum entropy principle to derive equilibrium distributions one may propose an ansatz with free parameters. How should the ansatz look like?

1. From lattice-gas cellular automata (FHP, FCHC, PI) and the Koelman model we know that terms quadratic in $\boldsymbol{u}$ and $\boldsymbol{c}_i \cdot \boldsymbol{u}$ in the equilibrium distributions yield the nonlinear advection term of the Navier-Stokes equation; no higher moments are required.
2. The free parameters of the ansatz should depend only on the mass density and the speeds $|\boldsymbol{c}_i|$ but not on the directions of the $\boldsymbol{c}_i$.

This suggests the following ansatz with ten free parameters:

$$\begin{aligned} F_i &= A_0 + D_0 \boldsymbol{u}^2 && i = 0 \\ F_i &= A_1 + B_1 \boldsymbol{c}_i \cdot \boldsymbol{u} + C_1 (\boldsymbol{c}_i \cdot \boldsymbol{u})^2 + D_1 \boldsymbol{u}^2 && i = 1, 2, 3, 4 \\ F_i &= A_2 + B_2 \boldsymbol{c}_i \cdot \boldsymbol{u} + C_2 (\boldsymbol{c}_i \cdot \boldsymbol{u})^2 + D_2 \boldsymbol{u}^2 && i = 5, 6, 7, 8. \end{aligned} \tag{5.4.1}$$

The definitions of mass and momentum densities give three scalar constraints

$$\rho := \sum_i F_i = \underbrace{A_0 + 4(A_1 + A_2)}_{= \rho} + \boldsymbol{u}^2 \underbrace{(D_0 + 4D_1 + 4D_2 + 2C_1 + 4C_2)}_{= 0} \tag{5.4.2}$$

$$\boldsymbol{j} := \sum_i \boldsymbol{c}_i F_i = \underbrace{(2B_1 + 4B_2)}_{= \rho} \boldsymbol{u}. \tag{5.4.3}$$

5.4.1 Multi-scale analysis

The multi-scale analysis proceeds as in Section 5.2.3 up to Eq. (5.2.31) inclusively. Not until the calculation of the momentum flux tensor $P^{(0)}_{\alpha\beta}$ the specific form of the equilibrium distribution has to be taken into account:

$$
\begin{aligned}
P^{(0)}_{\alpha\beta} := & \sum_i c_{i\alpha}c_{i\beta}F^{(0)}_i \\
= & \sum_{i=1}^{4} c_{i\alpha}c_{i\beta}\left[A_1 + B_1\boldsymbol{c}_i\cdot\boldsymbol{u} + C_1(\boldsymbol{c}_i\cdot\boldsymbol{u})^2 + D_1\boldsymbol{u}^2\right] \\
& + \sum_{i=5}^{8} c_{i\alpha}c_{i\beta}\left[A_2 + B_2\boldsymbol{c}_i\cdot\boldsymbol{u} + C_2(\boldsymbol{c}_i\cdot\boldsymbol{u})^2 + D_2\boldsymbol{u}^2\right] \\
= & \left(2A_1 + 4A_2\right)\delta_{\alpha\beta} + \left(2C_1u_\alpha^2 + 4C_2\boldsymbol{u}^2\right)\delta_{\alpha\beta} \\
& + 8C_2u_\alpha u_\beta\left(1-\delta_{\alpha\beta}\right) + \left(2D_1 + 4D_2\right)\boldsymbol{u}^2\delta_{\alpha\beta}
\end{aligned}
$$

with $\boldsymbol{u} = (u, v) = (u_1, u_2)$. The goal is to transform the tensor

$$
P^{(0)}_{\alpha\beta} = \begin{pmatrix} 2A_1 + 4A_2 + 2C_1u^2 & 8C_2uv \\ +(4C_2 + 2D_1 + 4D_2)\boldsymbol{u}^2 & \\ & \\ 8C_2uv & 2A_1 + 4A_2 + 2C_1v^2 \\ & +(4C_2 + 2D_1 + 4D_2)\boldsymbol{u}^2 \end{pmatrix}
$$

into

$$
\rho\begin{pmatrix} u^2 & uv \\ uv & v^2 \end{pmatrix} + p\,\delta_{\alpha\beta}.
$$

The portion of the tensor which is independent of the flow velocity $\boldsymbol{u}$ yields the pressure p:

$$
p = 2A_1 + 4A_2.
$$

All other terms lead to the following constraints for the free parameters

$$
\begin{aligned}
4C_2 + 2D_1 + 4D_2 &= 0 \quad (\boldsymbol{u}^2 \text{ term in } P^{(0)}_{11} \text{ must vanish}) \\
2C_1 &= \rho \quad (u^2 \text{ term in } P^{(0)}_{11} \text{ must yield } \rho u^2) \\
8C_2 &= \rho \quad (uv \text{ term in } P^{(0)}_{12} \text{ must yield } \rho uv)
\end{aligned}
$$

and therefore

$$
C_1 = \frac{\rho}{2} \quad \text{and} \quad C_2 = \frac{\rho}{8}.
$$

The remaining eight unknowns (A_0, A_1, A_2, B_1, B_2, D_0, D_1, D_2) are constrained by only four linear equations

$$\begin{aligned} A_0 + 4(A_1 + A_2) &= \rho \\ 2B_1 + 4B_2 &= \rho \\ D_0 + 4D_1 + 4D_2 = -2C_1 - 4C_2 &= -\frac{3}{2}\rho \\ 2D_1 + 4D_2 &= -\frac{\rho}{2}. \end{aligned}$$

Therefore in addition some arbitrary restrictions can be imposed. Here is just one possibility:

$$\frac{A_0}{A_1} = \frac{A_1}{A_2} = \frac{B_1}{B_2} = \frac{D_0}{D_1} =: r \tag{5.4.4}$$

where r is a free parameter. Thus the coefficients are functions of r:

$$A_0 = \frac{r^2}{(r+2)^2}\rho, \quad A_1 = \frac{r}{(r+2)^2}\rho, \quad A_2 = \frac{1}{(r+2)^2}\rho$$

$$B_1 = \frac{r}{4+2r}\rho, \quad B_2 = \frac{1}{4+2r}\rho$$

$$D_0 = -\frac{r}{2+r}\rho, \quad D_1 = -\frac{1}{2+r}\rho, \quad D_2 = -\frac{r-2}{16+8r}\rho$$

$$p = \frac{2}{r+2}\rho = c_s^2\rho \tag{5.4.5}$$

The speed of sound

$$c_s = \sqrt{\frac{dp}{d\rho}} = \sqrt{\frac{2}{r+2}}$$

is tunable by the parameter r (compare Fig. 5.4.1).

The additional restriction

$$\frac{D_1}{D_2} = r$$

leads to a quadratic equation for r with solutions $r_1 = 4$ and $r_2 = -2$. The solution r_2 yields negative equilibrium distribution even at small Mach numbers and an infinite pressure. The solution $r = 4$ (by the way: C_1/C_2 also equals 4) leads to

$$A_0 = \frac{4}{9}\rho, \quad A_1 = \frac{1}{9}\rho, \quad A_2 = \frac{1}{36}\rho, \quad B_1 = \frac{1}{3}\rho, \quad B_2 = \frac{1}{12}\rho,$$

$$D_0 = -\frac{2}{3}\rho, \quad D_1 = -\frac{1}{6}\rho, \quad D_2 = -\frac{1}{24}\rho, \quad p = \frac{1}{3}\rho = c_s^2\rho$$

with the speed of sound

$$c_s = \frac{1}{\sqrt{3}}.$$

The equilibrium distribution read

Fig. 5.4.1. *The speed of sound c_s as a function of the parameter r.*

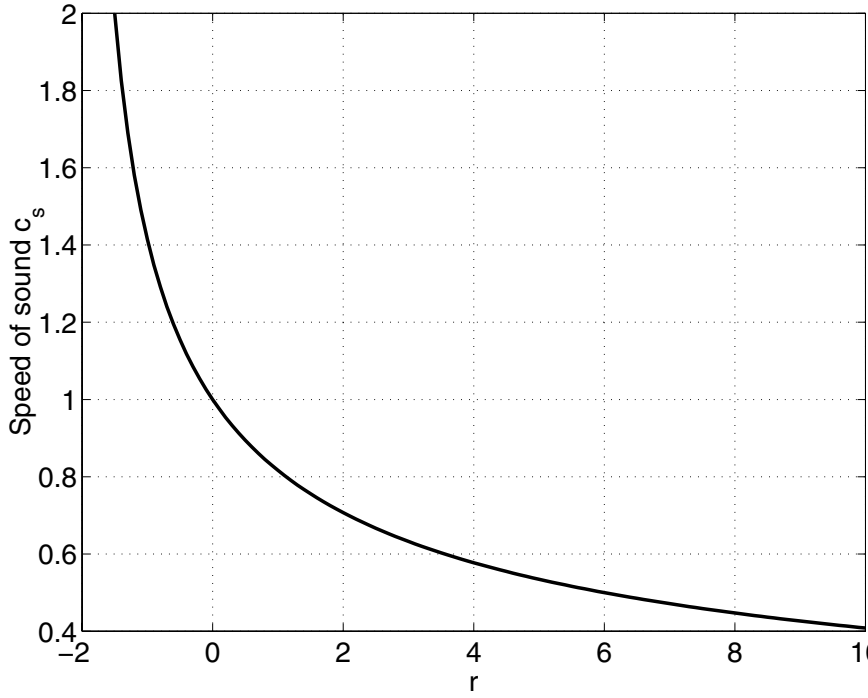

$$
\begin{aligned}
F_i &= \frac{4}{9}\rho \left[1 - \frac{3}{2}\boldsymbol{u}^2\right] && i = 0 \\
F_i &= \frac{1}{9}\rho \left[1 + 3\boldsymbol{c}_i \cdot \boldsymbol{u} + \frac{9}{2}(\boldsymbol{c}_i \cdot \boldsymbol{u})^2 - \frac{3}{2}\boldsymbol{u}^2\right] && i = 1, 2, 3, 4 \\
F_i &= \frac{1}{36}\rho \left[1 + 3\boldsymbol{c}_i \cdot \boldsymbol{u} + \frac{9}{2}(\boldsymbol{c}_i \cdot \boldsymbol{u})^2 - \frac{3}{2}\boldsymbol{u}^2\right] && i = 5, 6, 7, 8.
\end{aligned}
$$

The distribution functions are identical to those derived by the maximum entropy principle (compare Eq. 5.2.12 with $c = 1$)! These equilibrium distributions were also used by Martinez et al. (1994).
In summary, the equilibrium distribution have been derived in the current section by adjusting the free parameters of a plausible ansatz after the multi-scale analysis such that the desired macroscopic equations will result. For the model discussed above, there are not enough constraints to derive a unique solution for all free parameters. This freedom can be used, for example, to tune the speed of sound. The equilibrium distribution derived by the maximum entropy principle is a special case of the above calculated solutions.
The alternative approach to derive equilibrium distributions opens up the prospect to develop lattice Boltzmann models for other differential equations. From an ansatz for the equilibrium distributions and the conservation laws the desired properties of the macroscopic equations can be implemented into the microscopic model by appropriate choice of the free parameter after the multi-scale analysis. The ansatz method will be applied in the development of thermal LBM (Section 5.5) and LBM for the diffusion equation (Section 5.8).

5.4.2 Negative distribution functions at high speed of sound

Eq. (5.4.5) suggests that the speed of sound c_s might be tuned to arbitrary values by variing the parameter r. For small or even negative r, however, the distribution functions F_{si} become negative which leads to numerical instability very quickly. Let r_c be the critical r where one of the F_{si} first vanishes. It can be shown (see Exercise 5.4.2) that r_c depends on the velocity $\boldsymbol{u}$ as follows

$$r_c = \frac{2\boldsymbol{u}^2}{1 - \boldsymbol{u}^2} \tag{5.4.6}$$

and therefore

$$c_s < c_s(r_c) = \sqrt{1 - \boldsymbol{u}^2}. \tag{5.4.7}$$

The Navier-Stokes equation has been derived in the small Mach number limit. Thus

$$M_a := \frac{|\boldsymbol{u}|}{c_s} = \frac{|\boldsymbol{u}|}{\sqrt{1 - \boldsymbol{u}^2}} \tag{5.4.8}$$

should remain small compared to 1. Consequently $\boldsymbol{u}^2$ must remain small compared to 1 (singularity of M at $\boldsymbol{u}^2 = 1$) and therefore $c_s < 1$ (compare Fig. 5.4.2).

Fig. 5.4.2. *The Mach number M_a and the speed of sound c_s as a function of the speed $|\boldsymbol{u}|$.*

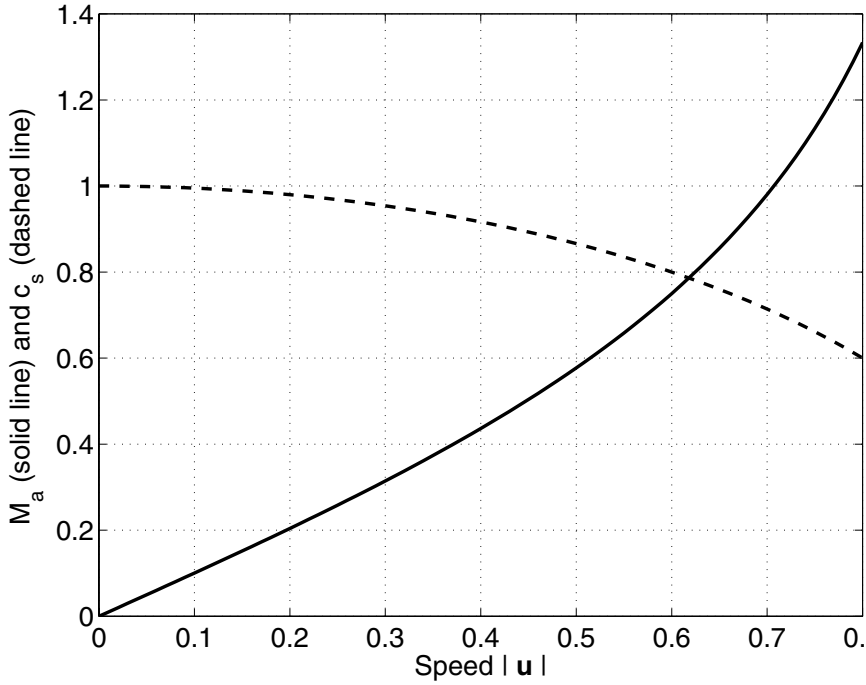

Exercise 5.4.1. (***)
Show that even when skipping the auxiliary constraints (5.4.4) while keeping $F_{si} > 0$ the speed of sound cannot exceed 1.

Exercise 5.4.2. (**)
Derive eq. (5.4.6).

Exercise 5.4.3. (***)
Calculate equilibrium distributions for an LBM for the Navier-Stokes equation in 2D over the D2Q7 lattice (FHP with rest particles). This model is called *pressure-corrected* LBM (PCLBM) because the pressure does not depend explicitly on the flow speed.

5.5 Hydrodynamic LBM with energy equation

Using the ansatz method described in Section 5.4 it is possible to develop hydrodynamic LBMs including an energy equation (so-called thermal models).

Alexander, Chen and Sterling (1993) proposed a thermal LBM over the D2Q13-FHP lattice (multi-speed FHP) with the following lattice velocities $\boldsymbol{c}_i$ (compare Fig. 3.3.8):

$$\begin{aligned}
\boldsymbol{c}_i &= (0,0) && i=0\\
\boldsymbol{c}_i &= \left(\cos\frac{2\pi k}{6}, \sin\frac{2\pi k}{6}\right) && i=1,2,...,6; \quad k=i\\
\boldsymbol{c}_i &= 2\left(\cos\frac{2\pi k}{6}, \sin\frac{2\pi k}{6}\right) && i=7,8,...,12; \quad k=i-6
\end{aligned}$$

For the equilibrium distributions they made an ansatz including terms up to third order in the flow velocity $\boldsymbol{u}$

$$F_i^{eq} = A_\sigma + B_\sigma \boldsymbol{c}_i\cdot\boldsymbol{u} + C_\sigma(\boldsymbol{c}_i\cdot\boldsymbol{u})^2 + D_\sigma \boldsymbol{u}^2 + E_\sigma(\boldsymbol{c}_i\cdot\boldsymbol{u})^3 + G_\sigma(\boldsymbol{c}_i\cdot\boldsymbol{u})\boldsymbol{u}^2, \quad (5.5.1)$$

whereby the 14 free parameters A_σ to G_σ depend only on mass and internal energy density. The index σ refers to the square of the speed which is equal to zero, one, or two.
The BGK kinetic equation

$$F_i(\boldsymbol{x}+\boldsymbol{c}_i, t+1) = (1-\omega)F_i + \omega F_i^{eq} \quad (5.5.2)$$

is applied.
Mass density (ρ), velocity ($\boldsymbol{u}$) and internal energy (ε_I) are defined as follows

$$\rho = \sum_i F_i \quad (5.5.3)$$

$$\rho\boldsymbol{u} = \sum_i \boldsymbol{c}_i F_i \quad (5.5.4)$$

$$\rho\varepsilon_I = \sum_i \frac{(\boldsymbol{c}_i-\boldsymbol{u})^2}{2} F_i. \quad (5.5.5)$$

The desired form of the macroscopic equations

$$\frac{\partial\rho}{\partial t} + \frac{\partial}{\partial x_\alpha}(\rho u_\alpha) = 0 \quad (5.5.6)$$

$$\rho\frac{\partial u_\alpha}{\partial t}+\rho u_\beta\frac{\partial u_\alpha}{\partial x_\beta}=-\frac{\partial p}{\partial x_\alpha}+\frac{\partial}{\partial x_\alpha}\left(\lambda\frac{\partial u_\gamma}{\partial x_\gamma}\right)+\frac{\partial}{\partial x_\beta}\left[\mu\left(\frac{\partial u_\beta}{\partial x_\alpha}+\frac{\partial u_\alpha}{\partial x_\beta}\right)\right] \quad (5.5.7)$$

$$\rho\frac{\partial \varepsilon_I}{\partial t}+\rho u_\beta\frac{\partial \varepsilon_I}{\partial x_\beta}=-p\frac{\partial u_\gamma}{\partial x_\gamma}+\frac{\partial}{\partial x_\beta}\left(\kappa\frac{\partial T}{\partial x_\beta}\right)+\mu\left(\frac{\partial u_\beta}{\partial x_\alpha}+\frac{\partial u_\alpha}{\partial x_\beta}\right)\frac{\partial u_\beta}{\partial x_\alpha}+\lambda\left(\frac{\partial u_\gamma}{\partial x_\gamma}\right)^2 \quad (5.5.8)$$

is obtained by the following choice for the coefficients (see Appendix 6.4)

$$A_0=\rho\left(1-\frac{5}{2}\varepsilon_I+2\varepsilon_I^2\right),\quad A_1=\rho\frac{4}{9}\left(\varepsilon_I-\varepsilon_I^2\right),\quad A_2=\rho\frac{1}{36}\left(-\varepsilon_I+4\varepsilon_I^2\right) \quad (5.5.9)$$

$$B_1=\rho\frac{4}{9}\left(1-\varepsilon_I\right),\quad B_2=\rho\frac{1}{36}\left(-1+4\varepsilon_I\right) \quad (5.5.10)$$

$$C_1=\rho\frac{4}{9}\left(2-3\varepsilon_I\right),\quad C_2=\rho\frac{1}{72}\left(-1+6\varepsilon_I\right) \quad (5.5.11)$$

$$D_0=\rho\frac{1}{4}\left(-5+8\varepsilon_I\right),\quad D_1=\rho\frac{2}{9}\left(-1+\varepsilon_I\right),\quad D_2=\rho\frac{1}{72}\left(1-4\varepsilon_I\right) \quad (5.5.12)$$

$$E_1=-\rho\frac{4}{27},\quad E_2=\rho\frac{1}{108} \quad (5.5.13)$$

$$G_1=G_2=0. \quad (5.5.14)$$

Alexander et al. (1993) give no statement concerning the uniqueness of the solution. The shear viscosity μ and the thermal conductivity κ are given by

$$\mu=\rho\varepsilon_I\left(\frac{1}{\omega}-\frac{1}{2}\right) \quad (5.5.15)$$

$$\kappa=2\rho\varepsilon_I\left(\frac{1}{\omega}-\frac{1}{2}\right) \quad (5.5.16)$$

(the compressional viscosity λ vanishes). Thus the Prandtl number is

$$Pr:=\frac{\mu}{\kappa}=\frac{1}{2}. \quad (5.5.17)$$

The pressure p reads $p=\rho\varepsilon_I$. The temperature T is proportional to the internal energy ε_I.

Exercise 5.5.1. (**)
Is it possible to define a thermal LBM over the D2Q9 lattice?

Exercise 5.5.2. (***)
Is it possible to choose the coefficients such that the Prandtl number is 1 or even becomes a tunable parameter?

Further reading:
Chen et al. (1995a,b) introduced an additional parameter in order to tune the Prandtl number. McNamara et al. (1995) discussed numerical instabilities of the models proposed by Alexander et al. (1993) and Chen et al. (1995a,b). Vahala et al. (1996) applied the model of Alexander et al. (1993) to free-decaying turbulence in 2D. McNamara et al. (1997) proposed a 3D thermal LBM with 27 velocities. They apply a Lax-Wendroff scheme in order to improve numerical stability. They performed simulations of Rayleigh-Bénard convection in 2D and compared the results with those of an explicit finite-difference (FD) solver. The computer times of LBM and FD are comparable whereas LBM requires significantly more memory and stability is significantly poorer. Thus they conclude that currently there is no potential advantage in using a thermal LBM over a conventional FD solver. Hu et al. (1997) consider the energy levels, ε_σ, of the three different speeds as free parameters and thereby are able to tune the ratio of specific heats, γ. Shan (1997) proposed a two-component LBGK in which temperature is advected as an passive scalar and simulated Rayleigh-Bénard convection. Pavlo et al. (1998a,b) investigate linear stability of thermal LBMs. The model of Alexander et al. (1993) has been revisited by Boghosian and Coveney (1998). They showed "that it is possible to achieve variable (albeit density-dependent) Prandtl number even within a single-relaxation-time lattice-BGK model". He et al. (1998), Vahala et al. (1998b).

5.6 Stability of lattice Boltzmann models

Lattice Boltzmann schemes do not have an H-theorem and therefore are subject to numerical instabilities (Sterling and Chen, 1996). Linear stability analysis has been performed for various LB models (D2Q7, D2Q9, D3Q15) and different background flows (homogeneous or shear flow) by Sterling and Chen (1996) and Worthing et al. (1997). The stability does not only depend on the background flow but also on the mass fraction parameters (α, β) of the equilibrium distributions and the grid size (stability decreases with increasing grid size).

5.6.1 Nonlinear stability analysis of uniform flows

The time evolution of BGK lattice Boltzmann models is described by the kinetic equation

$$F_m(\boldsymbol{x}+\boldsymbol{c}_m, t+1) = F_m(\boldsymbol{x}, t) - \omega\left[F_m(\boldsymbol{x}, t) - F_m^{(0)}(\boldsymbol{x}, t)\right] \tag{5.6.1}$$

Inspection of Eq. (5.6.1) shows that an initially uniform flow, in the sense

$$F_m(\boldsymbol{x}, t_0) = F_m(t_0),$$

will remain uniform at all later times and thus

$$F_m(t+1) = F_m(t) - \omega\left[F_m(t) - F_m^{(0)}(t)\right].$$

Furthermore, mass and momentum density are conserved and retain their initial value

$$\rho(\boldsymbol{x}, t) = \rho(t_0) = \rho_0, \quad \boldsymbol{j}(\boldsymbol{x}, t) = \boldsymbol{j}(t_0) = \boldsymbol{j}_0$$

and therefore

$$F_m(t+1) = F_m(t) - \omega\left[F_m(t) - F_m^{(0)}(\rho_0, \boldsymbol{j}_0)\right].$$

Subtracting $F_m^{(0)}(\rho_0, \boldsymbol{j}_0)$ on both sides leads to

$$\tilde{F}_m(t+1) = (1-\omega)\tilde{F}_m(t)$$

with $\tilde{F}_m(t) = F_m(t) - F_m^{(0)}(\rho_0, \boldsymbol{j}_0)$. The evolution is stable in the sense that the magnitude of $\tilde{F}_m$ does not increase with time ($|\tilde{F}_m(t+1)| \leq |\tilde{F}_m(t)|$) if

$$|1-\omega| < 1 \quad \rightarrow \quad 0 < \omega < 2 \quad \text{or} \quad \frac{1}{\omega} = \tau > \frac{1}{2}$$

(compare Fig. 5.6.1).

Fig. 5.6.1. *Stability range of BGK models.*

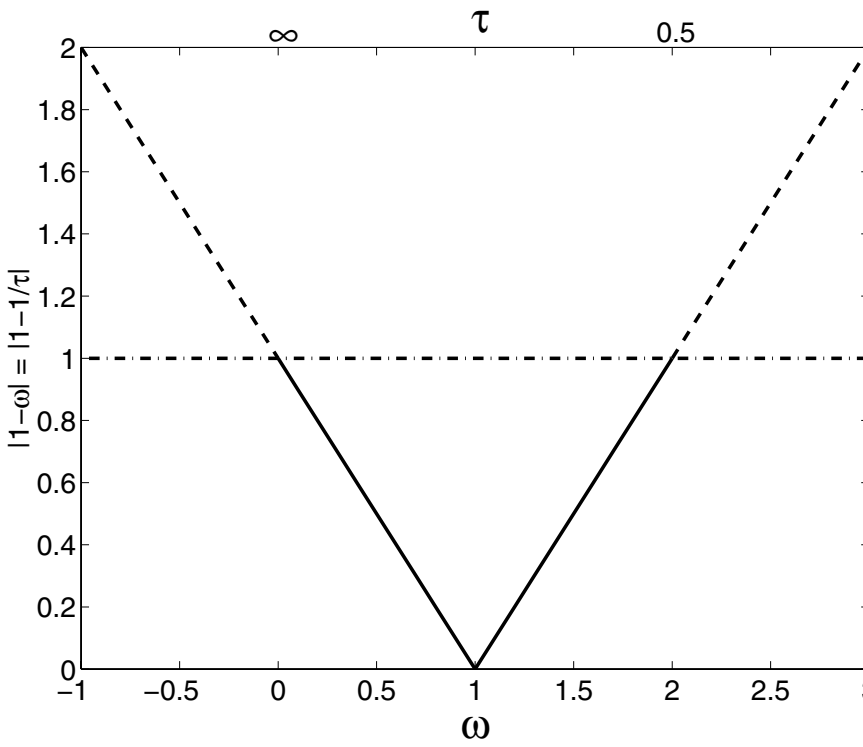

Exercise 5.6.1. (**)
Consider the kinetic equation

$$F_m(\boldsymbol{x}+\boldsymbol{c}_m, t+1) = F_m(\boldsymbol{x}, t) + \Omega_{ik}\left[F_k(\boldsymbol{x}, t) - F_k^{(0)}(\boldsymbol{x}, t)\right]$$

and show that for uniform flows the following equation holds

$$\tilde{\boldsymbol{F}}(t+1) = [\mathbf{I} + \boldsymbol{\Omega}]\tilde{\boldsymbol{F}}(t)$$

where the vector $\tilde{\boldsymbol{F}}(t)$ has components $\tilde{F}_m(t) = F_m(t) - F_m^{(0)}(\rho_0, \boldsymbol{j}_0)$.

In reality, a flow is never uniform in the strict sense because some noise is always around. Therefore we have to investigate whether small spatially varying perturbations grow or are damped with time. No general methods are known that allow stability analysis of arbitrary nonlinear systems. In each case you have to find special tricks (like, for instance, the construction of a Liapunov function). To get an idea of the stability properties of the nonlinear system one usually expands the system up to linear terms and investigates the stability of the resulting linear system. Before attacking the kinetic equation (5.6.1) we will discuss the *von Neumann stability analysis* for two simpler equations.

5.6.2 The method of linear stability analysis (von Neumann)

The Fourier method of John von Neumann is the standard method for stability analysis because it is applicable to arbitrary linear systems. As a first example we will consider the linear advection equation

$$\frac{\partial u}{\partial t} + c\frac{\partial u}{\partial x} = 0, \quad c > 0$$

which shall be solved numerically by the following finite difference scheme

$$u_{j,n+1} = u_{j,n} - \mu\,(u_{j,n} - u_{j-1,n}) \tag{5.6.2}$$

where $u_{j,n} = u(x_j, t_n)$, $x_j = j\Delta x$, $t_n = n\Delta t$, and $\mu = c \cdot \Delta t/\Delta x$. For the difference equation (5.6.2) we make the following ansatz ('poor man's Fourier transform')

$$u_{j,n} = U_n e^{ikx} = U_n e^{ikj\Delta x} \tag{5.6.3}$$

(the actual solution is the real part) where k is the wave number of the spatial perturbation. Inserting of (5.6.3) into (5.6.2) leads to

$$U_{n+1} = (1-\mu)U_n + \mu U_n e^{-ik\Delta x} = \lambda U_n$$

with

$$\lambda := 1 - \mu + \mu e^{-ik\Delta x}.$$

It follows that

$$|U_{n+1}| = |\lambda| \cdot |U_n| = |\lambda|^n \cdot |U_1|.$$

Stability in the sense that $|U_{n+1}|$ is bounded (i.e. $\lim_{n\to\infty} |U_{n+1}| < B < \infty$) yields the constraint

$$|\lambda| \leq 1.$$

Here we have

$$|\lambda|^2 = 1 - 2\mu(1-\mu)(1-\cos k\Delta x)$$

which is ≤ 1 when

$$0 \leq \mu = c\frac{\Delta t}{\Delta x} \leq 1$$

or

$$\frac{\Delta x}{\Delta t} \geq c \tag{5.6.4}$$

or

$$\boxed{0 \leq \Delta t \leq \frac{\Delta x}{c}.} \tag{5.6.5}$$

This is the stability condition we were looking for. According to Eq. (5.6.4) the 'grid speed' $c_{grid} := \Delta x/\Delta t$ has to be as fast or faster than the advection speed c (this holds in very similar form also for several spatial dimensions, for other explicit numerical schemes and other hyperbolic equations whereby the advection speed is eventually replaced by the speed of the fastes wave of the system).

As a second example we consider the diffusion equation

$$\frac{\partial T}{\partial t} = \kappa \frac{\partial^2 T}{\partial x^2}.$$

A finite difference approximation reads

$$T_{j,n+1} = T_{j,n} + \kappa \frac{\Delta t}{(\Delta x)^2} \left(T_{j+1,n} - 2T_{j,n} + T_{j-1,n}\right).$$

Inserting the ansatz

$$T_{j,n} = A_n e^{ikj\Delta x}$$

leads to

$$A_{n+1} = A_n + \mu' A_n \left(e^{ik\Delta x} - 2 + e^{-ik\Delta x}\right) = \lambda' A_n$$

with

$$\mu' = \kappa \frac{\Delta t}{(\Delta x)^2}$$

and

$$\lambda' = 1 - 2\mu'(1 - \cos k\Delta x)$$

The condition $|\lambda'| \leq 1$ yields the stability condition

$$0 \leq \mu' = \kappa \frac{\Delta t}{(\Delta x)^2} \leq \frac{1}{2}$$

or

$$\boxed{0 \leq \Delta t \leq \frac{(\Delta x)^2}{2\kappa}.} \tag{5.6.6}$$

5.6.3 Linear stability analysis of BGK lattice Boltzmann models

The following discussion is based on Worthing et al. (1997). The kinetic equation including external body forces $K_m(\boldsymbol{x},t)$ reads

$$F_m(\boldsymbol{x}+\boldsymbol{c}_m,t+1)=F_m(\boldsymbol{x},t)-\omega\left[F_m(\boldsymbol{x},t)-F_m^{(0)}(\boldsymbol{x},t)\right]+K_m(\boldsymbol{x},t) \quad (5.6.7)$$

where F_m are the distribution functions and $F_m^{(0)}$ are the equilibrium distribution functions. Expansion about time-independent but otherwise arbitrary distribution functions $F_m^{(bf)}$ ('background flow') leads to

$$\begin{aligned}
F_m(\boldsymbol{x},t) &= F_m^{(bf)}(\boldsymbol{x})+f_m(\boldsymbol{x},t)\\
F_m(\boldsymbol{x}+\boldsymbol{c}_m,t+1) &= F_m^{(bf)}(\boldsymbol{x}+\boldsymbol{c}_m)+f_m(\boldsymbol{x}+\boldsymbol{c}_m,t+1)\\
F_m^{(0)}(\boldsymbol{x},t) &= F_m^{(0)}(\{F_s(\boldsymbol{x},t)\})\\
&\approx F_m^{(0)}\left(\{F_s^{(bf)}(\boldsymbol{x})\}\right)+\sum_n\left(\frac{\partial F_m^{(0)}}{\partial F_n}\right)_{\{F_s^{(bf)}(\boldsymbol{x})\}}f_n(\boldsymbol{x},t)\\
K_m(\boldsymbol{x},t) &= K_m(\{F_s(\boldsymbol{x},t)\})\\
&\approx K_m\left(\{F_s^{(bf)}(\boldsymbol{x})\}\right)+\sum_n\left(\frac{\partial K_m}{\partial F_n}\right)_{\{F_s^{(bf)}(\boldsymbol{x})\}}f_n(\boldsymbol{x},t)
\end{aligned}$$

Inserting the expansions into the kinetic equation (5.6.7) results in

$$f_m(\boldsymbol{x}+\boldsymbol{c}_m,t+1)=G_m(\boldsymbol{x})+(1-\omega)f_m(\boldsymbol{x},t)+\sum_n J_{mn}(\boldsymbol{x})f_n(\boldsymbol{x},t)$$

where

$$\begin{aligned}
G_m(\boldsymbol{x}) &= F_m^{(bf)}(\boldsymbol{x})-F_m^{(bf)}(\boldsymbol{x}+\boldsymbol{c}_m)-\omega\left[F_m^{(bf)}(\boldsymbol{x})-F_m^{(0)}\left(\{F_s^{(bf)}(\boldsymbol{x})\}\right)\right]\\
&\quad +K_m\left(F_m^{(bf)}(\boldsymbol{x})\right)
\end{aligned}$$

and

$$J_{mn}=\left[\omega\frac{\partial F_m^{(0)}}{\partial F_n}+\frac{\partial K_m}{\partial F_n}\right]_{\{F_s^{(bf)}(\boldsymbol{x})\}}. \quad (5.6.8)$$

Here we are interested only in instabilities with exponential growth. Therefore we will neglect the time-independent term $G_m(\boldsymbol{x})$ which can lead to linear growth at most. The rectangular domain of length L and width W comprises a lattice with nodes at $(x_r=0,1,2,...,L;y_s=0,1,2,...,W)$. We will now Fourier transform the linear equation

$$f_m(\boldsymbol{x}+\boldsymbol{c}_m,t+1)=(1-\omega)f_m(\boldsymbol{x},t)+\sum_n J_{mn}(\boldsymbol{x})f_n(\boldsymbol{x},t). \tag{5.6.9}$$

The functions $f_m^{(k,l)}(t)$ and $f_m(x,y,t)$ are connected by the Fourier transform

$$f_m(x,y,t)=\sum_{k,l} f_m^{(k,l)}(t)e^{ikx2\pi/L}e^{ily2\pi/W}. \tag{5.6.10}$$

Consequently one obtains

$$\begin{aligned} & f_m(x+c_{x,m},y+c_{y,m},t+1) \\ = & \sum_{k,l} f_m^{(k,l)}(t+1)e^{ik(x+c_{x,m})2\pi/L}e^{il(y+c_{y,m})2\pi/W} \\ = & \sum_{k,l} f_m^{(k,l)}(t+1)e^{ikx2\pi/L}e^{ily2\pi/W}e^{ikc_{x,m}2\pi/L}e^{ilc_{y,m}2\pi/W} \end{aligned}$$

The analysis is further simplified by the assumption that the background flow (a shear layer or jet stream, for example) as well as the external forces depend only on y:

$$J_{mn}(y)=\sum_q J_{mn}^{(q)}e^{iqy2\pi/W}.$$

Inserting of the Fourier transforms into Eq. (5.6.9) one obtains

$$e^{ikc_{x,m}2\pi/L}e^{ilc_{y,m}2\pi/W}f_m^{(k,l)}(t+1)=(1-\omega)f_m^{(k,l)}(t)+\sum_{n,q} J_{mn}^{(q)}f_n^{(k,l-q)}(t)$$

Since the x modes remain uncoupled, they are considered independently via

$$e^{ikc_{x,m}2\pi/L}e^{ilc_{y,m}2\pi/W}f_m^{(l)}(t+1)=(1-\omega)f_m^{(l)}(t)+\sum_{n,q} J_{mn}^{(q)}f_n^{(l-q)}(t) \tag{5.6.11}$$

It can be shown (for some fine points see Worthing et al., 1997) that Eq. (5.6.11) can be written as a matrix iteration

$$\boldsymbol{f}_{t+1}=\mathcal{A}\boldsymbol{f}_t \tag{5.6.12}$$

where the vector $\boldsymbol{f}$ has components $f_m^{(l)}$. If the spectral radius (= magnitude of the largest eigenvalue) of $\mathcal{A}$, $\rho(\mathcal{A})$, is larger than unity, then the system is said to be linear unstable (this corresponds to the case $|\lambda|>1$ in the two examples with one component each discussed in Subsection 5.6.2). In case of uniform background flow and no external forcing considered by Sterling and Chen (1996) the matrix $\mathcal{A}$ reads

$$\boxed{\mathcal{A}=\boldsymbol{D}\left[(1-\omega)\,\boldsymbol{I}+\boldsymbol{J}\right]} \tag{5.6.13}$$

where $\boldsymbol{D}$ is a diagonal matrix with components

$$D_{mn} = e^{-ikc_{x,m}2\pi/L} e^{-ilc_{y,m}2\pi/W} \delta_{mn}, \tag{5.6.14}$$

$\boldsymbol{I}$ is the identity matrix (diagonal matrix with value 1 of all diagonal components) and the components of $\boldsymbol{J}$ are given by

$$J_{mn} = \omega \frac{\partial F_m^{(0)}}{\partial F_n}. \tag{5.6.15}$$

The matrix $\mathcal{A}$ (and therefore also its spectral radius $\rho(\mathcal{A})$) depends on the relative wave numbers ($\theta_x = 2\pi k/L$, $\theta_y = 2\pi l/W$), the uniform inital velocity (U), the collision parameter (ω) and the rest mass parameters (α, β; see below). Instability occurs if the maximal spectral radius (for given values of U, ω, α and β) becomes larger than 1 for any wave number:

$$\max_{\theta_x,\theta_y} \rho\left(\mathcal{A}\left[\theta_x, \theta_y, U, \omega, \alpha, \beta\right]\right) > 1. \tag{5.6.16}$$

The components of $\boldsymbol{J}$ may be calculated as follows. The equilibrium distributions for the models D2Q7, D2Q9 and D3Q15 are all of the form

$$F_m^{(0)} = \rho\left[A_m + B_m \boldsymbol{c}_m \cdot \boldsymbol{u} + C_m (\boldsymbol{c}_m \cdot \boldsymbol{u})^2 + D_m \boldsymbol{u}^2\right]$$

with constants A_m, ..., D_m. The derivatives of mass and momentum density with respect to F_n are easy to calculate:

$$\rho = \sum_n F_n, \quad \rightarrow \quad \frac{\partial \rho}{\partial F_m} = 1,$$

$$\boldsymbol{j} = \rho \boldsymbol{u} = \sum_n F_n \boldsymbol{c}_n, \quad \rightarrow \quad \frac{\partial \boldsymbol{j}}{\partial F_n} = \boldsymbol{c}_n$$

and consequently

$$\rho \boldsymbol{u}^2 = \frac{\boldsymbol{j}^2}{\rho}, \quad \rightarrow \quad \frac{\partial(\rho \boldsymbol{u}^2)}{\partial F_n} = \frac{2\boldsymbol{j}\frac{\partial \boldsymbol{j}}{\partial F_n}\rho - \frac{\partial \rho}{\partial F_n}\boldsymbol{j}^2}{\rho^2} = 2\boldsymbol{c}_n \cdot u - \boldsymbol{u}^2.$$

Finally we obtain

$$\begin{aligned} \frac{\partial F_m^{(0)}}{\partial F_n} &= A_m + B_m \boldsymbol{c}_m \cdot \boldsymbol{c}_n + C_m\left[2(\boldsymbol{c}_m \cdot \boldsymbol{c}_n)(\boldsymbol{c}_m \cdot \boldsymbol{u}) - (\boldsymbol{c}_m \cdot \boldsymbol{u})^2\right] \\ &\quad + D_m\left[2\boldsymbol{c}_n \cdot \boldsymbol{u} - \boldsymbol{u}^2\right]. \end{aligned}$$

The coefficients for the various models are listed below. The coefficients A_m include free parameters α and β (denoted as *rest mass parameters*) which can be tuned in order to improve stability.

FHP (D2Q7).

$$\begin{array}{llllll} A_m = \alpha, & B_m = 0, & C_m = 0, & D_m = -1; & m = 0 \\ A_m = \dfrac{1-\alpha}{6}, & B_m = \frac{1}{3}, & C_m = \frac{2}{3}, & D_m = -\frac{1}{6}; & m = 1, ..., 6. \end{array}$$

D2Q9.

$$\begin{array}{llllll} A_m = \alpha, & B_m = 0, & C_m = 0, & D_m = -\frac{2}{3}; & m = 0 \\ A_m = \beta, & B_m = \frac{1}{3}, & C_m = \frac{1}{2}, & D_m = -\frac{1}{6}; & m = 1, ..., 4 \\ A_m = \dfrac{1-\alpha-4\beta}{4}, & B_m = \frac{1}{12}, & C_m = \frac{1}{8}, & D_m = -\frac{1}{24}; & m = 5, ..., 8 \end{array}$$

D3Q15.

$$\begin{array}{llll} m = 0: & & & \\ A_m = \alpha, & B_m = 0, & C_m = 0, & D_m = -\frac{1}{2}. \\ m = 1, ..., 6: & & & \\ A_m = \beta, & B_m = \frac{1}{3}, & C_m = \frac{1}{2}, & D_m = -\frac{1}{6}. \\ m = 7, ..., 14: & & & \\ A_m = \dfrac{1-6\beta-\alpha}{8}, & B_m = \frac{1}{24}, & C_m = \frac{1}{16}, & D_m = -\frac{1}{48}. \end{array}$$

The eigenvalues of $\mathcal{A}$ have been calculated with a standard routine form MATLAB. The maximum eigenvalues for the D2Q7 (FHP) model with 1.) $(u, v) = (0.2, 0)$, $\alpha = 0.2$, $\theta_y = 0$ (solid line) and 2.) $(u, v) = (0.23, 0)$, $\alpha = 0.3$, $\theta_y = 0$ (broken line) are shown in Fig. 5.6.2 as a function of the relative wave number θ_x (the figure is identical to Figure 1 in Sterling and Chen (1996); this problem served as a test of the MATLAB script). For certain wave numbers the maximum eigenvalues become larger than unity and therefore the model is linear unstable for this choice of parameters. Detailed results on stability boundaries depending on the model parameters can be found in Sterling and Chen (1996) and Worthing et al. (1997).

5.6.4 Summary

The main results of Sterling and Chen (1996) and Worthing et al. (1997) can be summarized as follows:

– For the D2Q7 (FHP) model and homogeneous flow the wavenumber vector $\boldsymbol{k}$ of the most unstable mode is parallel to the velocity $\boldsymbol{u}$.

Fig. 5.6.2. *The maximum eigenvalues for the D2Q7 (FHP) model with 1.)* $(u, v) = (0.2, 0)$, $\alpha = 0.2$, $\theta_y = 0$ *(solid line) and 2.)* $(u, v) = (0.23, 0)$, $\alpha = 0.3$, $\theta_y = 0$ *(broken line) are shown as a function of the relative wave number* θ_x *(compare Fig. 1 in Sterling and Chen, 1996).*

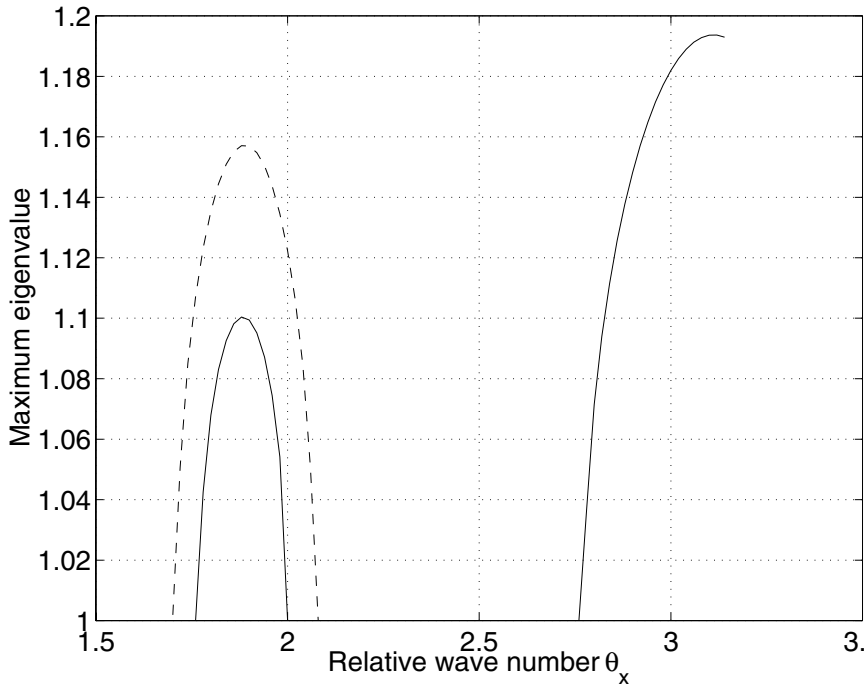

- For the D2Q9 model and homogeneous flow the wavenumber $|\boldsymbol{k}|$ of the most unstable mode is equal to about 2.3 ($\boldsymbol{k}$ is not necessary parallel to $\boldsymbol{u}$). An explanation for the 'magic' value 2.3 is not known.
- The stability domain as a function of the rest mass parameters α and β of the D2Q9 model shrinks with increasing lattice size. The 'canonical' values $\alpha = 4/9$, $\beta = 1/9$, which have been derived from maximum entropy principle (compare Section 5.2), lie inside one of the stability islands (compare Fig. 5.6.3).
- The D2Q7 model is less stable than the D2Q9 model in the sense that instability occurs already at smaller flow velocities (compare Fig. 2 in Sterling and Chen, 1996).
- The D2Q9 lattice is a projection of the D3Q15 lattice. Therefore it may be come at no big surprise that their linear stability properties for homogeneous background flows show some similarities. The wavenumber $|\boldsymbol{k}|$ of the most unstable mode is again equal to about 2.3 (Sterling and Chen, 1996).
- The stability domain shrinks further when the background flow includes shear. Please note that the usual linear stability analysis assumes a time-independent background flow whereas free shear layers decay by momentum diffusion. Therefore predictions from linear stability analysis are less reliable at high viscosities where the shear flow may decay before an instability has enough time to develop. Thus the unstable region is smaller than predicted (see, for example, Fig. 9 in Worthing et al., 1997). However, the linear stability analysis works fine in the low viscosity region (high Reynolds numbers) which is of most interest.

To the best of our knowledge linear stability analysis for D3Q19 and for thermal LB models is not available yet.

Exercise 5.6.2. (***)
Propose equilibrium distributions with rest mass parameters α and β for the D3Q19 model, investigate linear stability and compare the results with the linear stability properties of D3Q15.

Fig. 5.6.3. *Contour plot of the spectral radius as a function of the rest mass parameters α and β for the D2Q9 model. On a lattice with 64 times 64 grid points the stability region shrinks to small islands (domains inside the contour lines). The 'canonical' values $\alpha = 4/9$, $\beta = 1/9$, which have been derived from maximum entropy principle, lie inside one of the stability islands.*

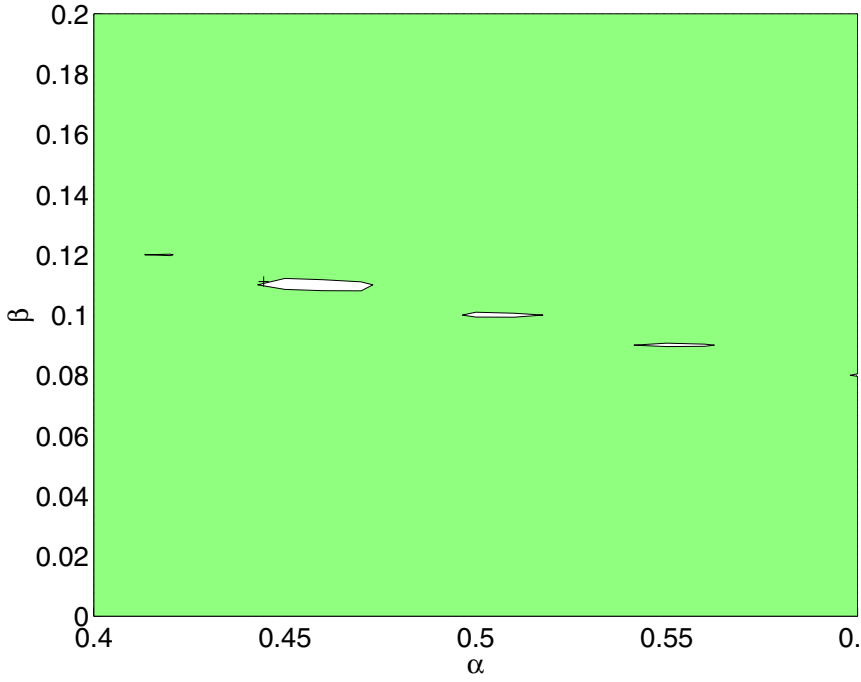

5.7 Simulating ocean circulation with LBM

Additional forces - wind stress, Coriolis force, and frictional forces - were implemented into a LB model with 9 lattice velocities in two dimensions (D2Q9). With this extended model it is possible to simulate the wind-driven circulation of a barotropic ocean. Model results are compared with analytical solutions of the linearized problem by Munk and with a finite difference model of the full nonlinear problem. The implementation of various boundary conditions and of body forces is discussed in some detail.

5.7.1 Introduction

Despite the rapid development of computer technology during the last decades, simulation of global ocean circulation is still limited by computer resources because of several small scale processes which are relevant for large scale features. Increasing computer power will not solve these problems during the next few years. More promissing is the development of new methods like 'active nesting' (Spall and Holland, 1991, Fox and Maskell, 1995 and 1996) to deal with small scale dynamics in selected areas or the application of other numerical methods like finite elements or LB models.
Because of the strict locality of the 'collisions' in LB models they are especially well suited for massive parallel computers. The code is extremely simple compared to typical ocean circulation models like MOM (Pacanowski et al., 1991). No elliptic equation has to be solved. Here the simplest case will be considered, namely the wind-driven circulation of a barotropic ocean in a rectangular domain. The main goal of this work is to test whether the LB model yields results which are in quantitative agreement with the analytical solution of the linearized problem and with the numerical (finite differences, finite volumes) solution of the nonlinear problem.

5.7.2 The model of Munk (1950)

One of the grand challenges of physical oceanography in the first half of the 20th century was the explanation of the western boundary currents like the Gulf Stream, the Agulhas or the Kuroshio. Ekman (1905 and 1923), Sverdrup (1947) and others had made important contributions to the theory of wind-driven circulation but could not explain the intensification of the flow near the western boundaries of oceanic basins. In the late 40ties in the time span of only two years different approaches for the basin-wide circulation were proposed by Stommel (1948) and Munk (1950) .
With the North Atlantic in mind Munk defined the following problem. Consider a rectangular ($L \times H$) flat-bottom barotropic (vertically integrated)

ocean which is driven by wind stress of the form (locally cartesian coordinates x, y where x is eastward and y northward)

$$T_x = -T_0 \cos\left(\frac{\pi}{H} y\right) \quad \text{and} \quad T_y = 0, \tag{5.7.1}$$

corresponding to westerly wind in mid latitudes and easterly wind in low latitudes. The Navier-Stokes equation contains only molecular diffusion as dissipative process. For large scale oceanic circulation molecular diffusion does not play a role. To get rid of the vorticity imparted by the wind Munk replaced the molecular viscosity coefficient, ν, by the so-called *eddy viscosity coefficient*, A, which is several orders of magnitude larger than ν. The *Laplacian friction*, $A\nabla^2 \boldsymbol{u}$, can be interpreted as a simple parameterization of subscale processes. The equation of motion thus reads

$$\frac{\partial \boldsymbol{u}}{\partial t} + (\boldsymbol{u}\boldsymbol{\nabla})\,\boldsymbol{u} + f\hat{\mathbf{u}} + \frac{1}{\rho}\boldsymbol{\nabla} p - A\nabla^2 \boldsymbol{u} - \boldsymbol{T} = 0 \tag{5.7.2}$$

with $\hat{\mathbf{u}} = (-v, u)$. The Coriolis parameter f is approximated by $f \simeq f_0 + \beta y$ (β-plane), where

$$f_0 = 2\Omega \sin\varphi_0 \quad \text{and} \quad \beta = \left(\frac{\partial f}{\partial y}\right)_{\varphi_0} = \frac{2\Omega \cos\varphi_0}{R}. \tag{5.7.3}$$

$R = 6371$ km is the mean radius of the Earth, $\Omega = 7.29 \cdot 10^{-5}$ s^{-1} the angular velocity of the Earth and φ_0 the reference latitude. $A \approx 10^4$ m^2 s^{-1} is the horizontal eddy viscosity coefficient. This value corresponds to a typical value of $200 - 250$ km for the widths of the western boundary currents (see Munk, 1950). The velocity $\boldsymbol{u}$ of an incompressible ($\boldsymbol{\nabla} \cdot \boldsymbol{u} = 0$) two-dimensional flow can be calculated from a *stream function* $\psi(x, y)$

$$u = -\frac{\partial \psi}{\partial y} \qquad \text{and} \qquad v = \frac{\partial \psi}{\partial x}. \tag{5.7.4}$$

Taking the curl of Eq. (5.7.2) to eliminate the pressure gradient one obtains the *vorticity equation*

$$\frac{\partial}{\partial t}\nabla^2 \psi + J(\psi, \nabla^2 \psi) + \beta \frac{\partial \psi}{\partial x} - A\nabla^4 \psi + \left(\frac{\partial T_y}{\partial x} - \frac{\partial T_x}{\partial y}\right) = 0 \tag{5.7.5}$$

where

$$J(a, b) = \frac{\partial a}{\partial x}\frac{\partial b}{\partial y} - \frac{\partial a}{\partial y}\frac{\partial b}{\partial x}$$

is the *Jacobi operator*.

The analytical solution of the linear Munk problem. For the stationary and linear case the vorticity equation (5.7.5) simplifies:

$$\nabla^4\psi - \frac{\beta}{A}\frac{\partial\psi}{\partial x} = -\frac{T_0}{A}\frac{\pi}{H}\sin\left(\frac{\pi}{H}y\right) \tag{5.7.6}$$

The characteristic length (*Munk scale*)

$$W_M = \left(\frac{A}{\beta}\right)^{1/3} \tag{5.7.7}$$

gives an estimate of the width of the western boundary current (see below). In order to resolve this current in the numerical simulation the grid spacing, $\boldsymbol{c}_i\Delta t$, has to be smaller than W_M (= 80 km for $\beta = 2 \cdot 10^{-11}$ m^{-1} s^{-1} and $A = 10^4$ m^2 s^{-1}).

Ideally one would like to derive an analytical solution with noslip conditions ($\boldsymbol{u} = 0$) on all boundaries (an ocean basin bounded by continents on all sides). In terms of the streamfunction ψ this would mean that $\psi = 0$ on all boundaries, $\partial\psi/\partial x = 0$ on the west and east boundary, and $\partial\psi/\partial y = 0$ on the south and north boundary. These conditions cannot easily be fulfilled exactly (consider the Fourier expansion of the meriodinal variation of the zonal wind stress: for each term Y_n of the series a solution X_n of the differential equation has to be constructed and the sum of all these terms has to fulfill the boundary conditions). Thus we will somewhat relax the constrains and allow slip conditions ($\psi = 0$, $\dfrac{\partial^2\psi}{\partial y^2}$) at the southern and northern boundaries (these boundary conditions are appropriate for an ocean gyre bounded on the west and east by continents, and on the south and north by other gyres circulating in the opposite direction).
The exact solution of Eq. (5.7.6) reads

$$\begin{aligned}\psi_{\mathrm{M,e}} \quad = \quad & -\frac{T_0\,H^3}{A\,\pi^3}\sin\left(\frac{\pi}{H}y\right) \\ & \cdot\left\{1 + e^{\alpha_r kx}\left[p_1\cos\left(\alpha_i kx\right) - p_2\sin\left(\alpha_i kx\right)\right] + p_3 e^{\alpha_3 kx} + p_4 e^{\alpha_4 kx}\right\}\end{aligned} \tag{5.7.8}$$

where $\alpha_{1,2} = \alpha_r \pm i\alpha_i$, α_3, and α_4 are roots of the characteristic equation

$$\left(\alpha^2 - \gamma^2\right)^2 = \alpha \tag{5.7.9}$$

and the coefficients p_1 to p_4 are derived from the boundary conditions. The α_n and p_n have to be calculated numerically (Exercise 5.7.3).

Exercise 5.7.1. (**)
Derive the exact solution (Eq. 5.7.8) and the characteristic Eq. (5.7.9) of the linear Munk model (hint: use a separation ansatz).

Exercise 5.7.2. (*)
For small γ find approximate solutions of the characterstic Eq. (5.7.9).

Exercise 5.7.3. (**)
Calculate the α_m and p_m $(m = 1, ..., 4)$ for $A = 10^3$ m^2 s^{-1}, mean latitude $\phi_0 = 30°$, $L = H = 2 \cdot 10^6$ m.

5.7.3 The lattice Boltzmann model

We apply the lattice Boltzmann model introduced in Section 5.2, i.e. the BGK kinetic equation (Eq. 5.2.9) over the D2Q9 lattice with the equilibrium distributions given in Eq. (5.2.12). In the simulations of the linear Munk problem the nonlinear terms of the distribution functions have been dropped:

$$\begin{aligned} F_i &= \frac{4}{9}\rho && i = 0 \\ F_i &= \frac{1}{9}\rho \left[1 + 3\frac{\boldsymbol{c}_i \cdot \boldsymbol{u}}{c^2}\right] && i = 1, 2, 3, 4 \\ F_i &= \frac{1}{36}\rho \left[1 + 3\frac{\boldsymbol{c}_i \cdot \boldsymbol{u}}{c^2}\right] && i = 5, 6, 7, 8. \end{aligned}$$

Here we will discuss some details of the coding of propagation, boundary conditions and forcing.
The grid consists of XMAX × YMAX sites where (XMAX-2) times (YMAX-2) points are 'wet' and the other sites are 'dry', i.e. they are located outside the domain. The boundary between land and ocean lies halfway between the dry and the neighboring wet site (Fig. 5.7.1).

Fig. 5.7.1. *Ocean model: lattice, wet (inside the dashed box) and dry (outside the dashed box) sites, slip or no-slip boundary conditions.*

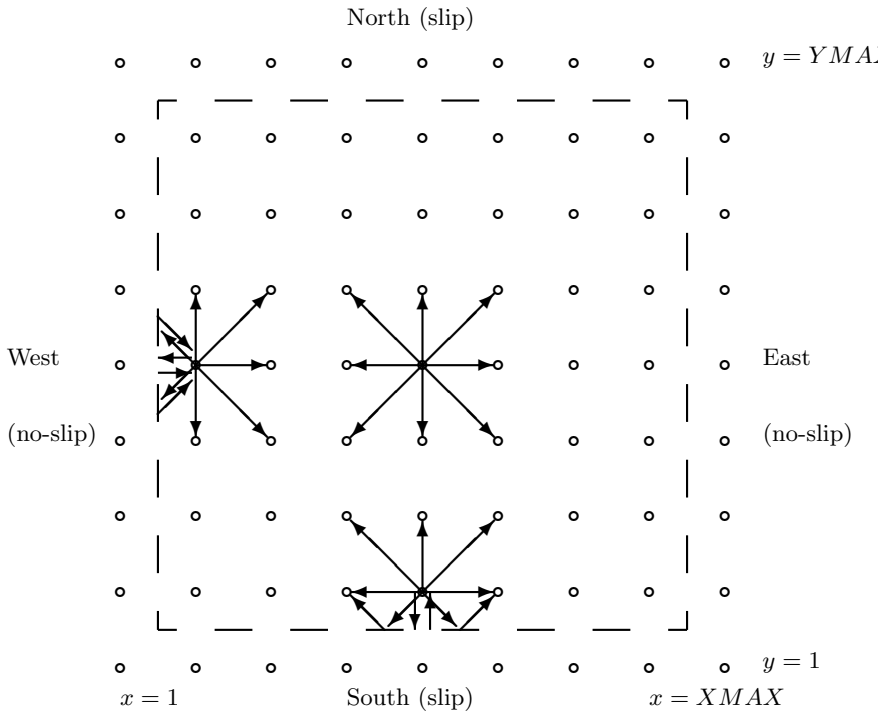

Propagation and boundary conditions. In the propagation step all distributions $F_i(\boldsymbol{x},t)$ (except the 'rest' distribution $F_0(\boldsymbol{x},t)$) of wet points proceed along the corresponding link (direction $\boldsymbol{c}_i$) to the neighbor site and are stored in a second array, say F_i':

$$F_i(\boldsymbol{x},t) \quad \Rightarrow \quad F_i'(\boldsymbol{x}+\Delta t\boldsymbol{c}_i,t). \tag{5.7.10}$$

Near the boundary on wet sites not all F_i' are occupied because no distributions are propagated from dry sites. On the other hand some distributions from sites near the boundary make it to dry sites. The latter distributions propagate back to wet sites according to the local boundary conditions, i.e. in case of no-slip boundary conditions the F_i' bounce back:

$$F_i(\boldsymbol{x},t) \quad \Rightarrow \quad F_i'(\boldsymbol{x}+\Delta t\boldsymbol{c}_i,t) \quad \Rightarrow \quad F_{Ii}'(\boldsymbol{x},t) \tag{5.7.11}$$

where F_{Ii}' is the distribution in the direction of $-\boldsymbol{c}_i$; in case of slip boundary conditions the distributions are reflected at the boundary:

$$F_i(\boldsymbol{x},t) \quad \Rightarrow \quad F_i'(\boldsymbol{x}+\Delta t\boldsymbol{c}_i,t) \quad \Rightarrow \quad F_{Ri}'(\boldsymbol{x}+\Delta t\boldsymbol{c}_{Ri},t) \tag{5.7.12}$$

where $\boldsymbol{c}_{Ri}$ is the lattice velocity that results from reflection of the lattice velocity $\boldsymbol{c}_i$ at the boundary and F_{Ri}' is the distribution in the direction of $\boldsymbol{c}_{Ri}$. After the propagation all dry sites are empty and all wet sites are occupied. This procedure obviously conserves total mass.

Forcing. As shown in Section 5.2 the inclusion of body forces requires changes of the distributions whereby spatial and temporal variations of the forcing have to be taken into account. Two difficulties immediately arise. When the time dependence of the forcing is not explicitely given in advance, the scheme becomes implicit, i.e. unknown values at the future time step are requested in the forcing term. This is indeed the case for the Coriolis force where the velocity at the new time step is required to calculate $\boldsymbol{K}(\boldsymbol{x}+\Delta t\boldsymbol{c}_i,t+\Delta t) = f\,(-u,v)_{\boldsymbol{x}+\Delta t\boldsymbol{c}_i,t+\Delta t}$. This problem can be solved by applying a predictor-corrector method. In the predictor, we use $[\boldsymbol{K}(\boldsymbol{x},t)+\boldsymbol{K}(\boldsymbol{x}+\Delta t\boldsymbol{c}_i,t)]/2$. In the corrector we evaluate the forcing term by using the previous iterate. One corrector seemed to be sufficient; without the corrector a numerical instability occurs after an integration time of several weeks.

The forcing should respect conservation of total mass. Mass is conserved at each lattice site in the case of the 'local forcing' because

$$\sum_i \boldsymbol{c}_i\boldsymbol{K}(\boldsymbol{x},t) = \boldsymbol{K}(\boldsymbol{x},t)\sum_i \boldsymbol{c}_i = 0. \tag{5.7.13}$$

On the other hand mass is in general not conserved locally under 'non-local forcing'

$$\sum_i \boldsymbol{c}_i\boldsymbol{K}(\boldsymbol{x}+\Delta t\boldsymbol{c}_i,t) \neq 0. \tag{5.7.14}$$

Nevertheless, total mass should (and can) be conserved. Problems arise near the boundaries where some forcing terms are not compensated (in terms of mass) by contributions from other sites. This can best be illustrated by an onedimensional example (Fig. 5.7.2; all forcings at $t + \Delta t$). $\boldsymbol{K}(\boldsymbol{x}_1)$ does not exists because $\boldsymbol{x}_1$ is a dry site; it is set to zero. $\boldsymbol{K}(\boldsymbol{x}_2)$ is not compensated. In order to compensate this term and to add some forcing at $\boldsymbol{x}_2$, $\boldsymbol{K}(\boldsymbol{x}_2)$ is added at $\boldsymbol{x}_2$ in such a way that after propagation the forcing at $\boldsymbol{x}_2$ is comparable to that at neighboring sites (the details of the algorithm depend on the type of boundary conditions).

Fig. 5.7.2. *External forcing: a onedimensional example. The arrows indicate compensation in terms of mass.*

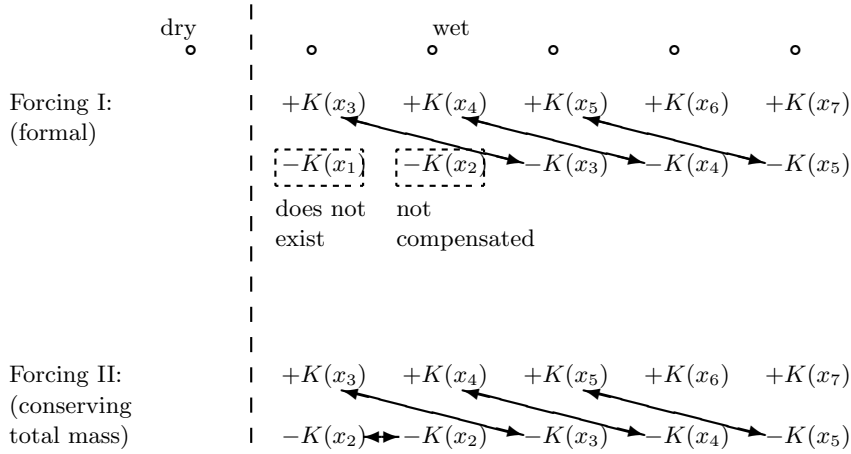

LB simulation of the linear Munk problem. The linear Munk problem was integrated in a 2000 km × 2000 km domain with central latitude at 30°N ($f_0 = 7.29 \cdot 10^{-5}$ s^{-1}, $\beta = 1.98 \cdot 10^{-11}$ s^{-1} m^{-1}). The eddy diffusivity coefficient $A = 10^4$ m^2 s^{-1} results in a width of the Munk layer $W_M = 80$ km which is almost twice the grid spacing ($\Delta x = 50$ km). The characteristic speed $U = 5 \cdot 10^{-4}$ m s^{-1} (linear regime!) is consistent with a wind stress coefficient $T_0 = 7.9 \cdot 10^{-10}$ m s^{-2}. The grid Reynolds number ($R_{e,g} = \dfrac{U \cdot \Delta x}{A} = 2.5 \cdot 10^{-3}$) is small compared to one.
In explicit numerical schemes the time step is limited by the fastest waves in the system (Courant, Friedrichs und Lewy, 1928). Rossby (planetary) waves are excited by the sudden onset of wind forcing. The free undamped waves are governed by

$$\frac{\partial}{\partial t}\nabla^2\psi + \beta\frac{\partial\psi}{\partial x} = 0. \tag{5.7.15}$$

Inserting the ansatz $\psi = \psi_0 e^{i(kx+ly-\sigma t)}$ (wavenumber $\boldsymbol{k} = (k,l)$, $k,l \geq 0$) into Eq. (5.7.15) one can readily derive the dispersion relation

$$\sigma(k,l) = -\frac{\beta k}{k^2+l^2} \tag{5.7.16}$$

which shows that Rossby waves live on the 'β effect', i.e. the fact that the rotation rate (as measured by the Coriolis parameter f) varies with latitude. The phase speed

$$v_{ph} = \frac{\sigma}{\kappa} = -\frac{\beta k}{\kappa^3} \quad \text{with} \quad \kappa = \sqrt{k^2+l^2} \tag{5.7.17}$$

is always negativ (westward propagating phase). Its magnitude becomes maximal for $k = 2\pi/L$ and $l = 0$ and reads

$$|v_{ph}|_{max} = \frac{\beta L^2}{4\pi^2} = 2 \text{ m s}^{-1}. \tag{5.7.18}$$

Thus the time step has to below $\Delta x / |v_{ph}|_{max} \approx 2500$ s. Integration with $\Delta t = 200$ s was numerically stable over the whole simulation time (15 weeks). The global kinetic energy (Fig. 5.7.3) increases over two weeks until it reaches a quasi steady state with oscillations due to Rossby waves. The mean (over several weeks in quasi steady state) velocity shows excellent agreement with the analytical solution (Fig. 5.7.4).

LB simulation in the nonlinear regime. In order to test the LBM under nonlinear conditions, simulations were performed in a closed (no-slip boundary conditions everywhere) basin of size 4000 km × 4000 km with central latitude at 30°N. The flow can be characterized by two dimensionless numbers: the *Rossby number*

$$R_o = \frac{U}{\beta L^2} \tag{5.7.19}$$

Fig. 5.7.3. *Time series of the global kinetic energy (LBM simulation of the linear Munk problem). The oscillations in the quasi steady state are due to Rossby waves.*

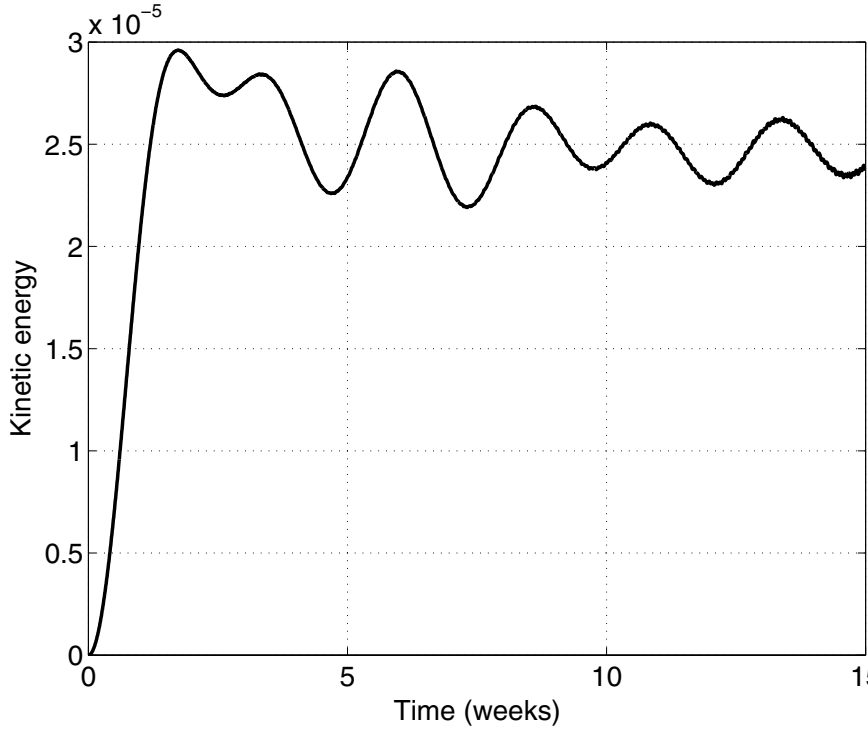

Fig. 5.7.4. *Isocontours of the velocity component u (times* 10^4*) show excellent agreement between the analytical solution (left) and the LBM result (right).*

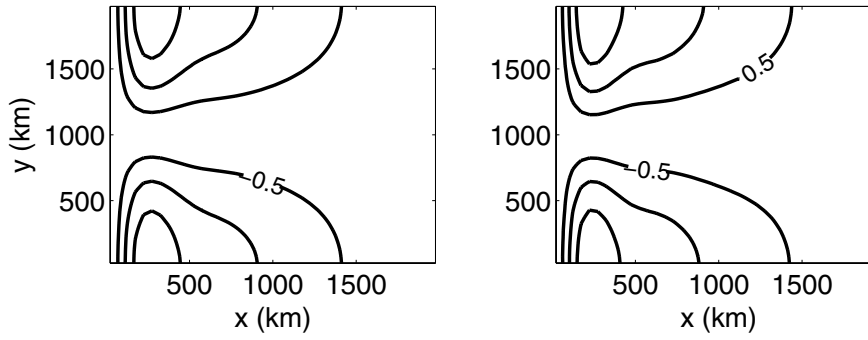

measures the ratio between the advection ($\boldsymbol{u}\boldsymbol{\nabla}\boldsymbol{u}$) and the β term ($\beta y\hat{\mathbf{u}}$), and the *Reynolds number*

$$R_e = \frac{U\,L}{A} \tag{5.7.20}$$

is the ratio between the advection and the friction term ($A\nabla^2\boldsymbol{u}$). The ratio of the Rossby and Reynolds number gives the *Ekman number*

$$E_A = \frac{A}{\beta L^3} \tag{5.7.21}$$

which measures the ratio between the friction and the β term. The Reynold number, $Re = \dfrac{U \cdot L}{A}$, was set to 80 and the Rossby number, $Ro = \dfrac{U}{\beta \cdot L^2}$, to $1.28 \cdot 10^{-3}$. $U = 0.4$ m s^{-1} and $A = 20300$ m^2 s^{-1} where calculated from Re and Ro. The grid spacing, $\Delta x = 40$ km, was chosen small than the Munk width, $W_M = 100$ km. The applied wind stress

$$T_x = -T_0 \sin^2 \frac{\pi y}{L}, \quad T_y = 0 \tag{5.7.22}$$

with $T_0 = 8 \cdot 10^{-7}$ m s^{-2} leads to the formation of a double gyre (Fig. 5.7.5).

Fig. 5.7.5. *LB simulation of a double gyre: isocontours of the stream function $\psi(x, y)$ (times 10^{-4}).*

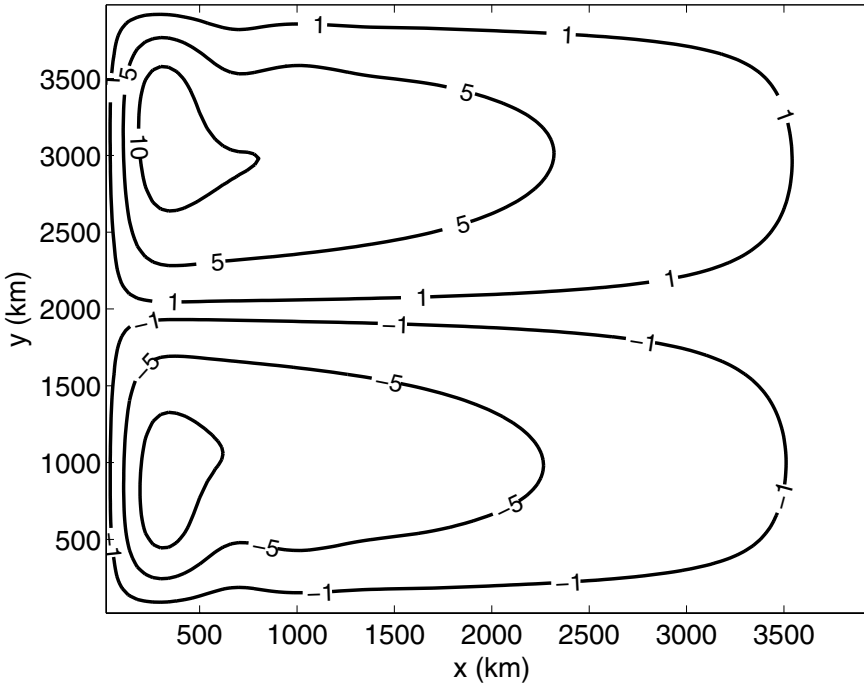

Exercise 5.7.4. (**)
A flow without any external body force can be characterized by a single dimensionless number (Reynolds number). A flow with one type of external body force requires two dimensionless numbers (Reynolds and Froude number; compare discussion of the similarity law in Section 1.3). Here we consider a flow with two types of body forces (Coriolis and wind stress). Do we need three (independent) dimensionless numbers to characterize the flow?

Exercise 5.7.5. (***)
The Navier-Stokes equation contains only molecular diffusion as dissipative process. For large scale oceanic circulation molecular diffusion does not play a role. To get rid of the vorticity imparted by the wind Stommel (1948) introduced *bottom friction* that is linear in the velocity $\boldsymbol{u} = (u, v)$. The appropriate equation of motion reads

$$\frac{\partial \boldsymbol{u}}{\partial t} + (\boldsymbol{u}\boldsymbol{\nabla})\,\boldsymbol{u} + f\hat{\mathbf{u}} + \frac{1}{\rho}\boldsymbol{\nabla} p + k_s \boldsymbol{u} - \boldsymbol{T} = 0 \tag{5.7.23}$$

with the (bottom) friction coefficient k_s. Taking the curl of Eq. (5.7.23) one obtains the *vorticity equation*

$$\frac{\partial}{\partial t}\nabla^2\psi + J(\psi, \nabla^2\psi) + \beta\frac{\partial \psi}{\partial x} + k_s\nabla^2\psi + \left(\frac{\partial T_y}{\partial x} - \frac{\partial T_x}{\partial y}\right) = 0. \tag{5.7.24}$$

For the stationary and linear case the vorticity equation (5.7.24) simplifies:

$$k_s\nabla^2\psi + \beta\frac{\partial \psi}{\partial x} = -\left(\frac{\partial T_y}{\partial x} - \frac{\partial T_x}{\partial y}\right). \tag{5.7.25}$$

The analytical solution of Eq. (5.7.25) in a rectangular ocean basin of length L and width H with $0 \le x \le L$ and $0 \le y \le H$ and the boundary conditions

$$\psi(0, y) = \psi(L, y) = \psi(x, 0) = \psi(x, H) = 0. \tag{5.7.26}$$

reads

$$\psi(x, y) \tag{5.7.27}$$
$$= \frac{T_0 H}{k_s \pi}\sin\left(\frac{\pi}{H}y\right)\left(1 - \frac{e^{\frac{\beta(L-x)}{2k_s}}\sinh(\alpha x) + e^{-\frac{\beta x}{2k_s}}\sinh(\alpha(L-x))}{\sinh(\alpha L)}\right)$$

where

$$\alpha = \sqrt{\frac{\beta^2}{4k_s^2} + \frac{\pi^2}{H^2}}. \tag{5.7.28}$$

This solution describes an asymmetrical gyre with a narrow intense western boundary current and a wide slow southward drift in the eastern part of the basin.
1. Write a LBM code for the Stommel problem. 2. Compare results of the LBM code with the analytical solution of the linear Stommel model. 3. Discuss the pattern of the gyre as a function of Rossby number.

Further reading: Salmon (1999).

5.8 A lattice Boltzmann equation for diffusion

The formulation of lattice-gas cellular automata (LGCA) for given partial differential equations is not straightforward and still requires 'some sort of magic'. Lattice Boltzmann models are much more flexible than LGCA because of the freedom in choosing equilibrium distributions with free parameters which can be set after a multi-scale expansion according to certain requirements. Here a LBM is presented for diffusion in an arbitrary number of dimensions (Wolf-Gladrow, 1995). The model is probably the simplest LBM which can be formulated. It is shown that the resulting algorithm with relaxation parameter $\omega = 1$ is identical to an explicit finite differences (EFD) formulation at its stability limit. Underrelaxation ($0 < \omega < 1$) allows stable integration beyond the stability limit of EFD. The time step of the explicit LBM integration is limited by accuracy and not by stability requirements.

The creation of LGCA for certain partial differential equations still seems to require 'some sort of magic' (compare quotation of Toffoli and Margulos, 1990, in Section 5.4). Here a simple LBM for diffusion is presented and it is shown how straightforward it is to derive such a model. In addition, the resulting algorithms are compared with an explicit finite difference (EFD) scheme.

5.8.1 Finite differences approximation

An explicit finite difference scheme for the diffusion equation

$$\boxed{\frac{\partial T}{\partial t} = \kappa \nabla^2 T} \tag{5.8.1}$$

(T is the concentration of a tracer, κ is the diffusion coefficient and ∇^2 is the Laplace operator in D dimensions in Cartesian coordinates) results from forward approximation in time and central differences in space

$$\begin{aligned} T^{(n+1)}_{k_1,k_2,\ldots,k_D} &= \frac{\kappa \Delta t}{(\Delta x)^2} \left(T^{(n)}_{k_1+1,k_2,\ldots,k_D} + T^{(n)}_{k_1-1,k_2,\ldots,k_D} + \right. \\ &\quad \left. \ldots + T^{(n)}_{k_1,k_2,\ldots,k_D+1} + T^{(n)}_{k_1,k_2,\ldots,k_D-1} \right) \\ &\quad + \left(1 - 2D \frac{\kappa \Delta t}{(\Delta x)^2} \right) T^{(n)}_{k_1,k_2,\ldots,k_D} \end{aligned}$$

where equidistant and equal spacing in all dimensions have been assumed. The scheme is stable for

$$0 < \Delta t \leq \frac{1}{2D} \frac{(\Delta x)^2}{\kappa}$$

(see, for example, Ames, 1977; compare Subsection 5.6.2 for the case $D = 1$). At the upper stability limit the scheme becomes especially simple

$$\begin{aligned} T^{(n+1)}_{k_1,k_2,\ldots,k_D} &= \Big(T^{(n)}_{k_1+1,k_2,\ldots,k_D} + T^{(n)}_{k_1-1,k_2,\ldots,k_D} \\ &\quad \ldots + T^{(n)}_{k_1,k_2,\ldots,k_D+1} + T^{(n)}_{k_1,k_2,\ldots,k_D-1}\Big) \Big/ (2D) \end{aligned}$$

that is T at the new time level is given by the mean over all neighbor values at the previous time level.

5.8.2 The lattice Boltzmann model for diffusion

> "... it is well known that 90° rotational invariance is sufficient to yield full isotropy for *diffusive* phenomena."
> Toffoli and Margulos (1990)

According to Toffoli and Margulos (1990) it is sufficient to use a square or a cubic lattice in two or three dimensions, respectively. The following model is applicable in an arbitrary number of dimensions. The grid velocities (vectors connecting neighboring grid points) are defined by

$$\boldsymbol{c}_{2n-1} = (0, 0, \ldots, 0, 1, 0, \ldots, 0), \quad \boldsymbol{c}_{2n} = (0, 0, \ldots, 0, -1, 0, \ldots, 0) \quad n = 1, 2, \ldots, D$$

where D is the dimension.
In general, the equilibrium distributions[6] $T^{(0)}_m$ depend on the conserved quantities (here only T), a number of parameters γ_k $(k = 0, 1, \ldots, N)$ and on the direction (index m). Here, grids with only one speed are considered and the equilibrium distribution functions $T^{(0)}_m$ do not independent on m. T is given as the sum over the distribution functions T_m

$$T(\boldsymbol{x}, t) = \sum_m T_m(\boldsymbol{x}, t) = \sum_m T^{(0)}_m(\boldsymbol{x}, t) \tag{5.8.2}$$

[6] We will use the notation T_m insteed of F_m for the distribution functions. The equilibrium distribution functions for pure diffusive problems, $T^{(0)}_m$, (diffusion of temperature or tracers) are simpler than those for flow problems, $F^{(0)}_m$.

where the summation runs over all directions ($m = 1, 2, ..., M = 2D$).
The diffusion equation is a linear differential equation. Hence it is reasonable to use a linear ansatz for $T_m^{(0)}$

$$T_m^{(0)} = \gamma_0 + \gamma_1 T. \tag{5.8.3}$$

Inserting (5.8.3) into (5.8.2) yields

$$\boxed{T_m^{(0)} = \frac{T}{2D}} \tag{5.8.4}$$

that is, all free parameters are already fixed by the definition of the tracer concentration. The diffusion coefficient κ will result from the multi-scale expansion as described below.

5.8.3 Multi-scale expansion

The LBM is defined by the grid, the equilibrium distribution $T_m^{(0)}$ and the kinetic equation

$$T_m(\boldsymbol{x} + \boldsymbol{c}_m, t+1) = (1-\omega) T_m(\boldsymbol{x}, t) + \omega T_m^{(0)}(\boldsymbol{x}, t) \tag{5.8.5}$$

which states that the distribution at the new time level $(t+1)$ at the neighboring site $(\boldsymbol{x} + \boldsymbol{c}_m)$ is a weighted sum of the distribution $T_m(\boldsymbol{x}, t)$ and the equilibrium distribution $T_m^{(0)}(\boldsymbol{x}, t)$. Models with parameter ω go under various names: 'enhanced collision' (Higuera et al., 1989), BGK (named after Bhatnagar, Gross and Krook, 1954; compare, for example, Qian et al., 1992), STRA ('single time relaxation approximation', Chen et al., 1991) or SOR ('successive over-relaxation', Qian et al., 1992). The LBM is stable for $0 < \omega < 2$. Now the macroscopic equations will be derived by a multi-scale analysis (compare Frisch et al., 1987, for an analogous procedure for LGCA). The distribution functions are expanded up to linear terms in the small expansion parameter ϵ

$$T_m = T_m^{(0)} + \epsilon T_m^{(1)} + \mathcal{O}(\epsilon^2).$$

From the kinetic equation (5.8.5) one can calculate an approximation of $T_m^{(1)}$

$$\begin{aligned} T_m(\boldsymbol{x} + \boldsymbol{c}_m, t+1) &= T_m(\boldsymbol{x}, t) + \partial_{x_\alpha} c_{m\alpha} T_m + \partial_t T_m + \mathcal{O}(\epsilon^2) \\ &= (1-\omega) \underbrace{T_m(\boldsymbol{x}, t)}_{= T_m^{(0)} + \epsilon T_m^{(1)} + \mathcal{O}(\epsilon^2)} + \omega T_m^{(0)}(\boldsymbol{x}, t) \end{aligned}$$

$\rightarrow$

$$\epsilon T_m^{(1)} = -\frac{1}{\omega} \partial_{x_\alpha} c_{m\alpha} T_m - \frac{1}{\omega} \partial_t T_m + \mathcal{O}(\epsilon^2).$$

Diffusion is a slow process on large spatial scales which suggests the following scaling (same as for the derivation of the Navier-Stokes equations in Frisch et al., 1987)

$$\begin{aligned} \partial_t &\rightarrow \epsilon^2 \partial_t^{(2)} \\ \partial_{x_\alpha} &\rightarrow \epsilon \partial_{x_\alpha}^{(1)}. \end{aligned}$$

The components of the grid velocities obey the following equations

$$\sum_m \boldsymbol{c}_m = 0$$

$$\sum_m c_{m\alpha} c_{m\beta} = 2\delta_{\alpha\beta}$$

and therefore

$$\sum_m \boldsymbol{c}_m T_m^{(0)} = \frac{T}{2D} \sum_m \boldsymbol{c}_m = 0.$$

Inserting the expansion and the scalings into the conservation relation for tracer concentration, one obtains up to second order in ϵ

$$\begin{aligned} 0 &= \sum_m [T_m(\boldsymbol{x} + \boldsymbol{c}_m, t+1) - T_m(\boldsymbol{x}, t)] \\ &= \sum_m [T_m(\boldsymbol{x}, t) + \underbrace{\epsilon^2 \partial_t^{(2)} T_m}_{\rightarrow \partial_t T} + \epsilon \partial_{x_\alpha}^{(1)} c_{m\alpha} T_m + \frac{1}{2} \epsilon^2 \partial_{x_\alpha}^{(1)} \partial_{x_\beta}^{(1)} c_{m\alpha} c_{m\beta} T_m^{(0)} \\ &\quad - T_m(\boldsymbol{x}, t) + \mathcal{O}(\epsilon^3)] \end{aligned}$$

and

$$\begin{aligned} \sum_m \epsilon \partial_{x_\alpha}^{(1)} c_{m\alpha} T_m &= \epsilon \partial_{x_\alpha}^{(1)} \underbrace{\sum_m c_{m\alpha} T_m^{(0)}}_{=0} + \sum_m \epsilon^2 \partial_{x_\alpha}^{(1)} c_{m\alpha} T_m^{(1)} + \mathcal{O}(\epsilon^3) \\ &= -\frac{1}{\omega} \sum_m \epsilon^2 \partial_{x_\alpha}^{(1)} \partial_{x_\beta}^{(1)} c_{m\alpha} c_{m\beta} T_m^{(0)} + \mathcal{O}(\epsilon^3) \qquad (5.8.6) \\ &= -\frac{1}{\omega} \frac{1}{D} \underbrace{\epsilon^2 \delta_{\alpha\beta} \partial_{x_\alpha}^{(1)} \partial_{x_\beta}^{(1)} T}_{\rightarrow \nabla^2 T} + \mathcal{O}(\epsilon^3) \end{aligned}$$

$$\sum_m \frac{1}{2} \epsilon^2 \partial_{x_\alpha}^{(1)} \partial_{x_\beta}^{(1)} c_{m\alpha} c_{m\beta} T_m^{(0)} = \frac{1}{2D} \epsilon^2 \delta_{\alpha\beta} \partial_{x_\alpha}^{(1)} \partial_{x_\beta}^{(1)} T$$

and finally

$$\frac{\partial T}{\partial t} = \kappa \nabla^2 T$$

with

$$\boxed{\kappa = \left(\frac{1}{\omega} - \frac{1}{2}\right)\frac{1}{D}.} \tag{5.8.7}$$

5.8.4 The special case $\omega = 1$

For $\omega = 1$ the kinetic equation (5.8.5) reduces to

$$T_m(\boldsymbol{x} + \boldsymbol{c}_m, t+1) = T_m^{(0)}(\boldsymbol{x}, t)$$

and the diffusion coefficient is $\kappa = \dfrac{1}{2D}$. This LBM is identical to the finite difference scheme at the stability limit. The right hand side of the kinetic equation is just the mean value of the nearest neighboring sites and the diffusion coefficient is the maximal value allowed by the stability condition. For the LBM the diffusion coefficient is expressed in the units $\Delta t = \Delta x = 1$; the diffusion coefficient at the stability limit of the EFD reads

$$\kappa = \frac{1}{2D}\frac{(\Delta x)^2}{\Delta t} = \frac{1}{2D}.$$

This scheme requires only two arrays in memory: the tracer concentrations at two time levels.

5.8.5 The general case

In the general case one has to store $M = 2D$ distributions in addition to the tracer concentrations at two time levels. What do we gain from this extra cost? In the range $0 < \omega < 1$ (underrelaxation) the diffusion coefficient κ is larger than the value at the stability limit of the EFD scheme while we still keep $\Delta t = \Delta x = 1$. In contrast to EFD, the LBM is stable in this parameter range.

5.8.6 Numerical experiments

To test the predictions of the LBM outlined above the one-dimensional diffusion equation was integrated. As initial conditions, values of an analytical solution were used, namely

$$T(x, t_i) = \frac{1}{2\sqrt{\pi \kappa t_i}} \exp\left[-\frac{x^2}{4\kappa t_i}\right].$$

The integration starts at $t_i = 15/\kappa(\omega)$ and ends at $t_f = 75/\kappa(\omega)$, thus the time interval depends on $\kappa(\omega)$, but in each case the integration starts with the same numerical values and ends after the maximum decreases from ≈ 0.073 to ≈ 0.033. Fig. 5.8.1 shows the results of such an integration for $\omega = 0.3$ together with the analytical solution and the initial values. By appropriate choice of ω, one can keep $\Delta t = 1$ for 'arbitrarily' large diffusion coefficients: the scheme is stable but the numerical error increases with increasing diffusion coefficient (compare Fig. 5.8.2). Thus, we have an explicit scheme (BGK-LBM) where the length of the time step is no longer limited by stability requirements. The large error at small values of ω stems from the fact that explicit approximations of parabolic equations act like a hyperbolic system with two real finite difference characteristics instead of only a single real characteristic of the continuous system (Ames, 1977).

5.8.7 Summary and conclusion

A very simple LBM for diffusion in an arbitrary number of dimensions is proposed. For $\omega = 1$ the resulting algorithm is identical to an explicit finite difference scheme at its stability limit. Thus the LBM scheme is not only stable, but automatically picks the maximal allowed diffusion coefficient κ to ensure stability of the EFD scheme.
For LGCA the transport coefficients depend on the collision rules which are never optimal in the sense that they yield only a certain approximation of the (continuous) local equilibrium functions (compare the various FHP models with and without rest particles in Frisch et al., 1987, or the various collision rules proposed for FCHC by Hénon, 1987, Rem and Somers, 1989, and van Coevorden et al., 1994) whereas for LBM, the collisions (which do not show up explicitly) can create local equilibrium at each time step. By reducing the number of collision in LGCA one obtains models with higher diffusion coefficients while stability is assured. This can be regarded as a kind of underrelaxation.
In the BGK-LBM the diffusion coefficient κ is an adjustable parameter. Of special interest is the parameter range $0 < \omega < 1$. The use of information contained in the nonequilibrium distribution functions allows explicit stable integration beyond the stability limit of the EFD scheme. Thus, the time step is limited by accuracy and not by stability requirements.

Fig. 5.8.1. *Integration of the diffusion equation in one dimension by the BGK-LBM with* $\omega = 0.3$. *The integration starts at time* $t_i = 15/\kappa(\omega)$ *with initial values* $T(x, t_i) = \dfrac{1}{2\sqrt{\pi\kappa t_i}} \exp\left[-\dfrac{x^2}{4\kappa t_i}\right]$ *(dotted line) and ends at* $t_f = 75/\kappa(\omega)$. *The figure shows the numerical results (broken line) together with the analytical solution (solid line).*

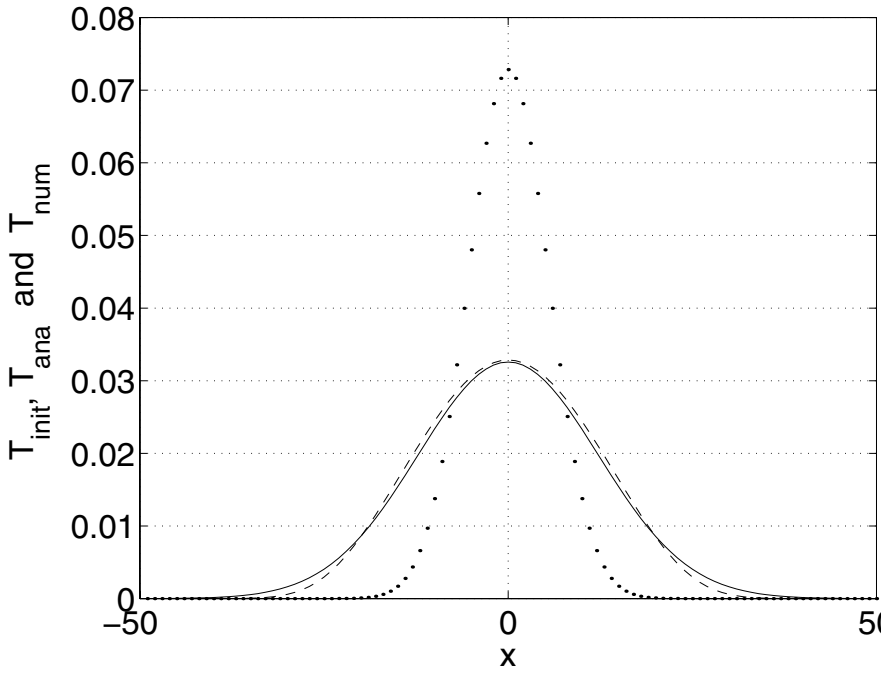

Fig. 5.8.2. *Integrations of the diffusion equation in one dimension by the BGK-LBM. The integration starts at time* $t_i = 15/\kappa(\omega)$ *with initial values* $T(x, t_i) = \frac{1}{2\sqrt{\pi\kappa t_i}} \exp\left[-\frac{x^2}{4\kappa t_i}\right]$ *and ends at* $t_f = 75/\kappa(\omega)$*. The plot shows the logarithm of the maximum error (*$max\{|T_{numerical\ solution} - T_{analytical\ solution}|\}$*) at the end of the integrations as a function of* ω*. The error increases at small values of* ω *(large values of the diffusion coefficients).*

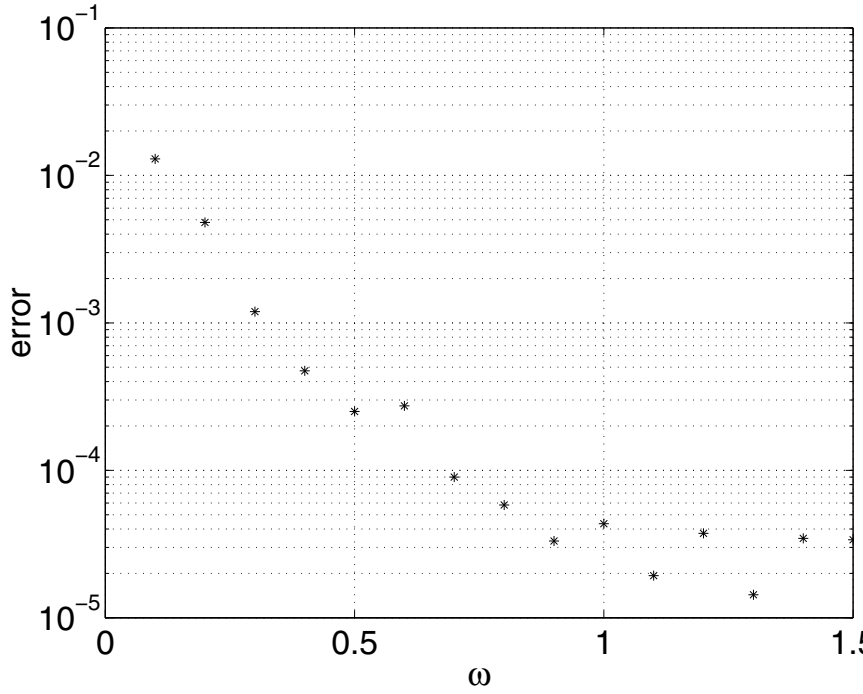

5.8.8 Diffusion equation with a diffusion coefficient depending on concentration

By a small modification the lattice Boltzmann model proposed above can be generalized to a model for a diffusion equation with a diffusion coefficient depending on concentration: The constant ω will be replaced by a function $\omega(T)$. The multi-scale analysis proceeds as before except for Eq. (5.8.6) where $1/\omega$ and the spatial derivative must not be exchanged:

$$\begin{aligned}
\sum_m \epsilon \partial^{(1)}_{x_\alpha} c_{m\alpha} T_m &= \epsilon \partial^{(1)}_{x_\alpha} \underbrace{\sum_m c_{m\alpha} T^{(0)}_m}_{=0} + \sum_m \epsilon^2 \partial^{(1)}_{x_\alpha} c_{m\alpha} T^{(1)}_m + \mathcal{O}(\epsilon^3) \\
&= -\sum_m \epsilon^2 \partial^{(1)}_{x_\alpha} \frac{1}{\omega(T)} \partial^{(1)}_{x_\beta} c_{m\alpha} c_{m\beta} T^{(0)}_m + \mathcal{O}(\epsilon^3) \\
&= -\frac{1}{D} \underbrace{\epsilon^2 \delta_{\alpha\beta} \partial^{(1)}_{x_\alpha} \frac{1}{\omega(T)} \partial^{(1)}_{x_\beta} T}_{\to \left[\boldsymbol{\nabla} \frac{1}{\omega(T)} \boldsymbol{\nabla} T \right]} + \mathcal{O}(\epsilon^3).
\end{aligned}$$

Thus the macroscopic equation reads

$$\boxed{\frac{\partial T}{\partial t} = \boldsymbol{\nabla} \left[\kappa(T) \boldsymbol{\nabla} T \right]} \tag{5.8.8}$$

with

$$\boxed{\kappa(T) = \left[\frac{1}{\omega(T)} - \frac{1}{2} \right] \frac{1}{D}.} \tag{5.8.9}$$

Comparison with an analytical solution. A few analytical solutions are known for the *nonlinear diffusion equation*

$$\frac{\partial T}{\partial t} = \frac{\partial}{\partial x} \left[\kappa(T) \frac{\partial T}{\partial x} \right] = \frac{\partial \kappa}{\partial T} \left(\frac{\partial T}{\partial x} \right)^2 + \kappa(T) \frac{\partial^2 T}{\partial x^2}. \tag{5.8.10}$$

For $\kappa(T) = T$ (Logan, 1994, p. 143; a misprint has been corrected) a solution reads

$$T(x,t) = \frac{1}{6t} \left(A^2 t^{2/3} - x^2 \right) \quad \text{for} \quad |x| < A t^{1/3} \tag{5.8.11}$$

and $T(x,t) = 0$ otherwise. Fig. 5.8.3 shows the comparison between the numerical solution by the lattice Boltzmann model and the analytical solution at $t = 210$ for initial conditions according to eq. (5.8.11) with $A = 5$, $t = 10$ inside the interval $|x| < A t^{1/3}$ and $T = 0$ otherwise. The agreement is very good.

Fig. 5.8.3. *Integration of the nonlinear diffusion equation (5.8.10) by the lattice Boltzmann model. The initial distribution is marked by circles. The numerical solution at* $t = 210$ *(solid line) is indistinguishable from the analytical solution (dashed-dotted line; not visible). The broken line shows the difference between numerical and analytical solution multiplied by* 100.

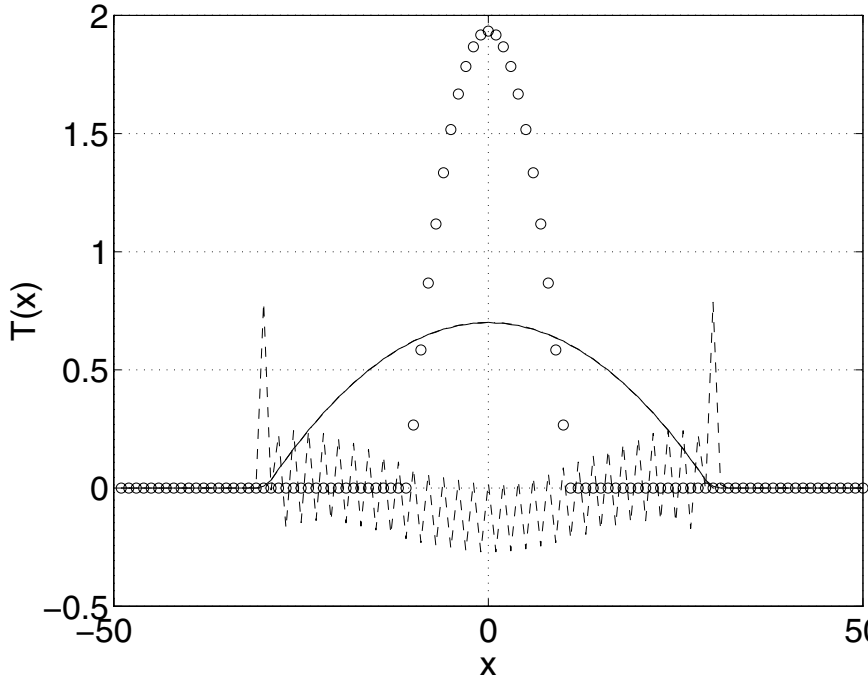

5.8.9 Further reading

Elton et al. (1990) proposed a LBM for a nonlinear diffusion equation in 2D. The collision operator is based on variants of the HPP model (extended by one- and two-particle collisions which conserve mass but not momentum). The diffusion coefficients are functions of the tracer density.
The LBM for reaction-diffusion systems by Dawson et al. (1993) lives on the FHP lattice (D2Q7) and applies the BGK approximation of the collision operator.
Qian and Orszag (1995) developed a LBM for reaction-diffusion equations. Their diffusion model is identical to that proposed by Wolf-Gladrow (1995).
Further reading: Sun (1998), van der Sman and Ernst (1999).
Finite differences: Teixeira (1999).

5.9 Lattice Boltzmann model: What else?

- Books: Rothman and Zaleski (1997).
- Review articles: Benzi, Succi and Vergassola (1992), Rothman and Zaleski (1994), Qian, Succi and Orszag (1995), Biggs and Humby (1998), Chen and Doolen (1998).
- Curvilinear coordinates, finite volumes, irregular grids, mesh refinement: Filippova and Hänel (1998a,b), He and Doolen (1997a,b), He (1997), Karlin and Succi (1998), Mei and Shyy (1998), Peng et al. (1998, 1999), Renwei and Wei (1998), Tölke et al. (1998, 1999), Karlin et al. (1999), Xi et al. (1999a,b).
- Flow past obstacles: Bernsdorf et al. (1998).
- Flow through porous media: Cancelliere et al. (1990), Aharonov and Rothman (1993), Gunstensen and Rothman (1993), Sahimi (1993), Buckles et al. (1994), Heijs and Lowe (1995), Martys and Chen (1996), Shan and Doolen (1996), Grubert (1997), Spaid and Phelan (1997; 1998), Angelopoulos et al. (1998), Bosl et al. (1998), Coveney et al. (1998), Dardis and McCloskey (1998a,b), Freed (1998), Kim et al. (1998), Koch et al. (1998), Koponen et al. (1998a,b), Maier et al. (1998a,b), Noble and Torczynski (1998), Waite et al. (1998; 1999), Berest et al. (1999), Bernsdorf et al. (1999), Inamuro et al. (1999), Verberg and Ladd (1999).
- Granular flow: Herrmann (1995), Tan et al. (1995), Herrmann et al. (1996).
- Multiphase flows: Gunstensen et al. (1991), Holme and Rothman (1992), Flekkøy (1993), Shan and Chen (1993, 1994), d'Ortona et al. (1995), Flekkøy et al. (1995), Orlandini et al. (1995), Flekkøy et al. (1996b), Halliday (1996), Halliday et al. (1996), Sofonea (1996), Swift et al. (1996), Gonnella et al. (1997; 1998; 1999), Hou et al. (1997), Kato et al. (1997), Wagner and Yeomans (1997; 1998; 1999), Angelopoulos et al. (1998), Chen et al. (1998a), Halliday et al. (1998), Holdych et al. (1998), Lamura et al. (1998; 1999), Masselot and Chopard (1998a), Theissen et al. (1998), Wagner (1998b), Yu and Zhao (1999).
- Magnetohydrodynamics (MHD): Chen et al. (1991), Succi et al. (1991), Martinez et al. (1994), Sofonea (1994).
- Compressible flows, Burgers equation: Alexander et al. (1992).
- Flow past fractal obstacles: Adrover and Giona (1997).
- Turbulence and large eddy simulation (LES): Frisch (1991), Benzi et al. (1996), Amati et al. (1996), Fogaccia et al. (1996), Hayot and Wagner (1996), Amati et al. (1997a,b), Succi (1998), Teixeira (1998).
- Flow in dynamical geometry (blood flow): Fang et al. (1998), Krafczyk et al. (1998a).

- Glacier flow: Bahr and Rundle (1995).
- Rayleigh-Bénard convection: Bartoloni et al. (1993), Massaioli et al. (1993), Benzi et al. (1994), Pavlo et al. (1998a) Vahala et al. (1998a).
- Rayleigh-Taylor instability: Nie et al. (1998), He et al. (1999a,b).
- Korteweg-de Vries equation: Yan (1999).
- Droplets: Schelkle et al. (1999), Xi and Duncan (1999).
- Crystal growth: Miller and Böttcher (1998).
- Wave propagation: Chopard and Luthi (1999).
- Maxwell's equations: Simons et al. (1999).
- Decoupling of spatial grid from the velocity lattice: Cao et al. (1997), Pavlo et al. (1998a).
- H-theorem for LBM: Karlin and Succi (1998), Karlin et al. (1998), Wagner (1998a), Karlin et al. (1999).
- Quantum mechanics: Succi and Benzi (1993), Succi (1996), Meyer (1997a,b; 1998).
- Related methods: Junk (1999).
- Further reading: Lavallée et al. (1989), Kingdon et al. (1992), McNamara and Alder (1992, 1993), Nannelli and Succi (1992), Qian (1993), Qian and Orszag (1993), Ladd (1993, 1994a,b), Chen et al. (1994), Punzo et al. (1994), Succi and Nannelli (1994), Elton et al. (1995), Hou et al. (1995), McNamara et al. (1995), Miller (1995), Ohashi et al. (1995), Reider and Sterling (1995), Succi et al. (1995), Wagner and Hayot (1995), Zou et al. (1995a,b), Flekkøy et al. (1996a), Elton (1996), (Burgers eq.) He et al. (1996), Kaandorp et al. (1996), Lin et al. (1996), Orszag et al. (1996), Rakotomalala et al. (1996), Sterling and Chen (1996), Chen and Ohashi (1997), Filippova and Hänel (1997, 1998c), Giraud and d'Humières (1997), Luo (1997a,b), Maier and Bernard (1997), Qi (1997; 1999), Qian (1997), Qian and Chen (1997), Stockman et al. (1997; 1998), Succi et al. (1997), van der Sman (1997), Warren (1997), Ahlrichs and Dunweg (1998), Aidun et al. (1998), Buick and Greated (1998), Buick et al. (1998), Chen (1998), Chen and Ohashi (1998), Chen et al. (1998b), Chenghai (1998), De Fabritiis et al. (1998), Giraud et al. (1998), He and Zhao (1998), Kandhai et al. (1998a,b; 1999), Krasheninnikov and Catto (1998), Luo (1998), Succi and Vergari (1998), Takada and Tsutahara (1998), Ujita et al. (1998), Xu and Luo (1998), Yan (1998), Yan et al. (1998; 1999), Kendon et al. (1999), Klar (1999).

5.10 Summary and outlook

Because LGCA and LBM are still in rapid development it is not possible to give an actual and complete picture of the whole field. Instead I have tried to introduce the basic models (HPP, FHP, FCHC, D2Q9) plus some personal favorites (like PI) together with methods from statistical mechanics (Chapman-Enskog expansion, BGK approximation, maximum entropy principle) which are necessary for the theory of LGCA or LBM but which are usually not part of the curriculum for students of physics or mathematics. Knowledge of these special methods is usually taken for granted in articles and even in reviews.

I am still fascinated by these new methods, and I guess, I am not alone. Although the emergence of new numerical methods is often driven by practical requirements by engineers and natural scientists, (applied) mathematicians usually take the lead in the development of the schemes. However, many researchers working on LGCA and LBM would call themselves most probably physicists. Why are these kind of schemes so attractive to them? At least three reason come to my mind. Firstly, both approaches are based on conservation laws. Physicists feel at home with conservation laws. The continuity equation and the Navier-Stokes equation express the conservation of mass and momentum. Certain conserved quantities are related (Noether theorem) to symmetry groups which allow us to derive equations of the fundamental field theories by the gauge principle. Secondly, LGCA and LBM require more (physical) theory than many other numerical methods. Whereas you can teach to a beginner how to create and apply the simplest schemes of finite differences or spectral methods to partial differential in a few hours, this seems not possible for LGCA, LBM, and finite elements. And the theory required stems from statistical mechanics (Chapman-Enskog expansion, maximum entropy principle) whereas for finite elements, for example, weak convergence in Sobolev spaces is more the backyard of mathematicians. Last but not least, it is fascinating to see the role of symmetry. The symmetry of the underlying lattice is still important on the macroscopic level. It took more than 10 years to discover that it is sufficient to replace a lattice with fourfold (HPP) by one with hexagonal (FHP) symmetry in order to obtain the correct form of the nonlinear advection term of the Navier-Stokes equation. The same symmetry requirement even led us into four dimensions (FCHC). Chiral symmetry has to be established by random processes (FHP). Spurious invariants have to be detected (still not solved in general) and then to be destroyed (for example: three-particle collisions in FHP) or not to be initialized or generated (Zanetti invariants). And finally consequences of missing symmetry has to be scaled away (symptomatic treatment of the violation of Galilean invariance).

As a final remark let me ask the question: What will be the future of LGCA and LBM? Will these schemes have outcompeted the traditional methods (fi-

nite differences, finite volumes, finite elements, spectral, semi-Lagrange, ...) in say five years from now? Or will we throw away these new schemes because they cannot compete with the fastest of the other schemes? The application of a wide variety of methods at the same time already indicates that currently (forever?) there does not exist a best scheme for all problems in the numerical solution of partial differential equations. Although finite elements are well established since decades (the first edition of the monograph by Zienkiewicz appeared already in 1967) the Modular Ocean Model (the work horse of physical oceanography) still applies finite volumes (Bryan, 1969; Semtner, 1997). And the traditional methods are still under development (the same is true for languages such as FORTRAN). Rood (1987) lists about 100 different numerical advection schemes and several new have been proposed since. LGCA and LB models have disadvantages (how to construct models for given differential equations, noise of LGCA, stability of LBM, large memory requirement of LBM) which prohibit the general replacement of well-established traditional methods.

On the other hand, LGCA and LB models have several advantages like flexibility with respect to domain geometry, locality of the collisions (well adapted to massively parallel computer) and low complexity of the code. Because LB models are based on conservation principles they are especially suited for long-time integrations (for instance: climate models). It has been shown already that LGCA and LB models can compete with traditional schemes in certain classes of problems. Therefore, it is almost certain that both methods will find their niches.